OUKA
The University of Osaka
Institutional Knowledge Archive

| | |
|---|---|
| Title | Studies on Electroweak Phase Transition Signatures - A Bridge Between Cosmological and Collider Phenomenology |
| Author(s) | Florentino, Ricardo Miguel |
| Citation | 大阪大学, 2026, 博士論文 |
| Version Type | VoR |
| URL | https://doi.org/10.18910/105643 |
| rights | |
| Note | |

*The University of Osaka Institutional Knowledge Archive : OUKA*

https://ir.library.osaka-u.ac.jp/

The University of Osaka

大阪大学
THE UNIVERSITY OF OSAKA

# Studies on Electroweak Phase Transition Signatures

A Bridge Between Cosmological and Collider Phenomenology

**Ricardo Miguel da Cunha Rosa Florentino**

Thesis to obtain the Doctor of Philosophy Degree in

**Physics**

Dedicated to my grandmother

# Acknowledgments

First, I would like to acknowledge Prof. Shinya Kanemura for supervising my thesis and for his careful guidance throughout my research. I also thank the other members of the doctoral thesis review committee—Prof. Masaharu Aoki, Prof. Tetsuya Onogi, Prof. Ryosuke Sato, and Prof. Kei Yagyu—for reading my thesis and providing valuable suggestions for improvement. I am grateful to the students, researchers, and professors at The University of Osaka, the University of Lisbon, and other institutions, with whom I had the pleasure of discussing physics. Finally, I would like to express my appreciation to my family, friends, and fellow karateka for their continued support throughout my doctoral studies and academic journey. I am deeply thankful to my father, Mário Florentino, and to my partner, Nguyễn Thanh Vân, for their unwavering understanding and encouragement.

# Abstract

One of the biggest issues plaguing modern physics is the observed value of the Baryon Asymmetry of the Universe. One of the most promising mechanisms to explain the observed Baryon Asymmetry of the Universe is Electroweak Baryogenesis. For Electroweak Baryogenesis to be successful, there must have occurred in the early universe a Strongly First Order Electroweak Phase Transition. In order for the Electroweak Phase Transition to be First Order, the sphaleron decoupling condition must be satisfied. The sphaleron decoupling condition requires large deviations in the Higgs triple self-coupling. The Higgs triple self-coupling measurements at colliders can thus be used to probe the nature of the Electroweak phase transition. Furthermore, first order cosmological phase transitions are capable of generating gravitational waves and even, in certain circumstances, primordial black holes. In extended scalar models, the main effects leading to these phenomena are the non-decoupling effects originating from loop correction from the new degrees of freedom. The Standard Model Effective Field Theory is not appropriate to describe non-decoupling effects, while the Higgs Effective Field Theory lacks predictive power. In order to consistently describe the non-decoupling effects from new physics in a model independent framework, the nearly-aligned Higgs Effective Field Theory must be used.

In this thesis, various topics on the Standard Model phenomenology, extended Higgs models, and cosmology of the electroweak phase transition are reviewed. The nearly-aligned Higgs Effective Field Theory, its validity, and its effectiveness in describing non-decoupling effects is also reviewed in detail. Then, a new observable is proposed as a probe for the nature of the Electroweak phase transition, the Higgs di-photon effective coupling. Towards this objective, the nearly-aligned Higgs Effective Field Theory is extended for the first time into its sub-leading order, chiral dimension 4, Lagrangian. This is necessary since, in the chiral formalism, loop induced interactions, like the Higgs di-photon, are only described by Lagrangians of this order. Furthermore, several classes of models are chosen as benchmark models for our analysis using the effective theory.

The non-decoupling effects on the Higgs di-photon couplings are analysed, and its importance once again proven. It was found that in models with charged scalars, large values of the Higgs triple self-coupling become easily constrained by Higgs di-photon

measurements, unless the new physics scale is high enough. Then, an analysis of signatures of the electroweak phase transition is performed for the benchmark models mentioned above. The sphaleron decoupling condition is taken into account, together with the phase transition completion condition, and perturbative unitarity. Various observables are analysed, such as the Higgs triple self-coupling, the Higgs di-photon coupling, gravitational waves, and primordial black holes. Besides corroborating the necessity of a large Higgs triple self-coupling, it is shown that models with charged scalars also necessitate large deviations on the Higgs di-photon coupling.

This thesis closes with discussions on the usage of future measurements to probe the nature of the Electroweak phase transition. First, a hypothetical scenario of Higgs di-photon coupling measurement at the HL-LHC is considered. In this scenario, it is shown how such measurements can be used to give tangible predictions on subsequent measurements of the Higgs triple self-coupling, in order to produce a Strongly First Order Electroweak Phase Transition. Secondly, hypothetical scenarios of Higgs triple self-coupling measurements at the HL-LHC and the various stages of the ILC are considered. It is shown that such measurements at the HL-LHC and the first and second stages of the ILC are incapable of decisively determining the nature of the electroweak phase transition by themselves. Even the last stage of the ILC is shown to only determine that the electroweak phase transition is first order, or that it is not first order, in some very fine-tuned circumstances. It is also shown that joining these measurements of the Higgs triple self-coupling, with the ones from the Higgs di-photon, can solve this issue and decisively determine the nature of the Electroweak phase transition in the future. This further motivates the use of the Higgs di-photon as a complementary probe of the nature of the Electroweak phase transition.

**Keywords:** Higgs; Higgs Couplings; Di-Photon; Effective Field Theory; naHEFT; Collider; Electroweak; Phase-Transition; Sphaleron; Gravitational Waves

# Contents

Acknowledgments . . . . . 5
Abstract . . . . . 7

**1 Introduction and Overview** **13**
1.1 Overview of this Thesis . . . . . 19

**I Background Review** **21**

**2 The Standard Model of Particle Physics** **22**
2.1 Particle Content . . . . . 23
2.2 The Higgs Mechanism . . . . . 24
2.3 Gauge Invariance . . . . . 25
2.4 Flavour Physics . . . . . 27
2.5 Custodial Symmetry . . . . . 29
2.6 Full Lagrangian . . . . . 32

**3 Higgs Sector Experimental Status** **33**
3.1 Higgs Mass . . . . . 33
3.2 Higgs Couplings . . . . . 34
3.3 Higgs Self-Coupling . . . . . 35
3.4 Electroweak Precision Parameters . . . . . 35

**4 Extended Higgs Models** **37**
4.1 The Two Higgs Doublet Model . . . . . 37
4.2 The Higgs Triplet Model . . . . . 40
4.3 The Georgi-Machacek Model . . . . . 41

**5 Cosmology of the Electroweak Phase Transition** **45**

5.1 The Baryon Asymmetry of the Universe . . . . . 46

5.2 Electroweak Baryogenesis . . . . . 47

5.3 The Sphaleron and Baryon Number Violation . . . . . 49

5.4 Bubble Nucleation and the Completion Condition . . . . . 50

5.5 Sphaleron Decoupling Condition . . . . . 52

5.6 Gravitational Waves from First Order Phase Transitions . . . . . 53

5.7 Primordial Black Hole Generation . . . . . 56

**II Exploring First Order EWPT using the naHEFT** **59**

**6 The nearly-aligned Higgs Effective Field Theory** **60**

6.1 The electroweak chiral Lagrangian . . . . . 61

6.2 The naHEFT leading order Lagrangian . . . . . 62

6.3 Finite Temperature Corrections . . . . . 65

6.4 Validity as an Effective Theory . . . . . 67

**7 Loop induced decays in the naHEFT** **71**

7.1 Sub-leading order Lagrangian . . . . . 72

7.2 Parameter Setup . . . . . 73

7.3 The effective $h\gamma\gamma$ interaction . . . . . 74

**8 Analysis of Electroweak Phase Transition Signatures** **79**

8.1 Gravitational Wave Spectra . . . . . 80

8.2 Parameter Scan . . . . . 81

**9 Further Discussions** **85**

9.1 Coupling Predictions . . . . . 85

9.2 Future Collider Phenomenology . . . . . 88

**10 Summary and Conclusions** **93**

**A Theoretical Constraints on the naHEFT** **97**

A.1 Vacuum Stability . . . . . 98

A.2 Perturbative Unitarity . . . . . 99

Bibliography 107

# Chapter 1

# Introduction and Overview

Throughout the 20th century the Standard Model of Particle Physics has emerged as one of the most successful theories of nature. Build upon the theory of the strong nuclear force Quantum Chromodynamics [1, 2, 3, 4, 5], the Glashow-Weinberg-Salam theory of Electroweak unification [6, 7, 8], and the Brout-Englert-Higgs-Guralnik-Hagen-Kibble mechanism [9, 10, 11, 12, 13], also known simply as the Higgs mechanism, it provides a complete quantum field theoretic description of all known fundamental particles and their interactions. After many decades of experimental scrutiny, it has been proved to be remarkably accurate [14], standing as the cornerstone of modern physics. The validation of the full framework was accomplished in 2012 with the discovery of the Higgs boson by two experiments at CERN, ATLAS [15] and CMS [16], confirming the Higgs mechanism responsible for electroweak symmetry breaking, and generating mass terms for the rest of the fields. Despite it's success, the Higgs sector remains largely untested. It's central role in mass generation and it's unique nature as a scalar field make it specially sensitive to phenomena beyond the Standard Model, making Higgs precision phenomenology one of the primary focuses of the current high energy physics community.

Despite it's tremendous success, the Standard Model is widely believed to be an incomplete description of natural phenomena. This comes from the existence of several observed phenomena for which the Standard Model offers no explanation. These include the observed Baryon Asymmetry of the Universe [17], the existence of Dark Matter [17], and the origin of neutrino masses and oscillations [18]. The framework also presents various theoretical challenges. These include the observed pattern of

fermion masses and mixing, the hierarchy problem associated with the stability of the Higgs mass, and the absence of a quantum description of gravity. These issues hint at the existence of a higher energy scale beyond which a more complete theory must appear, making the Standard Model likely a low energy effective theory of the phenomena present above this scale. Since many of these open questions couple directly or indirectly to the phenomenology of electroweak symmetry breaking, the Higgs sector becomes a natural playground to explore the effects of new physics phenomena.

Following the observational and theoretical limits of the Standard Model, the Higgs sector presents itself as a uniquely sensitive portal to explore new physics phenomena. Being the only observed scalar field, the Higgs field's couplings and self-interactions are not protected by the models symmetries in the same way interactions involving only fermions and gauge bosons are, making them specially sensitive to alterations coming from heavy or hidden sectors. The measurement of deviations in the Higgs couplings to fermions, gauge bosons, or itself, would therefore provide indirect evidence of new physics beyond the Standard Model. Extended scalar sector present in many new physics models, such as models with additional electroweak singlets [19, 20, 21, 22, 23, 24, 25, 26, 27], doublets [28, 29, 30, 31, 20, 32, 33, 34, 35, 36, 37, 38, 39, 40, 41, 42, 43, 27], or triplets [44, 45, 46, 47, 48, 49, 20], can alter the shape of the Higgs potential, modify the dynamics of electroweak symmetry breaking, and generate observable signatures in collider experiments. Precision measurements of Higgs related observables at the LHC and future colliders, combined with electroweak precision measurements and flavour physics constraints, become a powerful window for exposing and constraining new physics phenomena through the scalar sector. Moreover, alterations in the Higgs potential in extended scalar sectors also have tremendous impact to early universe cosmology. Due to finite temperature corrections to the field equations, at temperatures above the electroweak scale, the electroweak symmetry is intact. Then, when crossing the electroweak scale, the universe undergoes a phase transition and spontaneous symmetry breaking takes place through the Higgs mechanism. The dynamics of this phenomena, known as the Electroweak Phase Transition, is extremely dependent on the shape of the scalar potential.

The Baryon Asymmetry of the Universe can be explained by various models with extended Higgs sectors. In order to produce the correct baryon asymmetry, these

models must utilise a mechanism that satisfies the three Sakharov conditions [50]. One promising mechanism satisfying these conditions is Electroweak Baryogenesis [51] which takes place during the Electroweak Phase Transition. In order to satisfy the Sakharov condition of departure from thermal equilibrium, this transition must be a first order phase transition. Then, the condition of Baryon number violation can be accomplished through the sphaleron solution to the field equations [52, 53], only if the sphaleron decouples right after the phase transition. A phase transition satisfying the sphaleron decoupling condition, is called a Strongly First Order Electroweak Phase Transition. Finally, the condition of C and CP violation is accomplished from new CP violating terms in the scalar sector.

The Electroweak Phase Transition within the Standard Model framework is a smooth crossover phase transition [54], and as such, it does not satisfy the Sakharov condition of departure from thermal equilibrium. In addition, the only CP-violation term in the Standard Model, the Cabibbo-Kobayashi-Maskawa phase, is known to be too small to explain the observed baryon asymmetry [55, 56]. As for the sphaleron decoupling condition, its validity is strongly dependent on large values for the Higgs triple self-coupling [57, 58, 22, 59]. The nature of the Electroweak Phase Transitions can then be explored through precise measurements of the triple Higgs coupling. This means that extended Higgs sectors, specially the ones with a strong Higgs self-coupling, are crucial for the onset of Electroweak Baryogenesis. Deviations in this coupling can have two origins, mixing angles with new scalars, or radiative corrections from new physics. Mixing angles are strongly constrained from Higgs coupling measurements [60, 61], and generally lead to a decrease in the coupling value. This leaves radiative corrections as the likely origin for strong couplings. Even though the Higgs self coupling has not been measured precisely so far [61, 62], it will be measured precisely by future collider experiments. For instance, the High-Luminosity HLC is expected to measure the triple Higgs self-coupling with a precision of 50% [63], while the International Linear Collider running at 1TeV is expected to do so with at least 10% precision [64].

First order phase transitions in the early universe are capable of generating cosmological imprints. In particular, stochastic gravitational wave backgrounds can be generated by a first order electroweak phase transition, which can be detected in the future by gravitational wave observers [22, 59, 65]. The peak frequency of such gravitational

waves is of the order $10^{-1} - 10^{-4}$Hz, which is within the reach of future space-based interferometers like LISA [66], DECIGO [67], TianQin [68], Taiji [69], and the BBO [70]. Another example of cosmological imprints left by the electroweak phase transition are Primordial Black Holes. These can be formed by a method of delayed first order phase transition. They have recently been confirmed to be useful for the test of first order phase transitions [71, 72, 73, 74, 75, 76, 77, 78, 79, 80, 81, 82, 83]. In the case of the electroweak phase transition, the generated black holes have a mass of around $10^{-5}$ solar masses. This parameter region was contained up to a black hole fraction of $10^{-2}$ by Subaru HSC [84] and OGLE [85]. Future experiments, like PRIME [86] and the Roman Telescope [87], are expected to further constrain this area of the parameter space. These connections to cosmology make the Higgs sector an undeniable bridge between particle phenomenology and early universe cosmology, serving as motivation for the study of Higgs couplings, extended scalar potentials, and their thermal evolution and dynamics in the early universe. Exploring the interplay between collider phenomenology and early universe cosmological signatures reveals to be a powerful strategy to test beyond the Standard Model physics in a complementary and experimentally testable way.

When exploring effects of new physics in the Higgs sector, it is often convenient to use a framework capable of describing deviations from the Standard Model without specifying a specific ultraviolet complete model. With that end in mind, Effective Field Theories (EFTs) give a a model-independent framework capable of systematic parametrization of effects originating from physics at a higher scale through higher dimensional operators. In the context of Higgs physics, there are two widely used EFT approaches. The Standard Model EFT (SMEFT) [88, 89, 90] assumes the observed Higgs field to be part of the same electroweak doublet present in the Standard Model, with symmetry braking following the same pattern as the Standard Model, making it suitable for describing small deviations that decouple from the Standard Model for a new physics scale much larger than the electroweak scale. The Higgs EFT (HEFT) [91, 92, 93, 94, 95, 96, 97, 98, 99] relaxes this assumption by treating the Higgs as a generic scalar and allowing for a non-linear realization of electroweak symmetry breaking, which accommodates the presence of large deviations from the Standard Model, and also non-decoupling effects generated from loop correction from new physics,

which do not decouple for large new physics scales [100, 101, 102]. Besides allowing for a systematic description of modified Higgs couplings, EFTs are also suitable to incorporate finite-temperature corrections to the field theory, which is essential for the study of electroweak phase transitions and their cosmological signatures. It is thus evident that EFTs offer a consistent framework to study the dynamics of beyond the Standard Model Higgs sectors and both their collider and cosmological phenomenology.

The nearly-aligned Higgs EFT (naHEFT) [103, 104, 105, 106] was introduced as a subset of the HEFT, constructed with the added assumption that the observed Higgs boson is close to the alignment limit. In this regime, the Higgs field has close characteristics to the Standard Model Higgs at tree level, while not constrained to belonging to the it's doublet as in SMEFT, allowing the naHEFT to retain the flexibility to systematically describe large non-decoupling loop corrections to the Higgs couplings. This means that correction on couplings such as the triple Higgs coupling appear not from tree-level mixing effects, but from loop effects from new physics, just as we expect for the occurrence of a strongly first order electroweak phase transition. Thus, the naHEFT is the perfect framework to study phenomenology related to the electroweak phase transition. The loop induced corrections to the Higgs self coupling are of particular importance, for altering the scalar potential in such a way to allow for a strongly first order electroweak phase transition, while staying in the alignment limit at tree level. The quantum corrected scalar potential is then responsible for generating the necessary barrier between vacua and enabling the strong phase transition, while maintaining consistency with current Higgs measurements. By implementing the non-linear structure of the HEFT while focusing on a nearly-aligned Higgs field, the naHEFT constitutes a robust and tractable framework for connecting Higgs collider phenomenology with the dynamics of electroweak symmetry breaking and it's cosmological observables.

Given the situation explained so far, the central goal of this thesis in to investigate new phenomenological paths to probe the nature of the Electroweak Phase Transition. The main way to do this at the moment are: measuring the Higgs triple self coupling with precision in future colliders, like the ILC; and detecting gravitational waves with future space based observers, like LISA and DECIGO. Both these options depend on experiments that won't start running until the mid to late 2030's. A third option has

been introduced, detecting primordial black holes, with experiments running in a more timely manner. This option, however, is only possible in a very fine-tuned section of the parameter space. To deal with this issue, this thesis introduces a novel way of probing the electroweak phase transition, thorough measurements of the Higgs to di-photon decay. The LHC results for this effective interaction have recently been improved to 9% by ATLAS [107] and 8% by CMS [108], and is expected to be measured with 1.8% accuracy by the HL-LHC [109]. This interaction would then be a very good alternative to the aforementioned options to probe the nature of the electroweak phase transition. We show this to be possible because the same non-decoupling effects from new physics that cause a sizeable triple Higgs, high enough to produce a strongly first order phase transition, will also affect the effective interaction between the Higgs and two photons. In order to study this effects, we introduce for the first time the next to leading order terms in the nearly-aligned Higgs EFT necessary to properly describe this effective interaction. We also calculate the parameter space of the naHEFT capable of generating a strongly first order phase transition, and the parameter space leaving detectable cosmological imprints. We then study the interplay between the four mentioned observable: the triple Higgs self-coupling, the effective Higgs di-photon interaction, gravitational waves, and primordial black holes. We show not only that the Higgs di-photon interaction is capable of testing the parameter space in a meaningful way by itself, but also that it can complement the other observables in a unique way that is impossible with only the other three observables. We also show how this complementarity will help us approve or rule out specific models once we measure the effective Higgs di-photon interaction at the HL-LHC and at least one more of these observables with enough precision. Finally, we discuss how measurements of the triple Higgs self-coupling at the ILC will help to constrain the parameter space. Through this unique approach, this work intends to serve as a steeping stone in understanding how we can use all the available cosmological and collider observables to consistently test the nature of the electroweak phase transition in the years to come.

## 1.1 Overview of this Thesis

The rest of this Thesis is organized into two parts. Part I provides the background necessary to follow the main work of this theses by presenting modern reviews on relevant topics. Part II, on the other hand, its more focused on the original research conducted for this thesis, from it's theoretical setup, to the main analysis. The work in this part was published in the journal Physics Letter B [105] or as a conference proceedings of the International Workshop on Future Linear Colliders [106]. I now provide a short summary for each of these parts.

Part I starts with Chapter 2 by reviewing the Standard Model theoretical framework, detailing it's scalar, gauge, and fermion sectors, including an introduction to the Higgs mechanism and to the concept of custodial symmetry. Chapter 3 provides a review on the current status of Higgs sector phenomenology, including the most precise measurements at colliders of the Higgs mass and couplings to other particles and to itself, and the status of electroweak precision phenomenology. Chapter 4 explores relevant ultraviolet complete extensions of the Standard Model with extended scalar sectors, including the Two Higgs Doublet Model, the Higgs Triplet Model, and the Georgi-Machacek model, and it's varied Higgs sector phenomenology. Chapter 5 then shifts into early universe cosmology, namely by exploring the subject of Electroweak Phase Transition, including the concept of Electroweak Baryogenesis, the sphaleron process, the formation and nature of a measurable stochastic gravitational wave background from strongly first order phase transitions, and the generation of primordial black holes from the advent of a delayed first order phase transition.

Part II starts with Chapter 6 by introducing the nearly-aligned Higgs Effective Field Theory formalism, stemming from the electroweak chiral Lagrangian, into it's full leading order Lagrangian and it's finite temperature corrections, and finishes by setting up the framework used in the remainder of this work. Chapter 7 expands the nearly-aligned Higgs Effective Field Theory to include next to leading order terms necessary for the calculation of loop induced decays like the $h \to \gamma\gamma$ and $h \to Z\gamma$, and provides a study of the effective Higgs coupling $\kappa_{\gamma\gamma}$ using this formalism. Chapter 8 provides the main analysis of this research, explaining the calculation of the detectability of the gravitational waves spectra at interferometers, and a full parameter space scan of the occurrence of a Strongly First Order Electroweak Phase Transition, and all the signa-

tures described before. Chapter 9 deepens the discussion further by discussing how to complement this data with $\kappa_3$ and $\kappa_{\gamma\gamma}$ phenomenology at colliders, and how future colliders, like the International Linear Collider, will impact this work in the future. Finally, chapter 10 provides a summary of the topics discussed in this thesis, and the main conclusions to be taken from this study.

# Part I

# Background Review

# Chapter 2

# The Standard Model of Particle Physics

The Standard Model of Particle Physics is a Quantum Field Theory theory locally invariant under the non-abelian Lie group

$$SU(3)_C \times SU(2)_L \times U(1)_Y, \tag{2.1}$$

where the $SU(3)_C$ subgroup refers to the theory of Quantum Chromodynamics [1, 2, 3, 4, 5] which describes the strong nuclear force, while the $SU(2)_L \times U(1)_Y$ subgroup refers to the theory of Glashow-Salam-Weinberg [6, 7, 8] which describes the electroweak interactions, a unified theory of electromagnetism and the weak nuclear force. By combining these gauge theories with the Higgs mechanism [9, 10, 11, 12, 13], the Standard Model became the best theory of fundamental phenomena to date. The purpose of this chapter is to review the theoretical framework in which this model is build upon, with a stronger focus on the Higgs sector. In Section 2.1 the particle content of the model is summarized, with explanations on their relations to the gauge groups in Equation 2.1. In Section 2.2 the scalar potential is introduced, and the Higgs mechanism is explained. In Section 2.3 gauge invariance is introduced into the model, and the effect of the Higgs mechanism to the gauge bosons in explained. In Section 2.4 the Yukawa Lagrangian is introduced and the basics of flavour physics arising from fermion mixing is explained. In Section 2.5 an important property of the Standard Model Higgs potential, custodial symmetry, is explained, which will be useful later for the discution

| Fermions | $SU(3)_C$ | $SU(2)_L$ | $Y$ |
|---|---|---|---|
| $q_L$ | **3** | **2** | $1/6$ |
| $u_R$ | **3** | **1** | $2/3$ |
| $d_R$ | **3** | **1** | $-1/3$ |
| $l_L$ | **1** | **2** | $-1/2$ |
| $e_R$ | **1** | **1** | $-1$ |

Table 2.1: First generation of fermions introduced into the standard model with their gauge group representations and hypercharge.

of non-linear effective field theories. Finally, in Section 2.6, the full Lagragian on the Standard Model is given.

## 2.1 Particle Content

The gauge symmetries in Equation 2.1 give rise to three sets of massless vectorial gauge bosons

$$G_\mu^{a=1,8}, \qquad W_\mu^{a=1,3}, \qquad B_\mu, \tag{2.2}$$

which act as mediators for their respective interactions.

A total of fifteen fermion fields are introduced. These are divided into three generations with identical properties, apart from their Yukawa couplings, and consequently, their mass. Table 2.1 lists the fermion families, along with their representations under the non-abelian gauge groups, and their hypercharge under the $U(1)_Y$ gauge group. The indices $L, R$ indicate the chirality of the fields. The electroweak doublets can be further explicitly written as

$$q_L = \begin{pmatrix} u_L \\ d_L \end{pmatrix}, \qquad l_L = \begin{pmatrix} \nu_L \\ e_L \end{pmatrix}, \tag{2.3}$$

such that we get chirality pairs for both the types of quarks and the electrons. Many new physics models naturally introduce the right handed neutrino with trivial gauge variance.

A single scalar field is introduced, the Higgs field, which is a singlet under the strong

group and a doublet under the electroweak group, with hypercharge 1/2

$$\Phi = \begin{pmatrix} \phi^+ \\ \phi^0 \end{pmatrix}, \qquad Y_\Phi = 1/2, \tag{2.4}$$

the importance of which is explored in the next section.

## 2.2 The Higgs Mechanism

In the Standard Model, the Higgs field is subject to the following scalar potential

$$V = -\mu^2|\Phi|^2 + \lambda|\Phi|^4, \tag{2.5}$$

with both $\mu^2 > 0$ and $\lambda > 0$. This potential has the infamous Mexican hat shape, leading to a minima degenerate under three of the four degrees of freedom of the potential. Expanding the field around this minima results in a vacuum expectation value $v$ in the forth direction, which can be taken to the real part of the lower component without loss of generality, resulting into

$$\Phi = \begin{pmatrix} G^+ \\ \frac{1}{\sqrt{2}}(v + h + G^0) \end{pmatrix}. \tag{2.6}$$

Introducing this expression into the potential and solving the minimum condition

$$\frac{\partial V}{\partial h} = 0, \tag{2.7}$$

reveals the vacuum expectation value to be

$$v = \sqrt{\frac{\mu^2}{\lambda}}, \tag{2.8}$$

which can be used to replace $\mu^2$ by $v$ in the potential. Further, solving the two point function condition

$$\frac{\partial^2 V}{\partial h^2} = m_h^2, \tag{2.9}$$

leads to the formula for the mass of the Higgs field

$$m_h^2 = 2\lambda v^2, \tag{2.10}$$

which can be used to replace $\lambda$ by $m_h^2$ in the potential. The potential is thus written as

$$V = \frac{m_h^2}{2}h^2 + \frac{m_h^2}{2v}h^3 + \frac{m_h^2}{8v^2}h^4, \tag{2.11}$$

and we are left with only one physical scalar degree of freedom, the Higgs boson $h$. The remaining three degrees of freedom $G^{0,\pm}$ disappear from the potential and are thus the unphysical Goldstone bosons resulting from the spontaneous symmetry breaking of the electroweak gauge group as predicted by the Nambu-Goldstone theorem.

## 2.3 Gauge Invariance

Invariance under the Standard Model gauge groups is accomplished by forfeiting the use of the usual space-time derivative in favour of the generalised covariant derivative defined as

$$D_\mu = \partial_\mu + ig_c T_a^c G_\mu^a + igT_a W_\mu^a + ig'YB_\mu, \tag{2.12}$$

where $g_c$, $g$, and $g'$ are the respective gauge couplings, $T_a^c$ acts as $\lambda_a/2$ on $SU(3)_c$ triplets and as null to singlets, with $\lambda_a$ being the Gell-Mann matrices which generate the group, $T_a^c$ acts as $\tau_a/2$ on $SU(2)$ doublets and as null to singlets, with $\tau_a$ being the Pauli matrices which generate the group, and $Y$ is the hypercharge operator that acts accordingly to each field is it applied to.

When applied to the fermions we get

$$\mathcal{L}_\psi = \sum_\psi i\bar{\psi}\not{D}\psi, \tag{2.13}$$

where I make use of the Dirac slash notation $\not{D} = \gamma^\mu D_\mu$ with $\gamma^\mu$ being the Dirac matrices that generate the Clifford algebra $Cl_{1,3}(\mathbb{R})$. This Lagrangian is responsible for the strong and electroweak interactions between the fermions mediated by the gauge bosons.

When applied to the Higgs field we get

$$\mathcal{L}_\Phi = D^\mu \Phi^\dagger D_\mu \Phi, \tag{2.14}$$

which after expanding the Higgs around the potential minima leads to various terms. Some of these terms depend on the derivatives of the Goldstone bosons $\partial_\mu G^{0,\pm}$. These can be absorbed into the Gauge boson with a proper gauge transformation. The Lagrangian then becomes of the form

$$\begin{aligned}\mathcal{L}_\Phi \supset & \frac{1}{2}(\partial h)^2 + \frac{g^2 v^2}{8}(W^{1\mu} - iW^{2\mu})(W^1_\mu + iW^2_\mu) \\ & + \frac{v^2}{4}(g' B^\mu - g W^{3\mu})(g' B_\mu - g W^3_\mu),\end{aligned} \tag{2.15}$$

which introduces mass terms for the gauge bosons. It is then appropriate to move to their mass eigen-basis

$$W^+_\mu = \frac{1}{\sqrt{2}}(W^1_\mu - iW^2_\mu), \tag{2.16}$$

$$W^-_\mu = \frac{1}{\sqrt{2}}(W^1_\mu + iW^2_\mu), \tag{2.17}$$

$$Z_\mu = \cos(\theta_W) W^3_\mu - \sin(\theta_W) B_\mu, \tag{2.18}$$

$$A_\mu = \sin(\theta_W) W^3_\mu + \cos(\theta_W) B_\mu, \tag{2.19}$$

where $\theta_W$ is the Weinberg angle which satisfies

$$\cos(\theta_W) = \frac{g}{g_Z}, \tag{2.20}$$

$$\sin(\theta_W) = \frac{g'}{g_Z}, \tag{2.21}$$

and

$$g_Z = \sqrt{g^2 + g'^2}. \tag{2.22}$$

The final form of the Lagrangian is thus

$$\mathcal{L}_\Phi = \frac{1}{2}(\partial h)^2 - m^2_W W^{+\mu} W^-_\mu - \frac{m^2_Z}{2} Z^\mu Z_\mu, \tag{2.23}$$

where the gauge bosons obtained the masses

$$m_W^2 = \frac{g^2 v^2}{4}, \tag{2.24}$$

$$m_Z^2 = \frac{g_Z^2 v^2}{4}. \tag{2.25}$$

These mass terms spontaneously break the electroweak gauge invariance in the degrees of freedom represented by these three fields thanks to the Higgs mechanism, leaving the unbroken subgroup $U(1)_{EM}$ corresponding to the still massless boson $A_\mu$, responsible for the propagation of the electromagnetic interaction. The electromagnetic charge operator can be retroactively defined as

$$Q = T_3 + Y, \tag{2.26}$$

such that the hypercharge conventions introduced for the fermions are consistent with their electromagnetic charges.

Finally, the gauge boson are made dynamic by the introduction of their kinetic Lagrangian

$$\mathcal{L}_G = -\frac{1}{4} G^a_{\mu\nu} G_a^{\mu\nu} - \frac{1}{4} W^a_{\mu\nu} W_a^{\mu\nu} - \frac{1}{4} B_{\mu\nu} B^{\mu\nu}, \tag{2.27}$$

where

$$V^a_{\mu\nu} = \partial_\mu V_\nu - \partial_\nu V_\mu + g f_{abc} V^b_\mu V^c_\nu, \tag{2.28}$$

and $f_{abc}$ are the structure constants of the respective gauge groups.

## 2.4 Flavour Physics

The Yukawa Lagrangian of the Standard Model is

$$\mathcal{L}_Y = \bar{q}_L \tilde{\Phi} Y_u u_R + \bar{q}_L \Phi Y_d d_R + \bar{l}_L \Phi Y_e e_R + h.c., \tag{2.29}$$

where $\tilde{\Phi} = i\tau_a \Phi^*$. There are quite a few vector spaces implicit in this expression. First, there's the Dirac spinor space in which acts on all the fermions which are contracted as $\bar{\psi}\psi$. Second, there's the $SU(3)_c$ space acting on the quarks which are contracted as $\bar{q}q$. Third there's the $SU(2)_L$ scape acting on left handed fermions contracted with the Higgs doublet as $\bar{\psi}_L \Phi$. Lastly there's the family space with three dimensions where the Yukawa matrices $Y_\psi$ are acted on the right by a fermion column vector, and on the left by a fermion row vector.

After spontaneous symmetry breaking, mass terms proportional to $v$ are generated by the Higgs mechanism. The fields can then by brought to the mass eigenstates by

$$\psi_L^m = V_L^\psi \psi_L, \tag{2.30}$$

$$\psi_R^m = V_R^\psi \psi_R, \tag{2.31}$$

for $\psi = u, d, e$, where $V_{L,R}^\psi$ are flavour space matrices that diagonalise the Yukawa matrices such that

$$M_u = \frac{v}{\sqrt{2}} V_L^u Y_u^\dagger V_R^{u\dagger}, \tag{2.32}$$

$$M_d = \frac{v}{\sqrt{2}} V_L^d Y_d V_R^{d\dagger}, \tag{2.33}$$

$$M_e = \frac{v}{\sqrt{2}} V_L^e Y_e V_R^{e\dagger}, \tag{2.34}$$

are the diagonal mass matrices for the fermions, with real positive eigenvalues.

When diagonalising the fermions in their kinetic Lagrangian in Equation 2.13, the following interaction terms appear

$$\mathcal{L}_\psi \supset \mathcal{L}_J = eA_\mu J_A^\mu + g_Z Z_\mu J_Z^\mu + \frac{g}{\sqrt{2}} \left( W_\mu^+ J_W^\mu + W_\mu^- J_W^{\mu\dagger} \right), \tag{2.35}$$

where we introduce the electromagnetic coupling constant

$$e = \frac{g g'}{g_Z}, \tag{2.36}$$

which corresponds experimentally to the electron charge. The currents in this interac-

tion Lagrangian are given by

$$J_A^\mu = \frac{2}{3}\bar{u}\gamma^\mu u - \frac{1}{3}\bar{d}\gamma^\mu d - \bar{e}\gamma^\mu e, \tag{2.37}$$

$$J_Z = \bar{l}\gamma^\mu P_L T_3 l + \bar{q}\gamma^\mu P_L T_3 q - \sin^2\theta_W J_A^\mu, \tag{2.38}$$

$$J_W^\mu = \bar{u}\gamma^\mu P_L V_{CKM} d + \bar{e}\gamma^\mu P_L \nu, \tag{2.39}$$

where a sum in flavour space is implicit. Here we introduced a new flavour space matrix

$$V_{CKM} = V_L^u V_L^{d\dagger}, \tag{2.40}$$

commonly known as the Cabibbo–Kobayashi–Masukawa matrix, which is responsible for generating charged flavour changing charged currents mediated by $W_\mu^\pm$, that allow violation of flavour number within the Standard Model. On the other hand, flavour changing neutral currents are suppressed within the Standard Model due to the Glashow-Iliopoulous-Maiani mechanism.

## 2.5 Custodial Symmetry

The Higgs field can alternatively be represented as a matrix

$$\mathbf{\Phi} = (\tilde{\Phi}, \Phi) = \begin{pmatrix} \phi^{0*} & \phi^+ \\ -\phi^- & \phi^0 \end{pmatrix}, \tag{2.41}$$

such that the scalar potential can be written as

$$V = -\frac{\mu^2}{2}\,\mathrm{Tr}\{\mathbf{\Phi}^\dagger\mathbf{\Phi}\} + \frac{\lambda}{4}\,\mathrm{Tr}\{\mathbf{\Phi}^\dagger\mathbf{\Phi}\}^2, \tag{2.42}$$

and the kinetic Lagrangian as

$$\mathcal{L}_\Phi = \frac{1}{2}\,\mathrm{Tr}\{(D_\mu\mathbf{\Phi})^\dagger D^\mu\mathbf{\Phi}\}, \tag{2.43}$$

where the covariant derivative should be taken as

$$D_\mu\mathbf{\Phi} = \partial_\mu\mathbf{\Phi} + igT_a W_\mu^a\mathbf{\Phi} - ig' B_\mu\mathbf{\Phi}T_3, \tag{2.44}$$

with the special attention to the added $T_3$ in the $U(1)_Y$ term which acts on the right of the target field. This formulation reveals that the scalar sector is actually invariant not only on the electroweak symmetry group, but also on the more general global symmetry $SU(2)_L \times SU(2)_R$, under which the Higgs field transforms as

$$\mathbf{\Phi} \to U_L \mathbf{\Phi} U_R, \qquad U_L \in SU(2)_L, \qquad U_R \in SU(2)_R, \tag{2.45}$$

for which the electroweak group is a subgroup. After spontaneous symmetry breaking, the vacuum expectation value of the Higgs field takes the form

$$\langle \mathbf{\Phi} \rangle = \frac{1}{\sqrt{2}} \begin{pmatrix} v & 0 \\ 0 & v \end{pmatrix}, \tag{2.46}$$

which is still invariant under a subset of the global symmetry where $U_L = U_R$. The symmetry broken theory is then invariant under a global $SU(2)_V$ symmetry dubbed custodial symmetry. This remaining global symmetry is responsible for the degeneracy of the $W_\mu^a$ mass matrix after symmetry breaking. Let us now introduce the $\rho$ parameter as

$$\rho = \frac{m_W^2}{\cos^2\theta_W m_Z^2}, \tag{2.47}$$

The mentioned mass degeneracy, and hence the presence of custodial symmetry, is responsible for the relation $\rho = 1$ holding at tree level. Since the Yukawa sector is does not obey the custodial symmetry, loop correction to $\rho$ can deviate it from unity from next to leading order.

Some new physics models with extended scalar sectors do not have a custodialy symmetric scalar potential, such that $\rho$ can deviate from unity even at tree level. In fact, for a theory with an arbitrary number of scalar electroweak multiplets, the $\rho$ parameter is given by

$$\rho = \frac{\sum_i (t_i(t_i+1) - t_{3Vi}^2) v_i}{\sum_i 2 t_{3Vi}^2 v_i}, \tag{2.48}$$

where the sum goes over all the electroweak scalar multiplets, $t_i$ is such that $2t_i + 1$ is the multiplet's dimension, $v_i$ is their vacuum expectation value, and $t_{3Vi}$ is the $T_3$

eigenvalue corresponding to the electroweak vacuum. This equation indicates custodial symmetry is intact for models with only singlets, doublets, and septets, plus some other very high dimensional multiplets, while being broken by other types of multiplets, like triplets. Those others models are able to keep this parameter near unity only if they present a very small vacuum expectation value. As we will discuss in Chapter 4, exceptions to this rule exist. One notable exception is the general Two Higgs Doublet Model, where the most general potential is capable of breaking custodial symmetry. On the other hand, another notable exception is the Georgi-Machacek model, which introduces a scalar transforming as a triplet under both global symmetries in 2.45, and thus explicitly preserving custodial symmetry.

At the quantum level, custodial symmetry is not exact even in the Standard Model. Although the scalar potential preserves the global $SU(2)_L \times SU(2)_R$ symmetry at tree level, it is explicitly broken by hypercharge interactions and by the Yukawa sector, where fermions couple differently to the Higgs doublet. As a result, radiative corrections induce deviations of the $\rho$ parameter from unity. These effects first appear at one-loop order and are dominated by fermion mass splittings, in particular the large mass difference between the top and bottom quarks.

The leading one-loop correction to $\rho$ can be expressed in terms of the oblique parameter $T$, defined through $\Delta\rho \equiv \rho - 1 = \alpha T$, where $\alpha$ is the electromagnetic fine-structure constant. In the Standard Model, the dominant contribution is

$$\Delta\rho_{\text{SM}} \simeq \frac{3G_F}{8\sqrt{2}\pi^2}\left(m_t^2 - m_b^2\right), \tag{2.49}$$

which reflects the explicit custodial symmetry breaking induced by the Yukawa couplings. The experimental status on the electroweak precision parameters will be discussed in Section 3.4

In models with extended scalar sectors, additional one-loop contributions to $\rho$ arise from scalar mass splitting within custodial multiplets. Even if custodial symmetry is preserved at tree level, radiative corrections can break it unless the scalar spectrum respects the custodial $SU(2)_V$ symmetry. Consequently, maintaining $\rho \simeq 1$ beyond tree level typically requires either an exact custodial symmetry of the full Lagrangian or a near-degeneracy of scalar masses. This requirement places strong constraints on viable extensions of the Standard Model and motivates the custodial symmetric

construction of models such as the Georgi-Machacek model.

## 2.6 Full Lagrangian

The full Standard Model Lagrangian can be obtained by summing the contributions discussed throughout this chapter

$$\mathcal{L}_{SM} = \mathcal{L}_G + \mathcal{L}_\psi + \mathcal{L}_\Phi + \mathcal{L}_Y - V. \tag{2.50}$$

This Lagrangian serves as the backbone of modern particle physics, and most of it has been experimentally corroborated by numerous experiments. Nonetheless, the current measurements precisions still allow the Higgs sector to deviate from the predictions by this model. This sector thus becomes a very powerful tool for the search of new physics, and in the next chapter we review its phenomenological situation.

# Chapter 3

# Higgs Sector Experimental Status

Even thought the Standard Model has been put under experimental scrutiny for many decades so far [14], the Higgs sector is still widely untested. The purpose of this chapter is to review the current phenomenological status of the Higgs sector. The most important and up to date results from both ATLAS and CMS experiments at the LHC are presented for: the Higgs mass in Section 3.1; major Higgs couplings to Standard Model particles in Section 3.2; the Higgs triple self-coupling in 3.3; and the electroweak precision parameters, S, T, and U, in Section 3.4. For the relevant couplings, the kappa formalised is introduced and used.

## 3.1 Higgs Mass

The experiments at LHC produced several measurements of the Higgs boson mass. These include the combined Run-1 experiments [110], Run-2 experiments by ATLAS [111, 112], and those by CMS [113, 114]. Currently, the most precise measurement is the combined results by ATLAS on the di-photon and $ZZ$ channels [115]

$$m_H = 125.11 \pm 0.09(\text{stat.}) \pm 0.06(\text{syst.})\text{GeV} \qquad \text{(ATLAS)}, \tag{3.1}$$

while the current best single channel result comes from CMS's di-photon channel analysis [116]

$$m_H = 125.08 \pm 0.10(\text{stat.}) \pm 0.05(\text{syst.})\text{GeV} \qquad \text{(CMS)}. \tag{3.2}$$

| | ATLAS [107] | CMS [108] | HL-LHC[109] |
|---|---|---|---|
| $\kappa_t$ | $0.99 \pm 0.09$ | $0.92^{+0.09}_{-0.08}$ | 3.4% |
| $\kappa_b$ | $0.89^{+0.10}_{-0.09}$ | $0.98^{+0.13}_{-0.12}$ | 3.6% |
| $\kappa_\tau$ | $0.94 \pm 0.06$ | $0.91 \pm 0.07$ | 1.9% |
| $\kappa_\mu$ | $1.04^{+0.23}_{-0.30}$ | $1.09^{+0.20}_{-0.22}$ | 3.0% |
| $\kappa_W$ | $1.00 \pm 0.05$ | $1.03 \pm 0.06$ | 1.6% |
| $\kappa_Z$ | $0.96 \pm 0.05$ | $1.07 \pm 0.06$ | 1.6% |
| $\kappa_g$ | $0.99^{+0.07}_{-0.06}$ | $0.91^{+0.07}_{-0.06}$ | 2.4% |
| $\kappa_\gamma$ | $0.97 \pm 0.06$ | $1.10 \pm 0.07$ | 1.8% |
| $\kappa_{Z\gamma}$ | $1.36^{+0.30}_{-0.36}$ | $1.61^{+0.32}_{-0.35}$ | 6.8% |

Table 3.1: Current results from ATLAS [107] and CMS [108] experiments for the couplings of the Higgs boson to other particles using the kappa formalism, together with the expected measurement presision for said couplings by the HL-LHC [109]

The analysis of the entire Run-2 dataset is still to be made, and will be of great interest for Higgs sector phenomenology.

## 3.2 Higgs Couplings

When discussing measurements of the Higgs boson couplings, one very convenient formalism is the $\kappa$ framework, [117, 118], where the $\kappa$ parameters are introduced as

$$(\sigma \cdot \mathrm{BR})(i \to h \to f) = \frac{\sigma_i^{SM} \kappa_i^2 \cdot \Gamma_f^{SM} \kappa_f^2}{\Gamma_H^{SM} \kappa_H^2}, \tag{3.3}$$

where $k_H$ expresses the correction to the Higgs width to take into account the various coupling deviations. The rate relative to the SM value is then given by

$$\mu_i^f = \frac{\sigma \cdot \mathrm{BR}}{\sigma_{SM} \cdot \mathrm{BR}_{SM}} = \frac{\kappa_i^2 \cdot \kappa_f^2}{\kappa_H^2}, \tag{3.4}$$

and the Standard Model prediction are recovered by setting all $\kappa_i = 1$. Global fits on this formalism were made with the full Run-2 dataset of both ATLAS [107] and CMS [108]. The ATLAS results for $\kappa_\mu$ and $\kappa_{Z\gamma}$ also include data from Run 3. The results are summarized in Table 3.1, together with the respective precision expected at the HL-LHC [109]. These results are in strong agreement with the Standard Model expectations, giving strong constraints to new physics models.

## 3.3 Higgs Self-Coupling

The Higgs trilinear self-coupling $\kappa$ parameter is defined as the ratio between the observed coupling and it's Standard Model expectation

$$\kappa_3 = \frac{\lambda_3}{\lambda_3^{SM}}. \tag{3.5}$$

Currently, the most stringent result for the self-coupling is by the ATLAS experiment coming from combined di-Higgs and single Higgs production [119]

$$-1.2 < \kappa_3 < 7.2 \qquad \text{(ATLAS)}, \tag{3.6}$$

while the current results from the CMS experiment come solely from the di-Higgs production [120]

$$-1.39 < \kappa_3 < 7.02 \qquad \text{(CMS)}, \tag{3.7}$$

These results leave room for very large deviations from the Standard model expectation when it come to the Higgs self-coupling.

## 3.4 Electroweak Precision Parameters

Other strong constraint on new physics come from the electroweak precision parameters. These are used to parametrize deviation on the electroweak observable originating from new physics. The two-point functions of the gauge bosons are defined as [121]

$$ig^{\mu\nu}\Pi_{XY}(q^2) + (q^\mu q^\nu \text{ term}) = \int d^4x e^{-iqx}\langle J_X^\mu(x) J_Y^\nu(0)\rangle, \tag{3.8}$$

where the currents were defined in 2.39. The two-point functions can be expanded around the external momentum $q^2$ as

$$\Pi_{XY}(q^2) = \Pi_{XY}(0) + q^2\Pi'_{XY}(0) + \mathcal{O}(q^4), \tag{3.9}$$

| | Result | Correlation | | |
|---|---|---|---|---|
| $S$ | $0.021 \pm 0.096$ | 1 | 0.91 | $-0.62$ |
| $T$ | $0.040 \pm 0.012$ | 0.91 | 1 | $-0.83$ |
| $U$ | $0.008 \pm 0.092$ | $-0.62$ | $-0.83$ | 1 |

Table 3.2: Results from global fits [14] of the electroweak precision parameters S, T, and U.

where $\Pi'_{XY}(q^2)$ denotes the derivative in terms of $q^2$. The $\mathcal{O}(q^4)$ are proportional to the inverse of the new physics scale, and are thus negligible. In terms of these quantities, the electroweak precision parameters are [122]

$$\frac{\alpha}{4s_W^2 c_W^2} S = -\,\mathrm{Re}\left[\frac{\Pi_{ZZ}(m_Z^2) - \Pi_{ZZ}(0)}{m_Z^2} - \frac{c_W^2 - s_W^2}{c_W s_W}\frac{\Pi_{ZA}(m_Z^2)}{m_Z^2} - \frac{\Pi_{AA}(m_Z^2)}{m_Z^2}\right], \tag{3.10}$$

$$\alpha T = -\,\mathrm{Re}\left[\frac{\Pi_{WW}(0)}{m_W^2} - \frac{\Pi_{ZZ}(0)}{m_Z^2}\right], \tag{3.11}$$

$$\begin{aligned}\frac{\alpha}{4s_W^2} U = -\,\mathrm{Re}\Bigg[&\frac{\Pi_{WW}(m_W^2) - \Pi_{WW}(0)}{m_W^2} - c_W^2 \frac{\Pi_{ZZ}(m_Z^2) - \Pi_{ZZ}(0)}{m_Z^2} \\ &- 2 s_W c_W \frac{\Pi_{ZA}(m_Z^2)}{m_Z^2} - s_W^2 \frac{\Pi_{AA}(m_Z^2)}{m_Z^2}\Bigg],\end{aligned} \tag{3.12}$$

one of which corresponds to deviations in the aforementioned $\rho$ parameter

$$\rho = 1 + \alpha T. \tag{3.13}$$

Current global fits yield the results show in table 3.2 [14]. This results are in strong accordance with the Standard Model predictions, and leave thus strong constraints on new physics.

# Chapter 4

# Extended Higgs Models

In spite of the tremendous experimental success the Standard Model has achieved, it isn't without it's drawbacks. In order to tackle this issues, many models with extended scalar sector have been introduced. In this section, we give brief reviews on some of the most relevant of these models. In Section 4.1, a brief review of a class of models known as Two Higgs doublet models is given. Two model using scalar electroweak triplets are also reviewed, the Higgs Triplet Model, and the Georgi-Machacek model, in Sections 4.2 and 4.3 respectively.

## 4.1 The Two Higgs Doublet Model

Two Higgs Double Models (2HDM) are extensions of the Standard Model in which the scalar sector includes two scalar $SU(2)_L$ doublets with the same hypercharge as the Standard Model doublet

$$\Phi_{i=1,2} = \begin{pmatrix} w_i^+ \\ \frac{1}{\sqrt{2}}(\varphi_i + i z_i) \end{pmatrix}. \tag{4.1}$$

The Yukawa sector of the most general 2HDM leads to flavour changed neutral currents, which are strongly constrained by flavour experiments [123]. A common way to naturally satisfy this constraints is to introduced a softly broken $\mathbb{Z}_2$ symmetry into the model [124, 125, 126, 127, 128, 129, 130, 131, 29, 132]. Different assignments of this symmetry among the scalars and fermions lead to four different 2HDM models. In table 4.1 these models are presented by which doublet each right handed fermion couples

| Type | $u_R$ | $d_R$ | $e_R$ |
|---|---|---|---|
| I | $\Phi_2$ | $\Phi_2$ | $\Phi_2$ |
| II | $\Phi_2$ | $\Phi_1$ | $\Phi_1$ |
| X | $\Phi_2$ | $\Phi_2$ | $\Phi_1$ |
| Y | $\Phi_2$ | $\Phi_1$ | $\Phi_2$ |

Table 4.1: The four types of $\mathbb{Z}_2$ symmetric 2HDM, indicating which doublet couples to each fermion in the Yukawa Lagrangian for each of the types.

to in the Yukawa sector.

The scalar potential can be generally written as

$$\begin{aligned} V = &- \mu_1^2 \Phi_1^\dagger \Phi_1 - \mu_2^2 \Phi_2^\dagger \Phi_2 - (\mu_3^2 \Phi_1^\dagger \Phi_2 + h.c.) \\ &+ \lambda_1 (\Phi_1^\dagger \Phi_1)^2 + \lambda_2 (\Phi_2^\dagger \Phi_2)^2 + \lambda_3 (\Phi_1^\dagger \Phi_1)(\Phi_2^\dagger \Phi_2) \\ &+ \lambda_4 (\Phi_1^\dagger \Phi_2)(\Phi_2^\dagger \Phi_1) + \left[ \lambda_5 (\Phi_1^\dagger \Phi_2)^2 + h.c. \right], \end{aligned} \tag{4.2}$$

with $\mu_3^2$ and $\lambda_5$ complex, and the other parameters real. The $\mu_3^2$ term is responsible for the soft-breaking of the $\mathbb{Z}_2$ symmetry. After spontaneous symmetry breaking, both doublets acquire a vacuum expectation value

$$\varphi_i = v_i + h_i, \tag{4.3}$$

and the gauge bosons will obtain mass given by $\sqrt{v_1^2 + v_2^2}$, in place of the Standard Model $v$.

The physical scalar spectrum is composed of two CP-even scalars $h$ and $H$, a CP-odd scalar $A$, and a pair of charged scalars $H^\pm$. By usual convention, an angle $\alpha$ is responsible for diagonalizing the CP-even scalars, while an angle $\beta$ is responsible for diagonalizing the CP-even and charged scalars with the Goldstone bosons.

The phenomenology of two Higgs doublet models (2HDMs) is strongly controlled by the quartic couplings of the scalar potential and by the CP-even Higgs mixing angle $\alpha$. The couplings of the light CP-even Higgs boson $h$ to fermions and gauge bosons approach their Standard Model (SM) values when $\cos(\beta - \alpha) \to 0$.

One way this limit is realized is the *decoupling limit*, which occurs when the non-SM

Higgs states become heavy, in particular for large pseudoscalar mass $m_A$. In this case,

$$\sin\alpha \to -\cos\beta, \qquad \cos\alpha \to \sin\beta, \tag{4.4}$$

so that $\cos(\beta-\alpha) \to 0$ automatically. The SM-like behavior of $h$ then arises because the heavier scalar states effectively decouple from low-energy phenomenology.

A second, conceptually distinct possibility is the *alignment limit*, in which the Higgs mass eigenstate $h$ aligns with the direction of the electroweak vacuum expectation value in field space, independently of the masses of the additional scalars. This occurs when the parameters of the scalar potential satisfy a relation such as

$$M_{12}^2 \sin\beta = -(M_{11}^2 - m_h^2)\cos\beta, \tag{4.5}$$

which enforces $\cos(\beta-\alpha) = 0$ even when the non-SM Higgs bosons remain relatively light. In this case, the couplings of $h$ to fermions and weak gauge bosons are SM-like without requiring the decoupling of the additional scalar states.

The phenomenology of the two Higgs doublet models is highly dependent on the quartic couplings and the size of the mixing angle $\alpha$. The lightest CP-even Higgs boson acts like the SM Higgs boson for large values of $m_A$, $\sin\alpha \to -\cos\beta$, $\cos\alpha \to \sin\beta$, and $\cos(\beta-\alpha) \to 0$. If the quartic couplings are such that $M_{12}^2 \sin\beta = -(M_{11}^2 - m_h^2)\cos\beta$, the same behaviour is obtained. The latter scenario, which is particularly interesting because the found Higgs boson exhibits Standard Model-like properties, indicates a circumstance in which the couplings of heavy fermions and weak gauge bosons become the same as in the SM without disconnecting the remaining non-standard scalars. This scenario is called alignment.

As for custodial symmetry, it is easy to realise that the potential in 4.2 is custodial symmetric. Nonetheless, the custodial symmetry is preserved due to the presence of the $\mathbb{Z}_2$ symmetry. In fact, the more general non-$\mathbb{Z}_2$ symmetric 2HDM potential is not generally custodial symmetric, and explicit condition for custodial symmetry for it have been found [133, 134].

## 4.2 The Higgs Triplet Model

The Higgs Triplet model extends the Standard model by adding a complex charged electroweak triplet with hypercharge 1, that can be written as

$$\Delta = \frac{1}{\sqrt{2}} \begin{pmatrix} \Delta^{+} & \sqrt{2}\Delta^{++} \\ v_{\Delta} + \delta + i\xi & -\Delta^{+} \end{pmatrix}, \tag{4.6}$$

which includes a CP-even scalar $\delta$ with vacuum expectation value $v_{\Delta}$, a CP-odd scalar $\xi$, a singly charged scalar $\Delta^{+}$, and a doubly charged scalar $\Delta^{++}$.

The scalar potential can be written as

$$\begin{aligned} V = &- \mu_{\Phi}^2 \Phi^{\dagger}\Phi - \mu_{\Delta}^2 \,\mathrm{Tr}\{\Delta^{\dagger}\Delta\} + (\mu_3 \Phi^{T} i\tau_2 \Delta \Phi + h.c) \\ &+ \lambda_1 (\Phi^{\dagger}\Phi)^2 + \lambda_2 \,\mathrm{Tr}\{\Delta^{\dagger}\Delta\}^2 + \lambda_3 \,\mathrm{Tr}\{(\Delta^{\dagger}\Delta)^2\} \\ &+ \lambda_4 \Phi^{\dagger}\Phi \,\mathrm{Tr}\{\Delta^{\dagger}\Delta\} + \lambda_5 \Phi^{\dagger}\Delta\Delta^{\dagger}\Phi, \end{aligned} \tag{4.7}$$

with $\mu_3$ complex and the other parameters real. After symmetry breaking, there is mixing between the scalars, leading to the following physical states: two CP-even $h$ and $H$, one CP-odd $A$, one singly charged $H^{+}$, and one doubly charged $H^{++}$. One interesting property of this potential is that the $\mu_3$ term is not custodially symmetric. This allows the $\rho$ parameter to deviate from unity even at tree level. It's tree level expression is given by

$$\rho = \frac{1 + 2x^2}{1 + 4x^2}, \tag{4.8}$$

with $x = v_{\Delta}/v_{\Phi}$. This together with the electroweak precision measurements imposes a strong limit on the triplet vacuum expectation value of $v_{\Delta} < 8\text{GeV}$ [46], severely constraining the role of this Higgs triplet in the electroweak symmetry breaking. Furthermore, it has been shown that electroweak precision measurements also severely constrain the mass splittings $|m_{+} - m_{++}|$ and $|m_{+} - m_{A}|$ to be less than 50GeV [135].

This small value for the expectation value, on the other hand, can be used to generate a small mass for the neutrinos, without the need of introduction right handed

neutrinos, through the interaction

$$Y_\nu^{ij} l_i^T C^{-1} i\tau_2 \Delta l_j, \tag{4.9}$$

where $C$ is the charge conjugation matrix and $Y_\nu^{ij}$ is a complex symmetric coupling matrix. Efter symmetry breaking, the neutrinos obtain a mass matrix of the form

$$m_\nu^{ij} = \sqrt{2} v_\Delta Y_\nu^{ij}. \tag{4.10}$$

This term together with the usual neutrino seesaw produces what is known as the type-II seesaw mechanism [136].

The HTM puts forth the compelling chance of figuring out the characteristics of the neutrino mass matrix by using the LHC. In the event that the doubly-charged Higgs boson has a small enough mass and/or its interactions with $W^+W^+$ are adequately diminished, then its main method of breaking down is into pairs of leptons with the same charge, $H^{++} \to l_i^+ l_j^+$, from the Equation 4.9, one can clearly see that these disintegration pathways commonly violate lepton-flavour rules, with how often they occur being related to parts of the neutrino mass matrix [137].

Both the triplet vacuum expectation value, and the mass spectrum of the HTM are constrained by precise electroweak data [138, 47]. These restrictions favour a spectrum in which the mass difference between $H^+$ and $H^{++}$ is a few hundred GeV and $H^{++}$ is the lightest of the exotic bosons. In addition to favouring $H^{++}$ decays into $W^+W^+$ over same-sign di-leptons, the preferred triplet vacuum expectation value is a few GeV.

## 4.3 The Georgi-Machacek Model

By considering the SM doublet written as a (2,2) under $SU(2)_L \times SU(2)_R$ in Equation 2.41, it is obvious that the next simplest custodial symmetric construction transforms as a (3,3) [139, 140]. The Georgi-Machacek model directly tackles the $\rho$ parameter limitation by naturally incorporating custodial symmetry into it's setup, which consists of the SM doublet plus a new scalar transforming as a (3,3) under this symmetry group. However, it was suggested that significant adjustments to $\rho = 1$ are produced at one-loop [141], necessitating substantial fine-tuning to maintain agreement with EW accuracy

measurements. A complex electroweak triplet coupled with a real triplet is represented by these nine real degrees of freedom, and the scalar potential must be invariant under $SU(2)_R$. They transform as $1 \oplus 3 \oplus 5$ under the custodial $SU(2)_V$, with a CP-even neutral scalar in the custodial singlet, a CP-odd neutral scalar in the custodial triplet, and another CP-even neutral scalar in the custodial quintet.

The new fields can be written as

$$\Xi = \begin{pmatrix} \chi_3^* & \xi_1 & \chi_1 \\ -\chi_2^* & \xi_2 & \chi_2 \\ \chi_1^* & -\xi_1^* & \chi_3 \end{pmatrix}, \tag{4.11}$$

with $\xi_2$ being a real scalar while the rest are complex. The scalar potential can thus be written as

$$\begin{aligned} V = &- \mu_\Phi^2 \,\mathrm{Tr}\{\Phi^\dagger \Phi\} - \mu_\Xi^2 \,\mathrm{Tr}\{\Xi^\dagger \Xi\} + \mu_1 \,\mathrm{Tr}\{\Phi^\dagger T^a \Phi T^b\}(P^\dagger \Xi P)_{ab} \\ &+ \mu_2 \,\mathrm{Tr}\{\Xi^\dagger T^a \Xi T^b\}(P^\dagger \Xi P)_{ab} + \lambda_1 \langle \Phi^\dagger \Phi \rangle^2 + \lambda_2 \,\mathrm{Tr}\{\Xi^\dagger \Xi\}^2 \\ &+ \lambda_3 \,\mathrm{Tr}\{(\Xi^\dagger \Xi)^2\} + \lambda_4 \,\mathrm{Tr}\{\Phi^\dagger \Phi\} \,\mathrm{Tr}\{\Xi^\dagger \Xi\} + \lambda_5 \,\mathrm{Tr}\{\Phi^\dagger T^a \Phi T^b\} \,\mathrm{Tr}\{\Xi^\dagger T_a \Xi T_b\}, \end{aligned} \tag{4.12}$$

where the parameters are all real, $T_a$ acts as the $3 \times 3$ representation of the $SU(2)$ generators on the triplet, and we define

$$P = \frac{1}{\sqrt{2}} \begin{pmatrix} -1 & i & 0 \\ 0 & 0 & \sqrt{2} \\ 1 & i & 0 \end{pmatrix}. \tag{4.13}$$

The triplet vacuum expectation value is generated by the $\mu_1$ term such that the electroweak symmetry braking is accomplished by the scale

$$v^2 = v_\Phi^2 + 8 v_\Xi^2, \tag{4.14}$$

and after symmetry breaking we are left with an custodial quintet $H_5 = (H_5^{++}, H_5^+, H_5^0, H_5^-, H_5^{--})$ with mass $m_5$, a triplet $H_3 = (H_3^+, H_3^0, H_3^-)$ with mass $m_3$, and two singlets, $H_1$ with mass $m_1$, and $h$ to be identified with the measured 125GeV Higgs boson.

It is important to recognize that the GM triplets alone are adequate to account for

electroweak symmetry breaking and the presence of a 125 GeV neutral boson, along with a custodial triplet of Goldstone bosons. The complex doublet field in the GM framework is necessary to produce fermion masses through the conventional dimension four Yukawa couplings. This leads to the inquiry of whether it's possible to eliminate the chance that the 125 GeV boson is the neutral component of a custodial quintet instead of a custodial singlet, without referencing decays to fermions. A definitive answer is obtained by noting that the ratio of the branching fractions to $W$ versus $Z$ bosons is entirely dictated by the custodial symmetry characteristics of the boson. For a custodial quintet, the predicted ratio of the signal strength to $WW$ compared to that to $ZZ$ is expected to be $1/4$ of a SM Higgs boson [139, 140], and therefore it has already been excluded by the experiments.

Another noteworthy general characteristic of Higgs triplet models is that, following mixing, the SM-like neutral boson may exhibit stronger couplings to $WW$ and $ZZ$ than the SM predicts [142, 143]. This differs from scenarios involving additional doublets and singlets, which tend to decrease the $WW$ and $ZZ$ couplings compared to the SM. This highlights that LHC Higgs data cannot derive model-independent coupling strengths for the Higgs boson [118].

Due to the inherent custodial symmetry, the triplet vacuum expectation value in the GM model may be significantly larger than the doublet's. The custodial singlet neutral boson from the triplet interacts with the neutral boson from the doublet. Two intriguing special scenarios are the triplet expectation value being minimal and the 125 GeV boson resembling the SM with only slight deviations, and the 125 GeV boson primarily acts as the custodial singlet neutral boson derived from the electroweak triplets. The behaviour of the singly-charged and doubly-charged bosons resembles that of the HTM. The limitations on the GM model from precise electroweak data, LEP data, and present LHC data are outlined in [144].

# Chapter 5

# Cosmology of the Electroweak Phase Transition

The modern view on standard cosmology, the Lambda Cold Dark Matter Model (ΛCDM), predicts an Electroweak Phase Transition (EWPT) to have happened at a temperature $T \sim 300GeV$, or a time $t \sim 10^{-11}s$ after the Big Bang [145]. This phase transition is responsible for the spontaneous symmetry breaking of the Electroweak Gauge groups into electromagnetism, $SU(2)_L \times U(1)_Y \rightarrow U(1)_{EM}$, and generating the masses of the SM fermions and gauge bosons. Further, it is connected to various cosmological processes, namely baryogenesis, gravitational waves, and primordial black holes. The purpose of this chapter is to review the main concepts related to this phenomena. In Section 5.1 we give motivation for the topic by discussing the baryon asymmetry of the universe, and how can this problem be overcome by baryogenesis mechanisms. In Section 5.2 we review one of the most prominent methods of baryogenesis, electroweak baryogenesis, and why first order phase transitions play a crucial role in it. In Section 5.3 we describe the sphaleron solution to the electroweak field equations and how it can be used to generate baryon number. In Section 5.4 we explain how a first order phase transition takes place through the nucleation of bubble of the broken vacuum, and define the completion condition. In Section 5.5 we discuss the sphaleron decoupling condition necessary for successful electroweak baryogenesis. We call a strongly first order phase transition to one satisfying this condition. Finally, Sections 5.6 and 5.7 discuss the generation of gravitational waves and formation of primordial black holes from a strongly first order electroweak phase transition, respectively.

## 5.1 The Baryon Asymmetry of the Universe

On of the big questions in both modern cosmology and particle phenomenology is the large value observed of the Baryon Asymmetry of the Universe. The ratio of the numbers of baryon per photon in the universe can be measured from two sources: the Cosmic Microwave Background (CMB), whose current observed value is [14]

$$\frac{n_b}{n_\gamma} = (6.12 \pm 0.04) \times 10^{-10} \qquad \text{(CMB)}, \tag{5.1}$$

and the abundances of light elements from the Big Bang Nucleosynthesis (BBN), whose current observed value is [14]

$$\frac{n_b}{n_\gamma} = (6.040 \pm 0.118) \times 10^{-10} \qquad \text{(BBN)}. \tag{5.2}$$

In order to understand why this observed values are incompatible with the current theoretical framework, we note that a universe, at a temperature below 1GeV, and satisfying the initial condition

$$\frac{n_b}{n_\gamma} = 0, \tag{5.3}$$

develops baryon $n_b$ and anti-baryon $n_{\bar{b}}$ number densities according to the expression [146]

$$\frac{n_b}{n_\gamma} \simeq \frac{n_{\bar{b}}}{n_\gamma} \simeq \left(\frac{m_p}{T}\right)^{\frac{3}{2}} e^{-\frac{m_p}{T}}, \tag{5.4}$$

with $m_p$ the mass of the proton. The nucleons and anti-nucleons will decouple at a temperature of around 20MeV, by the time which the number densities are expected to take the following values [146]

$$\frac{n_b}{n_\gamma} \simeq \frac{n_{\bar{b}}}{n_\gamma} \simeq 10^{-18}, \tag{5.5}$$

which is many orders of magnitude smaller than the observed value. This is one of the big mysteries plaguing modern cosmology and particle physics communities.

To solve this issue, various mechanisms have been introduced to generate the ob-

served baryon number. In order to do so successfully, a mechanism must satisfy the three Sakharov conditions. These conditions are:

- Violation of baryon number;
- Violation of both C and CP;
- Departure from thermal equilibrium.

The first of these conditions, violation of baryon number, is trivially needed to generate baryons and anti-baryons in an unequal amount. The second condition needs a bit more reasoning to understand. Imagine a baryon generating process in a C conserving model. By C conservation the C conjugate process will have equal rate and cancel the net baryon number. In the same way, if we have CP conservation instead, the CP conjugate process would generate anti-baryons with opposite parity in an equal amount, once again cancelling the the net baryon number. This is why violation of both C and CP is required. Finally, the third condition is necessary since, according to statistical mechanics, a system in thermal equilibrium has no arrow of time, and all processes occur at the same rate as the opposite processes. This means that even with the inclusion of baryon number, C, or CP, violation processes, a system in thermal equilibrium will not be able, in practice, to generate net violation. This is why departure from thermal equilibrium is required.

A variety of baryogenesis mechanisms have been proposed over the decades. These include scenarios like leptogenesis [147], the Affleck-Dine mechanism [148], spontaneous baryogenesis [149], inflationary baryogenesis [150], mesogenesis [151], GUT baryogenesis [152], gravitational baryogenesis [153], and string baryogenesis [154]. In this work we focus on a mechanism known as Electroweak Baryogenesis, which is the topic of discussion of the next section.

## 5.2 Electroweak Baryogenesis

Electroweak Baryogenesis presents itself as one of the most promising baryogenesis models [155, 156, 157, 158, 159, 160, 161, 162, 163, 164, 165, 58, 166, 167, 168]. Since this mechanism takes place at the electroweak scale, many extended Higgs models can be used for this purpose. Also due to taking place at this scale, it will

be one of the best baryogenesis for testing at future colliders sensitive to Higgs precision physics. Finally, space focused experiments, like gravitational wave observers, will become precise enough in the future to test the universe back to the time of the electroweak scale. Since most other baryogenesis mechanisms happen at higher energy scales, Electroweak Baryogenesis is the most exiting from both theoretical and experimental points of view.

As expected for a baryogenesis mechanism, electroweak baryogenesis includes an environment that satisfies the Sakharok conditions. These are obeyed as follows [51]:

- Violation of baryon number: Sphaleron process;
- Violation of both C and CP: Extended scalar sectors;
- Departure from thermal equilibrium: First order phase transition.

The sphaleron is a saddle point solution in non-abelian gauge theories [52, 53]. The sphaleron process occurs when the fields transition between two vacuum states, through a topologically non-trivial path with non-zero winding number, that passes the sphaleron solution. In the case of the electroweak theory, this non-trivial path winds over the $SU(2)_L$ gauge space. This leads to violation of baryon number through the chiral anomaly [169, 170]. The C and CP violation can be easily achieved through the inclusion of CP violating terms in extended Higgs models. Finally, the occurrence of a first order electroweak phase transition leads to departure from thermal equilibrium, serving as a catalyst for the sphaleron process to occur and produce net baryon number violation. In the next few sections, the processes involved in this phase transition will be explained.

The dynamics of the electroweak phase transition within the SM was thoroughly studied in the 90's using lattice simulations [171, 172, 173, 174, 175, 176]. These simulations indicate that the transition is only first order for Higgs masses below approximately $72GeV$, other wise being crossover. This simulations were later further explored for the measured Higgs mass value of $125.1 \pm 0.3GeV$ [110] and confirmed to be crossover, taking place at a critical temperature of $159.5 \pm 1.5GeV$ [54]. Extensions of the Standard Model Higgs sector with more complex scalar potentials are thus needed for successful electroweak baryogenesis.

## 5.3 The Sphaleron and Baryon Number Violation

Within the electroweak theory, the sum between baryon and lepton number is not conserved. In fact, it's corresponding conserved current is given by

$$\partial_\mu J^\mu_{B+L} = \frac{n_g}{32\pi}\varepsilon^{\mu\nu\rho\sigma}(g^2 W^a_{\mu\nu}W^a_{\rho\sigma} + g'^2 B_{\mu\nu}B_{\rho\sigma}), \tag{5.6}$$

where $n_g$ is the number of fermion generations. Then, the variation of the baryon and lepton number sum can be calculated as

$$\Delta(B+L) = 2n_g \Delta N_{CS}, \tag{5.7}$$

with the variation in the Chern-Simons number is given by

$$\Delta N_{CS} = N_{CS}(t=+\infty) - N_{CS}(t=-\infty), \tag{5.8}$$

where the Chern-Simons number function can be defined as

$$N_{CS}(t) = \frac{g^2}{16\pi^2}\int d^3x \varepsilon^{ijk}\left(W^a_i \partial_j W^a_k + \frac{1}{3}\varepsilon_{abc}W^a_i W^b_j W^c_k\right). \tag{5.9}$$

When transitioning between degenerate vacua through a topologically non-trivial path, the variation in the Chern-Simons number will correspond to the winding number of that path through the $SU(2)_L$ space. This transition through topologically distinct vacua is called the sphaleron process, since it passes through the saddle point solution know as sphaleron. The simplest, but also the most likely, of such transitions, is the one with unity winding number, which leads to the variation

$$\Delta(B+L) = 2*3*1 = 6. \tag{5.10}$$

Thanks to the opposite combination $B-L$ being a conserved quantity with the Standard Model fermion structure, this directly leads to the baryon number variation

$$\Delta B = \Delta L = 3, \tag{5.11}$$

which demonstrates how the sphaleron process is capable of violating baryon number.

When transiting between topologically distinct vacua, the field must cross an energy barrier between the two, on top of which lies the sphaleron as a saddle point. At zero temperature, this transition can happened through quantum tunnelling, with a tunnelling rate given by [170]

$$\Gamma_{\text{sph}}^{\text{tun}} \propto e^{-8\pi^2/g^2}, \tag{5.12}$$

which is strongly suppressed by the $SU(2)_L$ coupling constant. Transition through quantum tunnelling is thus, in any practical terms, non-existent. This means this transition necessitates some borrowing of energy to aid in surpassing the barrier. At finite temperature, this energy borrowing can be given by temperature fluctuations, leading to the sphaleron process. The thermal transition rate is given by [177]

$$\Gamma_{\text{sph}}(T) \propto e^{-E_{\text{sph}}(T)/T}, \tag{5.13}$$

where the sphaleron energy is introduced as

$$E_{\text{sph}}(T) = \frac{4\pi v(T)}{g}\mathcal{E}(T), \tag{5.14}$$

and $v(T)$ is the value of the vacuum expectation value of the salar field as a function of temperature, and $\mathcal{E}(T)$ is a quantity that depends on the scalar potential of extended Higgs models, especially the triple Higgs self-coupling. The sphaleron energy determines the sphaleron transition rate, and as such, it is an important piece of information when dealing with extended Higgs sectors as tools for electroweak baryogenesis. Naturally, this value has been calculated for an extension on extended Higgs models [178, 179, 180, 181, 182, 183, 184, 185, 186, 195, 188, 189, 190].

## 5.4 Bubble Nucleation and the Completion Condition

Once the temperature of the universe drops to values in which the phase transition to the electroweak broken vacuum is probable enough, the transition, in the case of it being first order, will take place within nucleation bubbles throughout space. In order to calculate the nucleation rate of such bubbles, one must first find the classical bounce

solution by solving the equation

$$\frac{d^2\phi_b}{dr^2} + \frac{2}{r^2}\frac{d\phi_b}{dr} = \frac{\partial V_{\text{eff}}}{\partial \phi_b}, \qquad \left.\frac{d\phi_b}{dr}\right|_{r=0} = 0, \qquad \phi_b\big|_{r=+\infty} = 0, \tag{5.15}$$

from which one can calculate the three dimensional action of this solution

$$S_3(T) = \int d^3x \left[\frac{1}{2}\left(\vec{\nabla}\phi_b\right)^2 + V_{\text{eff}}(\phi_b, T)\right], \tag{5.16}$$

and finally, the nucleation rate is then given by [191]

$$\Gamma(T) \simeq T^4 \left(\frac{S_3(T)}{2\pi T}\right)^{3/2} e^{-S_3(T)/T}. \tag{5.17}$$

The characteristic nucleation temperature of the phase transition is defined as the temperature to which there is one bubble nucleating per Hubble volume. It can be obtained from the equation

$$\frac{\Gamma(T_n)}{H^4(T_n)} = 1, \tag{5.18}$$

where the Hubble parameter evolves with temperature as

$$H(T) \simeq 1.66 \frac{\sqrt{g_*(T)}T^2}{M_{\text{pl}}}, \tag{5.19}$$

with $M_{\text{pl}}$ the Planck mass, and $g_*(T)$ the effective degrees of freedom at a given temperature.

From observation, we know the whole observed universe has completed the electroweak phase transition, or there would be sections within where the Higgs expectation value is zero, and physical process would behave very differently. In order for the phase transition to be complete by today, we must have had at least a moment in time where there was one or more bubble nucleated per Hubble volume, or the universe expansion would have washed out the effects, and the phase transition wouldn't complete everywhere by today. This translates as the completion condition

$$\frac{\Gamma(T)}{H^4(T)} \geq 1, \tag{5.20}$$

being valid for at least some temperature.

## 5.5 Sphaleron Decoupling Condition

Once the bubbles of the broken vacuum nucleate, they start expanding. The expansion of the bubble walls interacts with the plasma creating a chiral asymmetry. The sphaleron process is then responsible for turning this chiral asymmetry into baryon asymmetry. As the bubble keeps expanding, the volume within the wall will be left with excess baryon number. This excess baryon number will quickly be washed out again by the sphaleron process, unless the sphaleron process quickly decouples. In such a case, the washout can be avoided, and we will be left with a net baryon number within the broken region. This excess baryon can explain in the observed baryon asymmetry of the universe.

The condition of avoiding the baryon number washout can be formulated as [160, 51, 177]

$$-\frac{1}{n_b}\frac{dn_b}{dt} < H(T), \tag{5.21}$$

which is often worked into the sphaleron energy as

$$\begin{aligned}\frac{E_{\text{sph}}(T)}{T} >& 38.849 + 7\ln\frac{v(T)}{T} - \ln\frac{T}{100\text{GeV}} \\ &- \frac{1}{2}\ln\frac{g_*}{106.75} + \ln\kappa(T) + \ln\left[2\mathcal{N}_{\text{tr}}(T)\mathcal{N}_{\text{rot}}(T)\frac{\omega_-(T)}{gv(T)}\right].\end{aligned} \tag{5.22}$$

The second line of this equation depends on various quantities that depend on the details of the extended scalar sectors, but this dependence is only logarithmic. It is thus considered a good approximation to use the Standard Model values at zero temperature of this quantities: the normalization factors for the translation and rotation zero modes $\mathcal{N}_{\text{tr}}(0) \simeq 7.6$ and $\mathcal{N}_{\text{rot}}(0) \simeq 11.2$ [192]; the negative mode frequency around the sphalerons $\omega_-(T) \simeq 0.81 g v(T)$[192]; and the fluctuation determinant $\kappa \simeq 0.12$ [193]. Using this approximation, and the formula for the sphleron energy, we get a condition

of the broken vacuum value at the transition temperature of [160, 194, 195]

$$\frac{v(T)}{T} > \frac{g}{4\pi\mathcal{E}(T)}\left[41.65 + 7\ln\frac{v(T)}{T} - \ln\frac{T}{100\text{GeV}}\right]. \tag{5.23}$$

This is known as the sphaleron decoupling condition. The quantity on the right hand side is often close to unity, as an example, the value is $1.1 \sim 1.2$ in the singlet extension of the Standard Model scalar sector [194]. Approximating this quantity by unity is a widely common approach. In our study using effective field theory, we utilize this approach. The sphaleron condition is thus stated as

$$\frac{v_n}{T_n} > 1, \tag{5.24}$$

where we use the nucleation temperature as the approximate temperature of the inside of the wall as it propagates, and $v_n$ is the broken vacuum value at such temperature.

## 5.6 Gravitational Waves from First Order Phase Transitions

First order phase transitions generate gravitational waves through different mechanisms. The study and detection of such gravitational waves is thus crucial in determining the nature and dynamics of the electroweak phase transition, and the viability of electroweak baryogenesis models. In this section we describe these generation mechanisms and the properties of said gravitational waves.

We define $T_*$ as the temperature of the thermal bath at the time $t_*$ when the gravitational waves are generated. By assuming there's no significant reheating taking place, we can consider this temperature equivalent to the nucleation temperature of the phase transition

$$T_* \approx T_n. \tag{5.25}$$

In order to define the nucleation temperature, consider the formula for the bubble nu-

cleation rate [210]

$$\Gamma(t) = A(t)e^{-S(t)}, \tag{5.26}$$

where $S$ is the Euclidean action of a critical bubble. We define $T_n$ as the temperature for which $\Gamma$ is large enough to give a probability of order one of one bubble nucleation within one horizon volume.

There are only a couple parameters that characterize the gravitational wave signal observed in cosmological phase transitions.

One of these parameters is the inverse time duration of the phase transition defined as

$$\beta \equiv -\frac{dS}{dt}\bigg|_{t=t_*} \simeq \frac{\dot{\Gamma}}{\Gamma}, \tag{5.27}$$

namely, being $H_*$ the Hubble parameter at $t_*$, the fraction $\beta/H_*$ directly correlates to the strength of the phase transition, and hence the strength of the gravitational wave signal. Since we consider $T_* \approx T_n$, we can calculate this fraction from

$$\frac{\beta}{H_*} = T_* \frac{dS}{dT}\bigg|_{T_*}. \tag{5.28}$$

The other key parameter is the ratio between the vacuum energy density released in the transition and the energy density of the radiation bath

$$\alpha \equiv \frac{\rho_{vac}}{\rho^*_{rad}}. \tag{5.29}$$

In this equation, we assume no significant reheating takes place, and

$$\rho^*_{rad} = \frac{g_*\pi^2 T_*^4}{30}, \tag{5.30}$$

with $g_*$ the number of relativistic degrees of freedom of the plasma at $t_*$.

In general, in a cosmological first order phase transition, there are three possible contributions to the generated gravitational wave spectrum:

- Collisions of bubble walls $\Omega_\phi$: Direct contribution from the scalar field itself;

- Sound waves $\Omega_{SW}$: From sound propagation after the collision but before the kinetic energy is dissipated to the plasma;

- Magnetohydrodynamics $\Omega_{MHD}$: At percolation the fully-ionized plasma generates Magnetohydrodynamic turbulence.

And the overall gravitational wave spectrum can be approximately calculated as

$$h^2\Omega_{GW} \simeq h^2\Omega_{\phi} + h^2\Omega_{SW} + h^2\Omega_{MHD}, \tag{5.31}$$

Which contribution to the spectrum is the most relevant depends on the dynamics of the phase transition. Namely, there are three different possible cases for the dynamics:

- Non-runaway bubbles: The bubbles reach a relativistic terminal velocity, and most of the signal comes from the bulk motion of the fluid. The bubble wall collision can thus be neglected;

- Runaway bubbles in plasma: The bubbles walls accelerate without bound and all the contributions must be considered;

- Runaway bubbles in vacuum: The plasma effects are negligible, and the walls accelerate without bound. The bubble collision is the only relevant contribution.

In the case of a strongly first order EWPT, the dynamics of non-runaway bubbles is generally assumed. Unfortunately, there is no known method to explicitly determine the terminal wall velocity. In simulations, it is used as an independent parameter taken to be close to the speed of light. In this work, we use $v_w = 0.95c$, as high values favour the production of detectable gravitational waves, in spite of the fact that it being difficult to assert the viability of electroweak baryogenesis in such scenario [196]. Further, the fraction between the magnetohydrodynamics contribution and the sound waves contribution is not exactly determined, but is considered to be small enough that we can neglect the former.

We thus consider only the sound wave contributions. The production of gravitational waves from acoustics is a very active area of research with many improvements to be expected in the future. For this work, it suffices us to use the numerical results in [197],

which can be reasonably fitted by [198]

$$h^2\Omega_{SW}(f) = 2.65 \times 10^{-6} \left(\frac{H_*}{\beta}\right) \left(\frac{k_v \alpha}{1+\alpha}\right)^2 \left(\frac{100}{g_*}\right)^{1/3} v_w S_{SW}(f), \tag{5.32}$$

which depends on the previous introduced quantities $\alpha$, $\beta$, $g_*$, $H_*$ and $v_w$. It also depends on the fraction of latent heat that is transformed into bulk motion of the fluid, which for a relativistic wall velocity is approximately

$$k_v \simeq \alpha(0.73 + 0.083\sqrt{\alpha} + \alpha)^{-1}, \tag{5.33}$$

and further complete expressions can be found in [199], which we use in this work. Finally, the frequency dependence is encapsulated in

$$S_{SW}(f) = \left(\frac{f}{f_{SW}}\right)^3 \left(\frac{7}{4 + 3(f/f_{SW})^2}\right)^{7/2}, \tag{5.34}$$

with the peak frequency being

$$f_{SW} = 1.9 \times 10^{-2} mHz \frac{1}{v_w} \left(\frac{\beta}{H_*}\right) \left(\frac{T_*}{100GeV}\right) \left(\frac{g_*}{100}\right)^{1/6}. \tag{5.35}$$

## 5.7 Primordial Black Hole Generation

As we have discussed, a SFOPT leads to a large density contrast between the inside and the outside of the nucleation bubbles. As this bubbles expand and collide, they start to fill the space in between them. Due to the probabilistic nature of the phase transition, is the probability is low enough, there will be a chance that a hole Hubble volume is left in the unbroken phase. If the contrast between the two regions is high enough, a region of over-density the size of at least a Hubble volume can collapse into a Primordial Black Hole (PBH) [74]. This situation is called a formation of primordial black holes through a delayed first order phase transition. Since the phase transition needs to be delayed enough, the threshold for primordial black hole generation is very close to the limit of the completion condition 5.20, in which case the transition is at risk of not happening at all in a Hubble volume and is never finished. This leaves only a very narrow parameter space available for primordial black hole generation by a

strongly first order electroweak phase transition, as is corroborated in this thesis.

The unbroken region inside the Hubble volume will have an energy density contrast to the broken region outside defined by

$$\delta \equiv \frac{|\rho_{in} - \rho_{out}|}{\rho_{out}}, \tag{5.36}$$

where $\rho_{in}$ and $\rho_{out}$ refer to the energy density inside and outside the delayed Hubble volume. If this exceeds the critical value $\delta_c = 0.45$ [200, 201], then there is formation of PBHs during the phase transition. Their mass is of the order of magnitude of the Hubble horizon mass at production time, which is roughly five orders bellow the solar mass for PBHs produced during the EWPT. The PBH fraction $f_{PBH}$ produced during the EWPT can calculated from the previous introduced quantities $\alpha$ and $\beta$, and it can be probed by current and future micro-lensing observations like the Subaru HSC, OGLE, PRIME, and the Roman Space Telescope. In this work, we apply the same treatment of Primordial Black Hole generation as in [76].

# Part II

# Exploring First Order EWPT using the naHEFT

# Chapter 6

# The nearly-aligned Higgs Effective Field Theory

Since the discovery of the Higgs boson, one of the main tasks of particle physics has been the investigation of it's properties as a probe of the underlying dynamics of electroweak symmetry breaking. While electroweak gauge interactions are typically constrained to order $\mathcal{O}(1\%)$ by electroweak precision measurements, the couplings between the Higgs boson and the Gauge bosons, as well as with the top quark, still allow deviations of $\mathcal{O}(10\%)$ to the SM predictions. Furthermore, the Higgs boson self couplings, and it's couplings with other fermions, allow for even larger deviations. Thus, it is natural to focus our attention on anomalous Higgs boson couplings, since these have high potential for large new physics effects, compared to other sectors.

For model independent studies, an appropriate effective field theory capable of describing anomalous Higgs boson couplings is necessary. The mostly used SMEFT is not suited to this end due to it's explicit approach on the Higgs boson gauge-variance. Allowing large new physics effects to dominate in the Higgs sector, by parametrizing the Higgs couplings in a gauge-invariant way, leads to the electroweak chiral Lagrangian as the low energy EFT, also known as the Higgs EFT (HEFT). This EFT approach is capable of accurately describing non-decoupling new physics effects, but it also has it's drawbacks. Namely, it is too wide of a framework, allowing for too much freedom in it's parameters, and thus not having any predictive power without explicit matching to UV models.

The nearly-aligned Higgs EFT (naHEFT) was introduced to tackle these issues. It

is build as a subset of the HEFT, under the constraint that the Higgs couplings are close to the SM at tree level. Thus, it manages to keep HEFT's freedom to accurately describe non-decoupling new physics, while at the same time being a more contained model with predictive power. Also, in the naHEFT, the deviation in the Higgs couplings come mainly from quantum effects, exactly the type needed to generate a strongly first order electroweak phase transition. It is thus the appropriate framework to study the dynamics of electroweak phase transition.

In this section we introduce the naHEFT. In Section 6.1 we provide the groundwork by introducing the chiral formalism of HEFT. In Section 6.2 we define the leading order Lagrangian of the naHEFT. In Section 6.3 we provide a treatment of finite temperature corrections within the naHEFT. Finally, in Section 7.2 we introduce the specific formalism and notations used in the rest of our work.

## 6.1 The electroweak chiral Lagrangian

The chiral formalism uses the Higgs form in Equation 2.41 and writes the fields as

$$(\tilde{\phi}, \phi) = \frac{1}{\sqrt{2}}(v + h)U, \tag{6.1}$$

so that it can be separated into two components. A gauge-variant non-linear representation of the Nambu-Goldstone bosons

$$U = \exp(i\tau_a \pi^a / v), \tag{6.2}$$

$$\pi^{\pm} = \frac{1}{\sqrt{2}}(\pi^1 \mp i\pi^2), \tag{6.3}$$

and the gauge-invariant Higgs boson $h$, allowing for the construction of a Lagrangian with anomalous Higgs boson couplings, as was noted beforehand.

Contrary to the SMEFT Lagrangian, the chiral Lagrangian is organized in power counting by chiral dimensions. This assigns 0 to each boson field, and 1 to each fermion bilinear, derivative, and gauge and Yukawa couplings, being equivalent to loop order with loop order $L$ equivalent to chiral dimension $2L + 2$. The tree level Lagrangian is thus of chiral dimension 2, while the one loop Lagrangian has chiral dimension 4.

## 6.2 The naHEFT leading order Lagrangian

The nearly-aligned Higgs Effective Field Theory (naHEFT) [103, 104] is an EFT framework that consistently characterizes non-decoupling effects of new physics. By assuming that the Higgs couplings are SM-like, and that BSM corrections come from quantum effects of new particles, the effective scalar potential can be described by a Coleman-Weinberg-like potential. In the naHEFT, the leading order effective Lagrangian is then given by

$$\mathcal{L}_2 = \mathcal{L}_{\text{SM}} + \mathcal{L}_{\text{BSM}}, \tag{6.4}$$

where $\mathcal{L}_{\text{SM}}$ is the SM Lagrangian, and $\mathcal{L}_{\text{BSM}}$ encapsulates the contributions from new physics and is defined as

$$\begin{aligned}\mathcal{L}_{\text{BSM}} =& \xi\Big[ -\frac{\kappa_0}{4}[\mathcal{M}^2(h)]^2 \ln\frac{\mathcal{M}^2(h)}{\mu^2} \\ &+ \frac{v^2}{2}\mathcal{F}(h)\,\text{Tr}\big\{D_\mu U^\dagger D^\mu U\big\} + \frac{1}{2}\mathcal{K}(h)\partial_\mu h\partial^\mu h \\ &- v\left(\bar{q}_L^i U\left[\mathcal{Y}_q^{ij}(h) + \hat{\mathcal{Y}}_q^{ij}(h)\tau^3\right]q_R^j + h.c.\right) \\ &- v\left(\bar{l}_L^i U\left[\mathcal{Y}_l^{ij}(h) + \hat{\mathcal{Y}}_l^{ij}(h)\tau^3\right]l_R^j + h.c.\right)\Big],\end{aligned} \tag{6.5}$$

The discovered Higgs field is represented here as a scalar $h$ singlet under the SM gauge groups. The Nambu-Goldstone bosons, on the other hand, are encapsulated under the non-linear representation:

$$U = \exp(i\tau_a\pi^a/v), \tag{6.6}$$

$$\pi^\pm = \frac{1}{\sqrt{2}}(\pi^1 \mp i\pi^2), \tag{6.7}$$

with the covariant derivative acting on $U$ as in Equation 2.44.

Regarding the constants present, $v$ is taken to be $246GeV$, $k_0$ represents the degrees of freedom of new physics, $\mu$ represents the renormalization scale, and $\xi = 1/(4\pi)^2$ is the loop expansion parameter. We are only interested at one loop and consequently will ignore all $\mathcal{O}(\xi^2)$ corrections.

The new physics is encoded in the various polynomials in $h$

$$\mathcal{M}^2(h) = \sum_{n=0} \frac{\mathcal{M}_n}{n!} \left(\frac{h}{v}\right)^n, \tag{6.8}$$

$$\mathcal{F}(h) = \sum_{n=1} \frac{f_n}{n!} \left(\frac{h}{v}\right)^n, \tag{6.9}$$

$$\mathcal{K}(h) = \sum_{n=1} \frac{k_n}{n!} \left(\frac{h}{v}\right)^n, \tag{6.10}$$

$$\mathcal{Y}_\psi^{ij}(h) = \sum_{n=1} \frac{y_{\psi,n}^{ij}}{n!} \left(\frac{h}{v}\right)^n, \tag{6.11}$$

$$\hat{\mathcal{Y}}_\psi^{ij}(h) = \sum_{n=1} \frac{\hat{y}_{\psi,n}^{ij}}{n!} \left(\frac{h}{v}\right)^n, \tag{6.12}$$

which satisfy $\mathcal{F}(0) = \mathcal{Y}_\psi^{ij}(0) = \hat{\mathcal{Y}}_\psi^{ij}(0) = 0$ in order to keep the parameters in the SM Lagrangian canonical.

The corrections in the kinetic term of the Higgs field affect its normalisation. The canonically normalised field is

$$\hat{h} = \int_0^h dh' \sqrt{1 + \xi \mathcal{K}(h')}, \tag{6.13}$$

$$h = \sum_{n=1}^{\infty} \frac{c_n}{n!} \hat{h}^n, \tag{6.14}$$

where

$$c_{n=1} = 1 - \frac{\xi}{2} k_0 + \mathcal{O}(\xi^2), \tag{6.15}$$

$$c_{n>1} = -\frac{\xi}{2} \frac{k_{n-1}}{v^{n-1}} + \mathcal{O}(\xi^2). \tag{6.16}$$

The part pertaining to the Goldstone bosons can be written as

$$\mathcal{L}_{NG} = \frac{v^2}{4} \left(1 + 2\frac{h}{v} + \frac{h^2}{v^2} + \xi \mathcal{F}(h)\right) \mathrm{Tr}\left[D_\mu U^\dagger D^\mu U\right], \tag{6.17}$$

$$= \frac{v^2}{4} \left(1 + 2\kappa_V \frac{\hat{h}}{v} + \kappa_{VV} \frac{\hat{h}^2}{v^2} + \mathcal{O}(\hat{h}^3)\right) \mathrm{Tr}\left[D_\mu U^\dagger D^\mu U\right], \tag{6.18}$$

where we introduced the couplings

$$\kappa_V = c_1 \left(1 + \frac{\xi}{2} f_1\right), \tag{6.19}$$

$$\kappa_{VV} = c_1^2 \left(1 + \frac{\xi}{2} f_2\right) + c_2 v \left(1 + \frac{\xi}{2} f_1\right). \tag{6.20}$$

And the Yukawa terms as

$$\mathcal{L}_Y = -\sum_{f=u,d,e} m_{fi} \left[\left(\delta^{ij} + \kappa_f^{ij} \frac{\hat{h}}{v} + \mathcal{O}(\hat{h}^2, \pi^2)\right)\right], \tag{6.21}$$

with the couplings

$$\kappa_u^{ij} = c_1 \left(\delta^{ij} + \xi(y_{q1}^{ij} + \hat{y}_{q1}^{ij}) \frac{v}{m_{ui}}\right), \tag{6.22}$$

$$\kappa_d^{ij} = c_1 \left(\delta^{ij} + \xi(y_{q1}^{ij} - \hat{y}_{q1}^{ij}) \frac{v}{m_{di}}\right), \tag{6.23}$$

$$\kappa_e^{ij} = c_1 \left(\delta^{ij} + \xi(y_{l1}^{ij} - \hat{y}_{l1}^{ij}) \frac{v}{m_{ei}}\right). \tag{6.24}$$

Finally, we wish to calculate the couplings of the Higgs potential from the n-point functions. Defining

$$d_n = -\frac{\partial^n \mathcal{L}_{naHEFT}}{\partial h^n}\Big|_{h=0}, \tag{6.25}$$

the stationary condition leads to

$$0 = c_1 d_1, \tag{6.26}$$

while the minimum condition reads

$$M_h^2 = c_1^2 d_2, \tag{6.27}$$

which are used to replace $m$ and $\lambda$ present in the SM part of the Higgs potential. The third and the fourth n-point functions give us the cubic and quartic self coupling of the

Higgs, which normalized by the SM value read

$$\kappa_3 = \frac{v}{3M_h^2}(c_1^3 d_3 + 3c_1 c_2 d_2), \tag{6.28}$$

$$\kappa_4 = \frac{v^2}{3M_h^2}(c_1^4 d_4 + 6c_1^2 c_2 d_3 + 4c_1 c_3 d_2 + 3c_2^2 d_2). \tag{6.29}$$

In this work, we consider the polynomials

$$\mathcal{M}^2(h) = (1-r)\Lambda^2 + r\Lambda^2\left(1+\frac{h}{v}\right)^2, \tag{6.30}$$

$$\mathcal{K}(h) = \frac{\kappa_0 \Lambda^2 r}{3v^2}\left[1-(1-r)\frac{\Lambda^2}{\mathcal{M}^2(h)}\right], \tag{6.31}$$

$$\mathcal{F}(h) = 0, \tag{6.32}$$

which come from assuming a number $\kappa_0$ of BSM scalars contributing significantly to the Higgs potential at one loop corrections, at a mass scale $\Lambda$, and with uniform non-decouplingness $r$.

In such a case, the relevant couplings are given by

$$\kappa_V = 1 - \kappa_0 \frac{\xi \Lambda^2 r^2}{6v^2}, \tag{6.33}$$

$$\kappa_{VV} = 1 - \kappa_0 \frac{\xi \Lambda^2 r^2}{6v^2}(3-2r), \tag{6.34}$$

$$\kappa_3 = 1 + \frac{4\xi\Lambda^4}{3v^2 M_h^2}\left[\kappa_0 r^3 - \kappa_0 \frac{M_h^2 r^2}{8\Lambda^2}(3-2r)\right], \tag{6.35}$$

$$\kappa_4 = 1 + \frac{16\xi\Lambda^4}{3v^2 M_h^2}\left[\kappa_0 r^3 \frac{3-r}{2} - \kappa_0 \frac{M_h^2 r^2}{16\Lambda^2}\frac{25-38r+16r^2}{3}\right]. \tag{6.36}$$

## 6.3 Finite Temperature Corrections

In order to study the dynamics of the EWPT transition, we must calculate the finite temperature corrections from new physics within our EFT formalism. This was done in [104] through a procedure in [202, 203, 204]. To that end, we first note that the BSM scalar potential

$$\mathcal{V}_{\text{BSM}}(h) = -\xi\frac{\kappa_0}{4}[\mathcal{M}^2(h)]^2 \ln\frac{\mathcal{M}^2(h)}{\mu^2}, \tag{6.37}$$

can be rewritten as

$$\mathcal{V}_{\text{BSM}}(h) = \frac{\kappa_0}{2} \int \frac{d^4 k_E}{(2\pi)^4} \ln[k_E^2 + \mathcal{M}^2(h)], \tag{6.38}$$

by ignoring the ultraviolet divergent and the constant terms that are irrelevant in this argument. We can then introduce the finite temperature corrections by performing the replacement

$$\int \frac{d^4 k_E}{(2\pi)^4} \ln[k_E^2 + \mathcal{M}^2(h)] \to T \sum_{n=-\infty}^{+\infty} \int \frac{d^3 k_E}{(2\pi)^3} \ln[\vec{k}_E^2 + w_n^2 + \mathcal{M}^2(h)], \tag{6.39}$$

where $T$ is the temperature and $w_n$ is the Matsubara frequency defined as

$$w_n = 2n\pi T, \tag{6.40}$$

for $k_0 > 0$, which is the case in our analysis. The finite temperature corrected potential can then be written as

$$\mathcal{V}_{\text{BSM}}(h, T) = \frac{\kappa_0}{2} T \sum_{n=-\infty}^{+\infty} \int \frac{d^3 k_E}{(2\pi)^3} \ln[\vec{k}_E^2 + w_n^2 + \mathcal{M}^2(h)]. \tag{6.41}$$

Further, we can decompose the above formula into a zero temperature part and a temperature dependent part as

$$\mathcal{V}_{\text{BSM}}(h, T) = \mathcal{V}_{\text{BSM}}(h) + \Delta\mathcal{V}_{\text{BSM,T}}(h, T), \tag{6.42}$$

with

$$\Delta\mathcal{V}_{\text{BSM,T}}(h, T) = 8\xi T^4 \kappa_0 J_{BSM}\left(\frac{\mathcal{M}^2(h)}{T^2}\right) \tag{6.43}$$

where a new function is introduced, whose definition is

$$J_{BSM}(x) = \int_0^\infty dk^2 k^2 \left(1 - e^{-\sqrt{k^2 - x}}\right). \tag{6.44}$$

This form for the finite temperature corrected potential is used for the evolution of the scalar vacuum during the EWPT.

## 6.4 Validity as an Effective Theory

The nearly aligned Higgs EFT validity has been tested and contrasted with the Standard Model EFT to great results [103, 104]. We now summarize these results.

In reference [103], the naHEFT is matched to a real scalar singlet model. The naHEFT Lagrangian is then written in terms of the SM electroweak doublet as

$$\mathcal{L}_{\text{naHEFT}} = \mathcal{L}_{SM} - \xi\frac{\kappa_0}{4}(M^2+\kappa_p|\Phi|^2)^2\left[\ln\frac{M^2}{\mu^2}+\sum_{n=1}^{\infty}\frac{(-1)^{n+1}}{n}\left(\frac{\kappa_p|\Phi|^2}{M^2}\right)^n\right] + \xi\frac{\kappa_0}{24}\frac{\kappa_p^2}{M^2}\sum_{n=0}^{\infty}\left(-\frac{\kappa_p|\Phi|^2}{M^2}\right)^n\partial_\mu|\Phi|^2\partial^\mu|\Phi|^2, \tag{6.45}$$

which is then truncated at canonical dimension 6 as

$$\mathcal{L}_{\text{naHEFT}}\big|_{\text{dim6}} = \mathcal{L}_{\text{SM}} - \frac{\xi}{2}\kappa_p\left[\kappa_0\left(\ln\frac{M^2}{\mu^2}+\frac{1}{2}\right)M^2|\Phi|^2+\kappa_0\left(\ln\frac{M^2}{\mu^2}+\frac{3}{2}\right)\kappa_p|\Phi|^4 + \kappa_0\frac{\kappa_p^2}{6M^2}|\Phi|^6-\kappa_2\frac{\kappa_p}{12M^2}\,\partial_\mu|\Phi|^2\,\partial^\mu|\Phi|^2\right] \tag{6.46}$$

so that it corresponds to the SMEFT. The evolution of the Higgs couplings $\kappa_V$ and $\kappa_3$ with the new physics scale for various values of the non-decouplingness is then compared for the calculations of the naHEFT, SMEFT, and the full UV theory. Their results are presented in Figure 6.1. The main takeaways from these plots is that both the naHEFT and the cut-off dim-6 are good at describing these couplings for small values of the non-decouplingness. For high values of the non-decouplingness, on the other hand, the dim-6 results start deviating considerably from the UV ones, while the naHEFT results remain remarkably accurate. This corroborates the affirmation that the naHEFT is the more appropriate formalism to accurately describe the non-decoupling effects from new physics.

In reference [104], the validity of the naHEFT is tested in the context of the study of the electroweak phase transition. Namely, the evolution of $v_n/T_n$ with the non-decouplingness is calculated. According to the sphaleron decoupling condition, if this quantity is above unity, the electroweak phase transition is a strongly first order phase transition. Their results are presented in Figure 6.2. The results for the naHEFT calculation are compared to the ones in the canonical dimension 6, 8, and 10

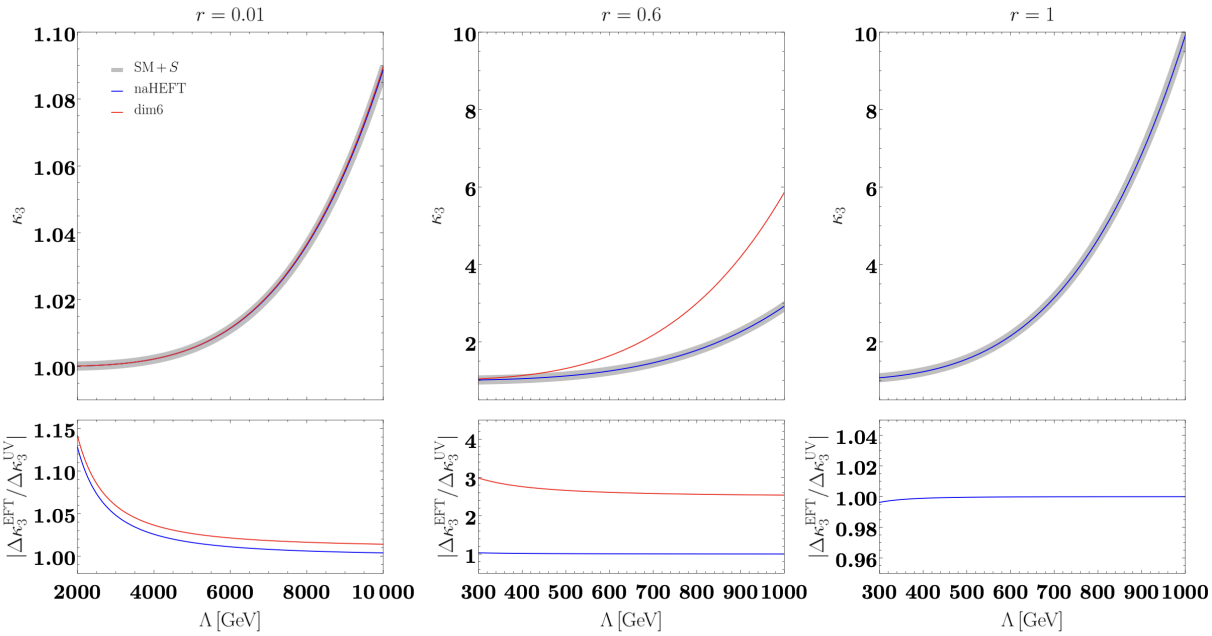



Figure 6.1: Figure taken from [103]. Shows the evolution of the Higgs triple self coupling with the cut-off scale of the respective EFT, for various values of the non-decouplingness $r = 0.01, 0.6, 1$. In blue is the naHEFT, red the dim-6 truncated theory, and in gray the UV calculation in the singlet scalar extension of the SM. Below are the ratio of the coupling variations of each EFT with the UV calculation. This figure motivates the use of the naHEFT to describe non-decoupling effects.

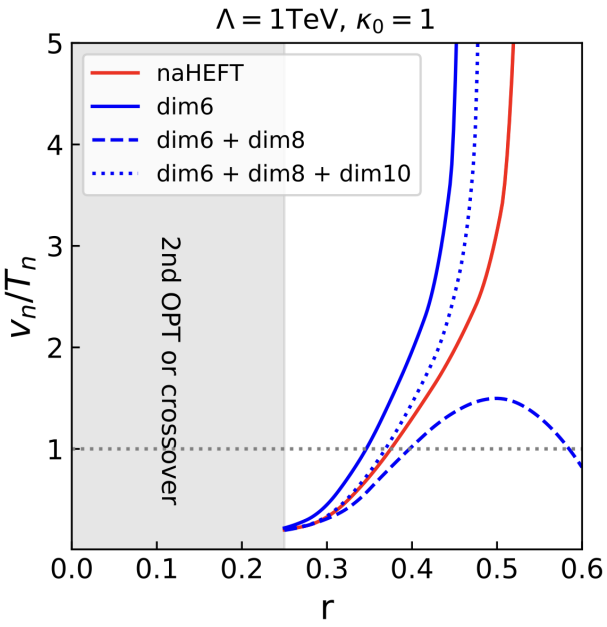



Figure 6.2: Figure taken from [104]. Shows the evolution of $v_n/T_n$ with the non-decouplingness in different effective theories, for a cut-off scale $\Lambda = 1\text{TeV}$ and number of degrees of freedom $\kappa_0 = 1$. In red is the naHEFT result, whine in blue filled, dashed, and dotted, is the dim-6, dim-8, and dim-10 truncated theories, respectively. For $v_n/T_n = 1$ the sphaleron decoupling condition is satisfied. When compared with UV calculation, the best value for $r$ satisfying sphaleron decoupling condition is the naHEFT result of $r \simeq 0.35$. This fiure motivates the use of naHEFT when studying the dynamics of the electroweak phase transition.

truncated effective theory. By looking at the plot, one can notice that for low values of the non-decouplingness, all the theories seem to match. One the non-decouplingness starts increasing, the truncated theories seem to deviate in different directions, while the naHEFT remains consistent in the middle of these. This shows once again that the naHEFT is the correct effective theory framework to study the dynamics of the electroweak phase transition, because this relies on the accurate description of non-decoupling effects.

# Chapter 7

# Loop induced decays in the naHEFT

The decay of the Higgs boson into two photons has been central in probing Standard Model phenomenology. In fact, it was the observation of an excess in the diphoton spectrum near 125GeV that provided one of the first and most compelling evidences for the existence of the Higgs boson itself [15, 16]. In spite of it's relatively small branching ratio, the Higgs to di-photon clean experimental signature make it one of the most powerful channels at the LHC.

One of the most unique features of the Higgs to di-photon decay is that it is a loop induced decay. This makes it a unique window into beyond the Standard Model physical degrees of freedom. In the context of the electroweak phase transition, within the new scalar degree of freedom that contribute to the strengthening of the Higgs triple self coupling and, consequently, the first order phase transition, the electrically charged degrees of freedom will also heavily influence the Higgs to di-photon decay. One of the main purposes of this thesis is to explore this correlation between the Higgs to di-photon and a first order electroweak phase transition, and how this channel can be used to probe the nature of the electroweak phase transition.

In this chapter we introduce for the first time the treatment of loop induced decays within the naHEFT formalism. Using the chiral formalism, loop induced decays, like the Higgs to di-photon and Higgs do $Z$-photon, appear only at chiral dimension 4. This terms are thus not included in any previous treatment of the naHEFT, which were focused on the leading order Lagrangian of chiral dimension 2. In Section 7.1 we introduce the terms of this sub-leading order Lagrangian relevant for these two loop induced decays. Then, in Section 7.2, we introduce the setup and notations used

in the analysis throughout the rest of this thesis. Finally, in Section 7.3, we study the behaviour of the $h\gamma\gamma$ effective interaction using our formalism, and compare with collider measurements.

## 7.1 Sub-leading order Lagrangian

Loop induced processes, like the $h \to \gamma\gamma$ and $h \to Z\gamma$, cannot be described with the leading order Lagrangian introduced previously. Their effects come from the sub-leading order Lagrangian

$$\begin{aligned}\mathcal{L}_4 = \xi\Big[&g'^2\mathcal{F}_B(h)\,\mathrm{Tr}\{B_{\mu\nu}B^{\mu\nu}\} + g^2\mathcal{F}_W(h)\,\mathrm{Tr}\{W_{\mu\nu}W^{\mu\nu}\} \\ &+gg'\mathcal{F}_{BW}(h)\,\mathrm{Tr}\big\{UB_{\mu\nu}U^\dagger W^{\mu\nu}\big\}\Big],\end{aligned} \tag{7.1}$$

where the polynomials can be written in the notation

$$\xi\mathcal{F}_B(h) = -\,a_{hBB}\frac{h}{v} + \mathcal{O}(h^2), \tag{7.2}$$

$$\xi\mathcal{F}_W(h) = -\,a_{hWW}\frac{h}{v} + \mathcal{O}(h^2), \tag{7.3}$$

$$\xi\mathcal{F}_{BW}(h) = -\,a_{hBW}\frac{h}{v} + \mathcal{O}(h^2). \tag{7.4}$$

Arranging this Lagrangian in terms of the physical gauge fields, we can derive the relevant terms

$$\mathcal{L}_4 = -\frac{1}{2}\frac{e^2}{v}a_{h\gamma\gamma}hF_{\mu\nu}F^{\mu\nu} - \frac{egc_W}{v}a_{hZ\gamma}hF_{\mu\nu}Z^{\mu\nu} + ..., \tag{7.5}$$

where

$$a_{h\gamma\gamma} = a_{hBB} + a_{hWW} - a_{hBW}, \tag{7.6}$$

$$a_{hZ\gamma} = \frac{1}{c_W^2}\left[-a_{hBB}s_W^2 + a_{hWW}c_W^2 - \frac{1}{2}a_{hBW}(c_W^2 - s_W^2)\right], \tag{7.7}$$

which are necessary for the loop induced decays $h \to \gamma\gamma$ and $h \to Z\gamma$.

Mirroring our treatment of the leading order Lagrangian, we assume form factors of

the form

$$\mathcal{F}_W(h) = \mathcal{F}_B(h) = \frac{b}{2} \ln \left[ \tilde{r} \left( 1 + \frac{h}{v} \right)^2 + 1 - \tilde{r} \right], \tag{7.8}$$

$$\mathcal{F}_{BW}(h) = 0, \tag{7.9}$$

where we again use the non-decouplingness $\tilde{r}$ of the particle contribution to this loop, and the new parameter $b$ representing the BSM charged particles in the loop which for a model with singly and doubly charged particles is $b = \frac{n_+ + 4n_{++}}{3}$.

We can now calculate the Higgs di-photon effective interaction coupling as

$$\kappa_{\gamma\gamma}^2 = \frac{\Gamma_{h\to\gamma\gamma}^{\text{EFT}}}{\Gamma_{h\to\gamma\gamma}^{\text{SM}}} \simeq \left| \kappa_V - \frac{br}{F_{\text{SM}}} \right|^2. \tag{7.10}$$

## 7.2 Parameter Setup

As a result of the discussion in the previous sections, the main new physics parameters affecting the discussed observables are:

- $\Lambda$ : the energy scale of the scalars contributing significantly to the Higgs self-coupling and Higgs di-photon coupling;
- $r$ : the non-decouplingness of those same scalar particles;
- $\kappa_0$ : the number of degree of freedom of those particles, subdivided as $\kappa_0 = n_0 + 2n_+ + 2n_{++}$:
  - $n_0$ : number of neutral scalars;
  - $n_+$ : number of singly charged scalars;
  - $n_{++}$ : number of doubly charged scalars.

where we made the natural assumption that those same charged scalars contribute to the BSM correction to the loop decays with the same non-decouplingness, i.e. $\tilde{r} = r$.

In order to study the EWPT using this formalism, we let the first two parameters run free in our analysis, while choosing specific benchmark models for the values of the number of scalar particles contributing to the Higgs self-coupling. We list the benchmark values that were considered with the respective example of BSM model:

- Singly charged singlet: $(n_0,\ n_+,\ n_{++}) = (0, 1, 0)$
- Real triplet: $(n_0,\ n_+,\ n_{++}) = (1, 1, 0)$
- 2HDM: $(n_0,\ n_+,\ n_{++}) = (2, 1, 0)$
- Doubly charged singlet: $(n_0,\ n_+,\ n_{++}) = (0, 0, 1)$
- Complex triplet: $(n_0,\ n_+,\ n_{++}) = (2, 1, 1)$
- Georgi-Machacek: $(n_0,\ n_+,\ n_{++}) = (3, 2, 1)$

## 7.3 The effective $h\gamma\gamma$ interaction

In Figure 7.1, the evolution of $\kappa_{\gamma\gamma}$ with the non-decouplingness $r$ is shown. The constraints from the ATLAS and CMS are shown in Figure 7.1 as orange and green regions, respectively. The constraint on $\kappa_{\gamma\gamma}$ from the CMS results is $\kappa_{\gamma\gamma} = 1.10 \pm 0.16$ at $95\,\%$ confidence level [61]. For the ATLAS, the current constraint is $\kappa_{\gamma\gamma} = 1.02 \pm 0.11$ at $95\,\%$ confidence level, where it is assumed that the $hgg$ coupling is the same as the SM prediction [205]. Figure 7.1 indicates that large values of $\Lambda$ lead to large deviations in $\kappa_{\gamma\gamma}$. The first three figures, which only vary in the number of neutral particles $n_0$, show that the presence of neutral particles can lead to larger deviations in the Higgs di-photon effective coupling. This effect is encoded within the $\kappa_V$ term present in $\kappa_{\gamma\gamma}$. The remaining three figures imply that extended Higgs models with doubly charged scalar bosons are strongly constrained by $h\gamma\gamma$ coupling measurements. These results are consistent with the previous results in the specific renormalizable models [45, 46, 206, 207]. The result in Figure 7.1 indicates that the value of $\kappa_{\gamma\gamma}$ becomes SM-like when one takes the decoupling limit $r \sim 0$. This behaviour is consistent with the decoupling theorem [208]. On the other hand, large values for the non-decouplingness can be constrained by $h\gamma\gamma$ coupling measurements at current and future collider experiments.

In Figure 7.2, the correlation between $\kappa_3$ and $\kappa_{\gamma\gamma}$ is shown. This figure indicates that high values of the scale of new physics lead to small values for $\kappa_{\gamma\gamma}$ and large values for $\kappa_3$. We note that the $h\gamma\gamma$ coupling may be measured with about $0.5\%$ accuracy in the future by combining HL-LHC results with those from the ILC running at $\sqrt{s} = 250\text{GeV}$

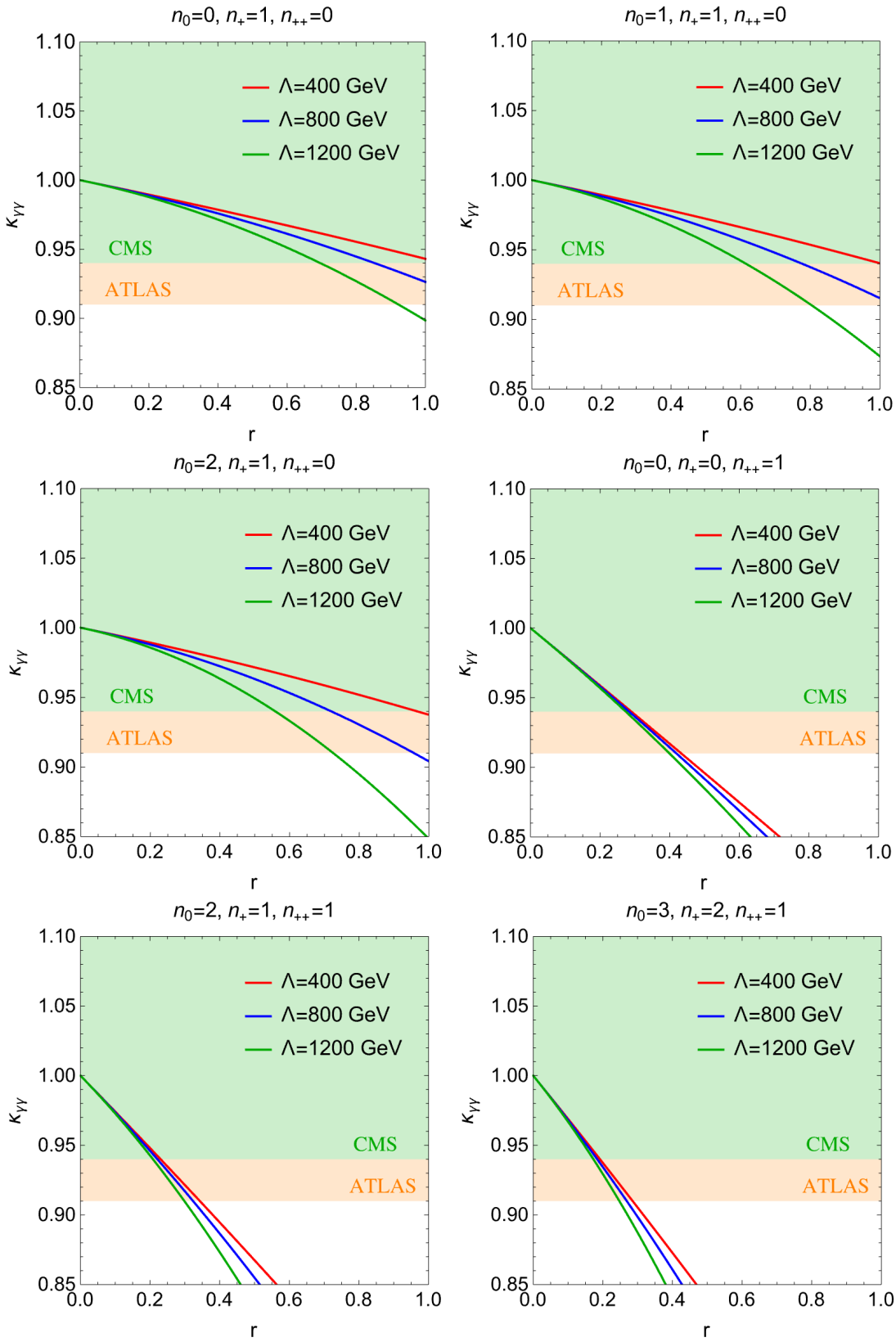



Figure 7.1: The relation between $\kappa_{\gamma\gamma}$ and the non-decouplingness $r$. The parameter $\Lambda$ corresponds to the mass scale of new particles. The green and orange regions indicate the current allowed regions from the CMS result [61] and the ATLAS result [205], respectively. The parameters $n_0$, $n_+$ and $n_{++}$ are the degrees of freedom of neutral, singly charged and doubly charged particles, respectively.

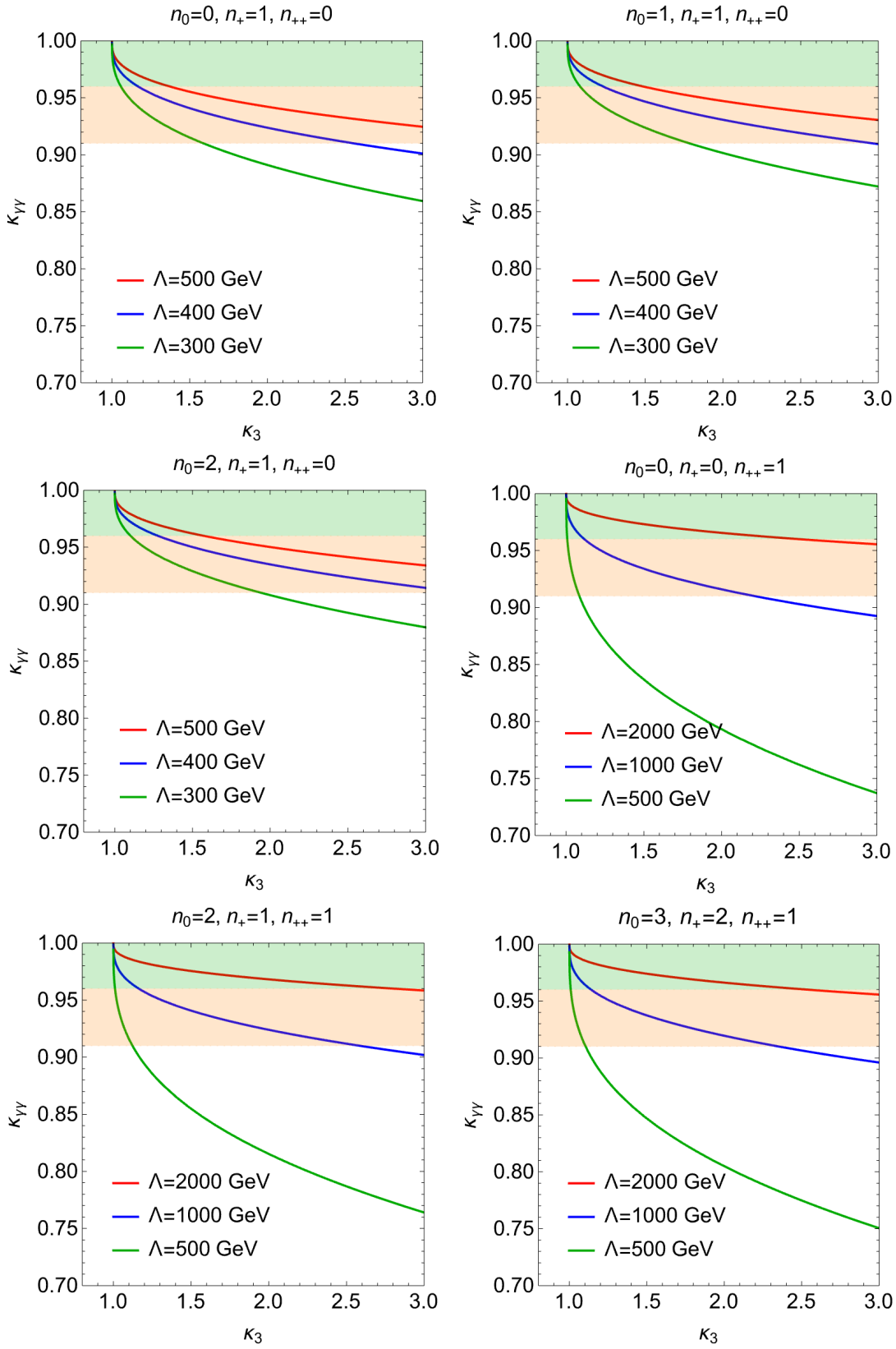



Figure 7.2: Correlation between $\kappa_3$ and $\kappa_{\gamma\gamma}$ for each benchmark point. The parameter $\Lambda$ corresponds to the mass scale of new particles. The green and orange regions indicate the current allowed regions from the CMS result [61] and the ATLAS result [205], respectively.

with 68% confidence level [64]. As we discussed previously and confirm later, the sphaleron decoupling condition in Equation (5.24) requires a large deviation in the $hhh$ coupling. Therefore, the new physics scale should be large to satisfy the condition in Equation (5.24) and precise $h\gamma\gamma$ measurement results simultaneously.

# Chapter 8

# Analysis of Electroweak Phase Transition Signatures

The advent of a strongly first order electroweak phase transition is crucial for the generation of baryon asymmetry through the method of electroweak baryogenesis. While the theoretical setup and conditions for this have been thoroughly discussed in previous chapters, the viability of this mechanism ultimately requires connection to experimental signatures. This chapter serves as comprehensive analysis of various phenomenological probes of the electroweak phase transition.

In Section 8.1 we discuss how the analysis of the gravitational wave spectra and their detectability at the future interferometers LISA and DECIGO is performed. Then, in Section 8.2 we perform a full parameter scan for various benchmark models. We include theoretical constraints on a first order phase transition, like the completion condition and the sphaleron decoupling condition, and unitarity bounds. We include experimental detectability of gravitational waves at LISA and DECIGO, and of primordial black holes by various experiments. We also study how measurements of triple Higgs coupling, and the Higgs di-photon interaction, can help to decipher this parameter space.

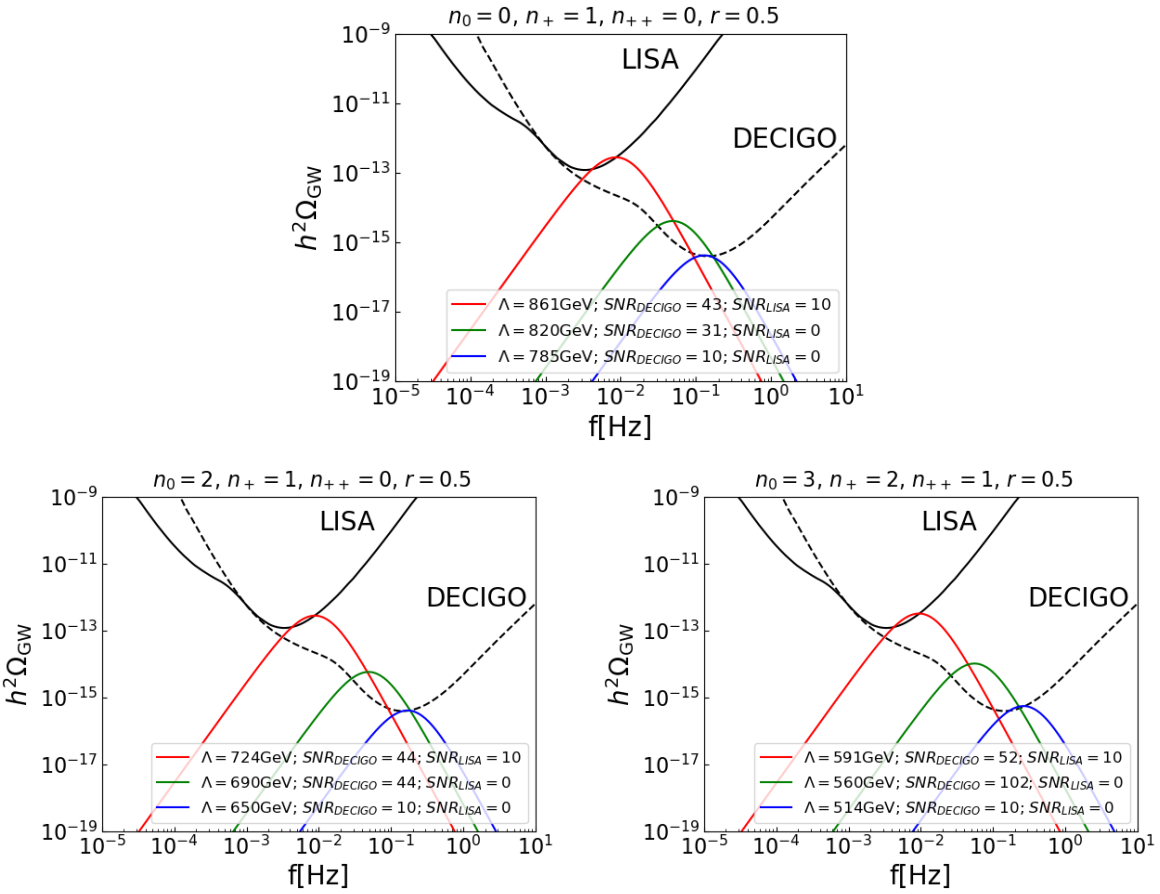



Figure 8.1: GW spectra in the naHEFT for each benchmark point. The parameters $r$ and $\Lambda$ correspond to the non-decouplingness and the mass scale of new particles, respectively. The black solid and dashed lines are the peak integrated sensitivity curves for LISA and DECIGO, respectively [209]. If the peak of GW spectra is higher than the sensitivity curves, the detectability criterion SNR $> 10$ is satisfied.

## 8.1 Gravitational Wave Spectra

To discuss the detectability of the GWs, we evaluate the signal-to-noise ratio [198]

$$\mathrm{SNR} = \sqrt{\mathcal{T} \int_{f_{\mathrm{min}}}^{f_{\mathrm{max}}} df \left[ \frac{h^2\Omega_{\mathrm{GW}}(f)}{h^2\Omega_{\mathrm{sens}}(f)} \right]^2}, \tag{8.1}$$

where $h^2\Omega_{\mathrm{sens}}(f)$ and $\mathcal{T}$ are the sensitivity and the observation duration of future space-based interferometers like LISA [66] and DECIGO [67]. We take $\mathcal{T} = 1.26 \times 10^8$ s for all GW experiments. In this work, we consider that the GWs can be detected if the condition SNR $> 10$ is satisfied [209].

In Figure 8.1, the prediction on GW spectra in three benchmark points is shown.

The black solid and dashed lines are the peak integrated sensitivity curves of LISA and DECIGO, respectively [209]. If the peak position of GW spectra is higher than the sensitivity curves, the detectability criterion SNR $> 10$ is satisfied. Therefore, the red benchmark points can be tested by LISA. On the other hand, all the benchmark points shown can be explored by DECIGO. We here assume that the wall velocity is $95\%$ of the speed of light.

## 8.2 Parameter Scan

In Figure 8.2, the parameter region, which can be explored by $h\gamma\gamma$, $hhh$ and GW observations, is shown for each model. The coloured solid lines are the contours of the $h\gamma\gamma$ coupling. The black dotted lines are contours of the deviation in the $hhh$ coupling. The upper-right white region does not satisfy the completion condition, and the phase transition never completes 5.20. In the lower-left white region, the sphaleron decoupling condition 5.24 is not satisfied, and the phase transition is not strongly first order. The black solid line indicates constraints from the perturbative unitarity bound. We here take into account the unitarity bound in the SM with $N$ scalar singlet fields as an example [59]. The red region can be explored by current and future microlensing observations such as Subaru HSC [84], OGLE [85], PRIME [86] and Roman telescope [87]. This PBH region is the same as the literature [76]. The green and dark green regions indicate the parameter region that can be tested at DECIGO and LISA, respectively. In the blue region, the first-order EWPT can be tested only by collider experiments. Figure 8.2 indicates that a criterion of the strongly first-order EWPT can be obtained in terms of the $hhh$ coupling by using precise $h\gamma\gamma$ coupling measurements and the condition (5.24). Also, Figure 8.2 indicates that the large deviation in the $h\gamma\gamma$ coupling is required to realize a strongly first-order EWPT in models with doubly charged particles.

In Figure 8.3, contours of the $hVV$ coupling are shown instead of the $hhh$ coupling contours in the same setup as Figure 8.2. We note that the $hVV$ coupling may be measured with $0.5\%$ accuracy by combining the HL-LHC with the ILC with $\sqrt{s} = 250$GeV at $68\%$ confidence level [64]. Therefore, the parameter region satisfying $\Lambda < 1$TeV and Equation (5.24) can be explored by future precise $hVV$ coupling measurements if $n_0 \geq 2$.

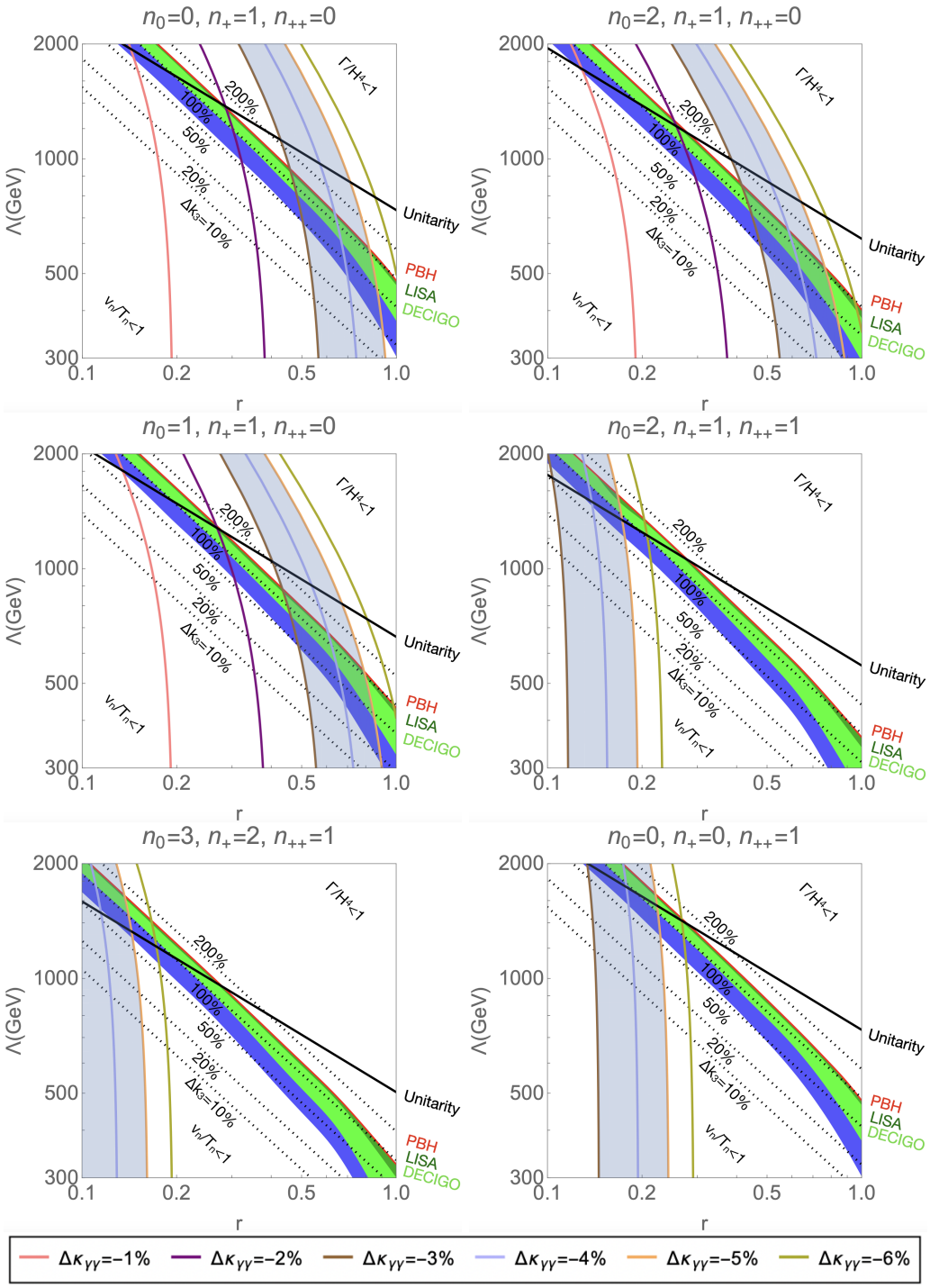



Figure 8.2: Parameter region explored by $h\gamma\gamma$, $hhh$ and GW observations. The parameters $r$ and $\Lambda$ correspond to the non-decouplingness and the mass scale of new particles, respectively. The values of $\Delta\kappa_3$ and $\Delta\kappa_{\gamma\gamma}$ are defined by $\Delta\kappa_3 \equiv \kappa_3 - 1$ and $\Delta\kappa_{\gamma\gamma} \equiv \kappa_{\gamma\gamma} - 1$, respectively. The upper right white region is constrained by the perturbative unitarity bound or the completion condition of the phase transition. In the lower-left white region, the condition (5.24) is not satisfied. The red region can be explored by Subaru HSC, OGLE, PRIME and Roman telescope. The green and dark green regions are explored by DECIGO and LISA, respectively. In the blue region, the first-order EWPT can be basically tested only by collider experiments.

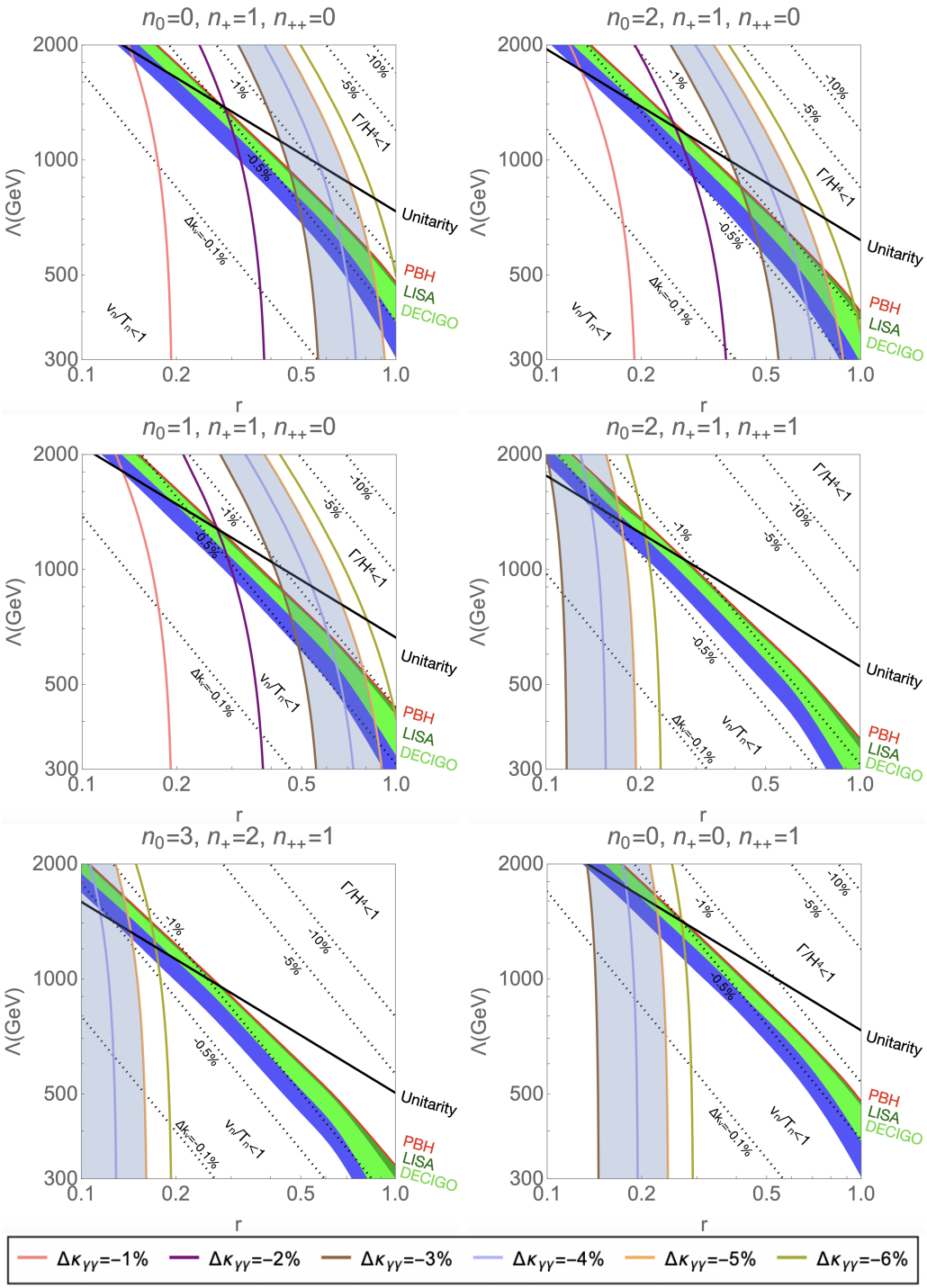



Figure 8.3: Parameter region explored by $h\gamma\gamma$, $hVV$ and GW observations. The parameters $r$ and $\Lambda$ correspond to the non-decouplingness and the mass scale of new particles, respectively. The black dotted lines are the contours of $hVV$ coupling. The value of $\Delta\kappa_V$ is defined by $\Delta\kappa_V \equiv \kappa_V - 1$. The definitions of other lines and regions are the same in Figure 8.2.

# Chapter 9

# Further Discussions

Here further motivation of the importance of $h \to \gamma\gamma$ measurements in determining the nature of the EWPT is provided. In Section 9.1 we discuss in detail the interplay between these signatures, and in specific, discuss how the Higgs di-photon interaction can come to play a unique role in deciphering the structure of the scalar sector when contrasted with the rest. In Section 9.2 we discuss in which scenarios the future colliders will be able to conclusively determine if a specific Higgs structure predicts a strongly first order electroweak phase transition or not, by considering hypothetical measurements at colliders, and how the Higgs di-photon measurements will be necessary to conclusively determine the nature of the phase transition in most cases.

## 9.1 Coupling Predictions

In Table 9.1, it is summarized that the prediction on the $hhh$ coupling to realize the strongly first-order EWPT when $\Delta\kappa_{\gamma\gamma} = -4\% \pm 1\%$ for each model. In the second column labelled "Required by $\frac{v_n}{T_n} > 1$ & $\frac{\Gamma}{H^4} > 1$", it is shown that the predictions on the $hhh$ coupling where the EWPT *can be* strongly first-order. The lower and upper bounds on $\Delta\kappa_3$ are determined by sphaleron decoupling condition and the completion condition of the phase transition, respectively. For the third column labelled "Conservative bound", the predictions on the $hhh$ coupling where the EWPT *is* strongly first-order are shown. It means that in the bounds shown in the third column, the sphaleron decoupling condition and the completion conditions are safely satisfied simultaneously. Thus, if the measured $hhh$ coupling matches the prediction shown in the third column labelled

| $(n_0,\ n_+,\ n_{++})$ | Required by $\frac{v_n}{T_n} > 1$ & $\frac{\Gamma}{H^4} > 1$ | Conservative bound |
|---|---|---|
| (0, 1, 0) | $137\,\% > \Delta\kappa_3 > 21\%$ | $114\,\% > \Delta\kappa_3 > 50\,\%$ |
| (1, 1, 0) | $143\,\% > \Delta\kappa_3 > 19\,\%$ | $115\,\% > \Delta\kappa_3 > 47\,\%$ |
| (2, 1, 0) | $135\,\% > \Delta\kappa_3 > 18\,\%$ | $114\,\% > \Delta\kappa_3 > 44\,\%$ |
| (0, 0, 1) | $153\,\% > \Delta\kappa_3 > 62\,\%$ | $148\,\% > \Delta\kappa_3 > 65\,\%$ |
| (2, 1, 1) | $160\,\% > \Delta\kappa_3 > 65\,\%$ | $150\,\% > \Delta\kappa_3 > 75\,\%$ |
| (3, 2, 1) | $136\,\% > \Delta\kappa_3 > 59\,\%$ | $153\,\% > \Delta\kappa_3 > 63\,\%$ |

Table 9.1: Predictions on the $hhh$ coupling for realizing the strongly first-order EWPT if $\Delta\kappa_{\gamma\gamma} = -4\% \pm 1\%$ for each model. The lower and upper bounds on $\Delta\kappa_3$ shown in the second column are determined by the sphaleron decoupling conditions and the completion condition of the phase transition, respectively. In the bounds shown in the third column, the condition sphaleron decoupling and the completion conditions are safely satisfied simultaneously. If the measured $hhh$ coupling matches the prediction shown in the third column, it is expected that the EWPT is strongly first-order. In the final column, corresponding candidates of the SM extensions are shown for each benchmark point.

"Conservative bound", it is expected that the electroweak phase transition occurring at the early Universe was a strongly first order phase transition. Therefore, we emphasize that the results in the third column are important in testing the strongly first-order EWPT.

In Reference [211], it has been confirmed that conservative predictions for the feasibility of the strongly first-order EWPT are given by $\Delta\kappa_3 > 80\%$ in several representative extended Higgs models. Our new results indicate that more precise criteria for the strongly first-order phase transition can be obtained by using precise $h\gamma\gamma$ coupling measurements. If the $hhh$ coupling measured at future colliders satisfies the prediction shown in Table 9.1, we can conclude whether the EWPT is strongly first-order or not. In addition, we can determine an upper bound on $\Lambda$ by combining precise $h\gamma\gamma$ coupling measurements and the completion condition for the phase transition. In the case with $(n_0, n_+, n_{++}) = (0, 1, 0)$, we can conclude that a new charged particle satisfying $\Lambda < 946\text{GeV}$ and $r > 0.457$ should exist if we confirm $\Delta\kappa_{\gamma\gamma} < -3\%$. If we cannot observe any new physics signal at future colliders, we can test the EWPT via the GW and PBH observations in addition to precise Higgs coupling measurements.

Moreover, Figure 8.2 indicates that lower bounds on the $h\gamma\gamma$ coupling can be obtained by combining the sphaleron decoupling condition with the perturbative unitarity bound. In Table 9.2, predictions on the $h\gamma\gamma$ coupling are summarized. If the measured

| $(n_0,\ n_+,\ n_{++})$ | Predictions on $\Delta\kappa_{\gamma\gamma}$ |
|---|---|
| (0,1,0) | -0.88% |
| (1,1,0) | -0.97% |
| (2,1,0) | -0.95% |
| (0,0,1) | -2.71% |
| (2,1,1) | -3.73% |
| (3,2,1) | -4.53% |

Table 9.2: Predictions on the $h\gamma\gamma$ coupling. If the measured $h\gamma\gamma$ coupling is larger than these predictions, the EWPT can be strongly first-order.

| Collider | $\Delta\kappa_3(1\sigma)$ |
|---|---|
| HL-LHC | 50% |
| $\text{ILC}_{250}$ | 49% |
| $\text{ILC}_{500}$ | 22% |
| $\text{ILC}_{1000}$ | 10% |

Table 9.3: Expected precision at one sigma of the triple Higgs coupling measurements at the HL-LHC and various stages of the ILC.

$h\gamma\gamma$ coupling is larger than these predictions, the EWPT can be strongly first-order.

Before closing this section, we comment on our analyses. In our analyses, it has been assumed that all new particles have the same mass and non-decouplingness. In general, a hierarchy between new particle masses can exist. To discuss the impact of the hierarchy, we consider the case with $(n_0, n_+, n_{++}) = (2, 1, 0)$. Although this setup is the same as that in the top-right panel of Figure 8.2, we here assume that the charged particle mass is heavier than the neutral particle mass. We also assume that the non-decouplingness of the charged particle is larger than that of the neutral particles. In Figure 7.1, it is shown that charged particles with larger $\Lambda$ and $r$ make the $h\gamma\gamma$ coupling large. Therefore, we can expect that the contour for the $h\gamma\gamma$ coupling in the right panel of Figure 8.2 is shifted to the left. On the other hand, the parameter region satisfying the condition (5.24) is shifted downward. Thus, we can expect that the bounds on the $hhh$ coupling and $\Lambda$ we obtained are not drastically changed. We have numerically confirmed that our predictions do not much change even if non-decouplingness and mass take slightly different values for each particle.

## 9.2 Future Collider Phenomenology

In this section we discuss in which scenarios the future colliders will be able to conclusively determine if a specific Higgs structure predicts a strongly first order electroweak phase transition or not. To this end, we consider hypothetical scenarios for measurements of the triple Higgs coupling at future colliders. The expected precision for the triple Higgs boson coupling measurements at the HL-LHC[1] and at the three stages, 250GeV, 500GeV, and 1TeV, of the ILC are presented in table 9.3. We use the bound from the ATLAS result for the triple Higgs coupling scaling factor given by $-0.4 < \kappa_3 < 6.3$ [62].

In figure 9.1 we consider the hypothetical scenario where the triple Higgs coupling is measured to be the same as the SM value, $\kappa_3 = 1$, at the various collider stages. The blue region represents the SFOPT allowed space, while the dashed lines represent the line for which the area below is allowed experimentally in this scenario, for each collider. Since all the lines are on top or above the blue area, except for the last stage of 1TeV of the ILC, we conclude that, in this scenario, only by the last stage of the ILC the SFOPT could be ruled out.

In figure 9.2 the hypothetical scenario where the triple Higgs coupling is measured at its ideal value for a SFOPT, $\kappa_3 = 1.8$, is considered for the various collider stages. The large dashed line represents the central value, while the smaller dashed lines bound the allowed area. Again, it can be seen that only the last stage of the ILC will be able to confirm the SFOPT by use of the triple Higgs coupling measurements alone. Note that this only happens for this ideal $\kappa_3$ value. Slight deviation would make it impossible to confirm the SFOPT even in the last ILC stage.

In figure 9.3 two hypothetical scenarios are considered, where the triple Higgs coupling scaling factor is measured as $\kappa_3 = 1.4$ and $\kappa_3 = 2.3$ in the left and right of the figure respectively. These represent different scenarios where not even the most accurate precision of the triple Higgs coupling would be able to determine the nature of the EWPT, since both situations present a central value contour that includes both sections with a SFOPT and without. The $\kappa_{\gamma\gamma}$ contours are shown on top, and reveal that mea-

[1] Recently, new machine learning techniques have been used to improve this value at the HL-LHC [213]. Even though we do not use this results, we point out that these results do not invalidate the conclusions taken from this discussion.

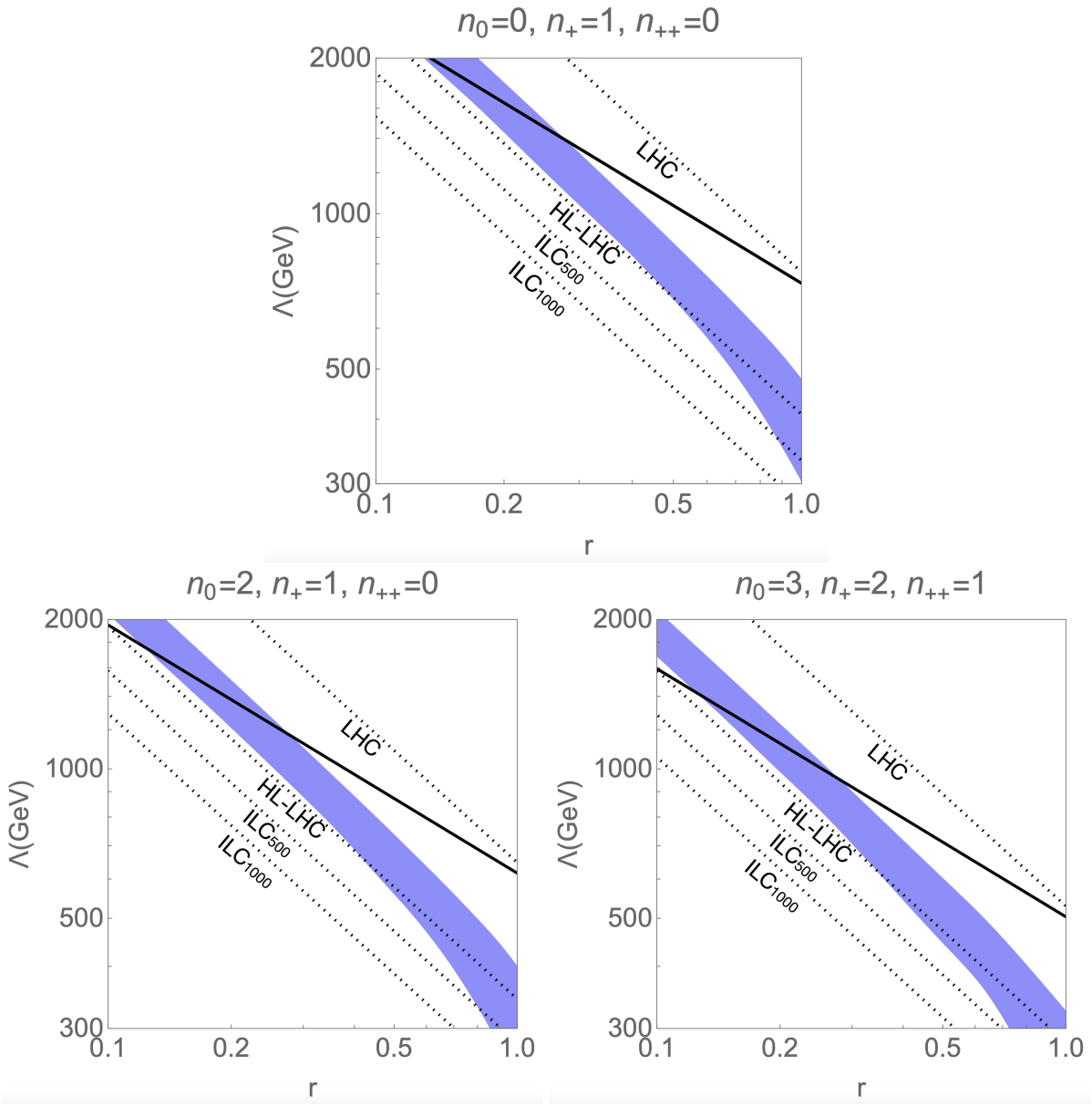



Figure 9.1: Scenario where $\kappa_3$ is measured as the standard model value, $\kappa_3 = 1$. The dotted lines represent the upper bounds each collider would impose with the uncertainties given in table 9.3.

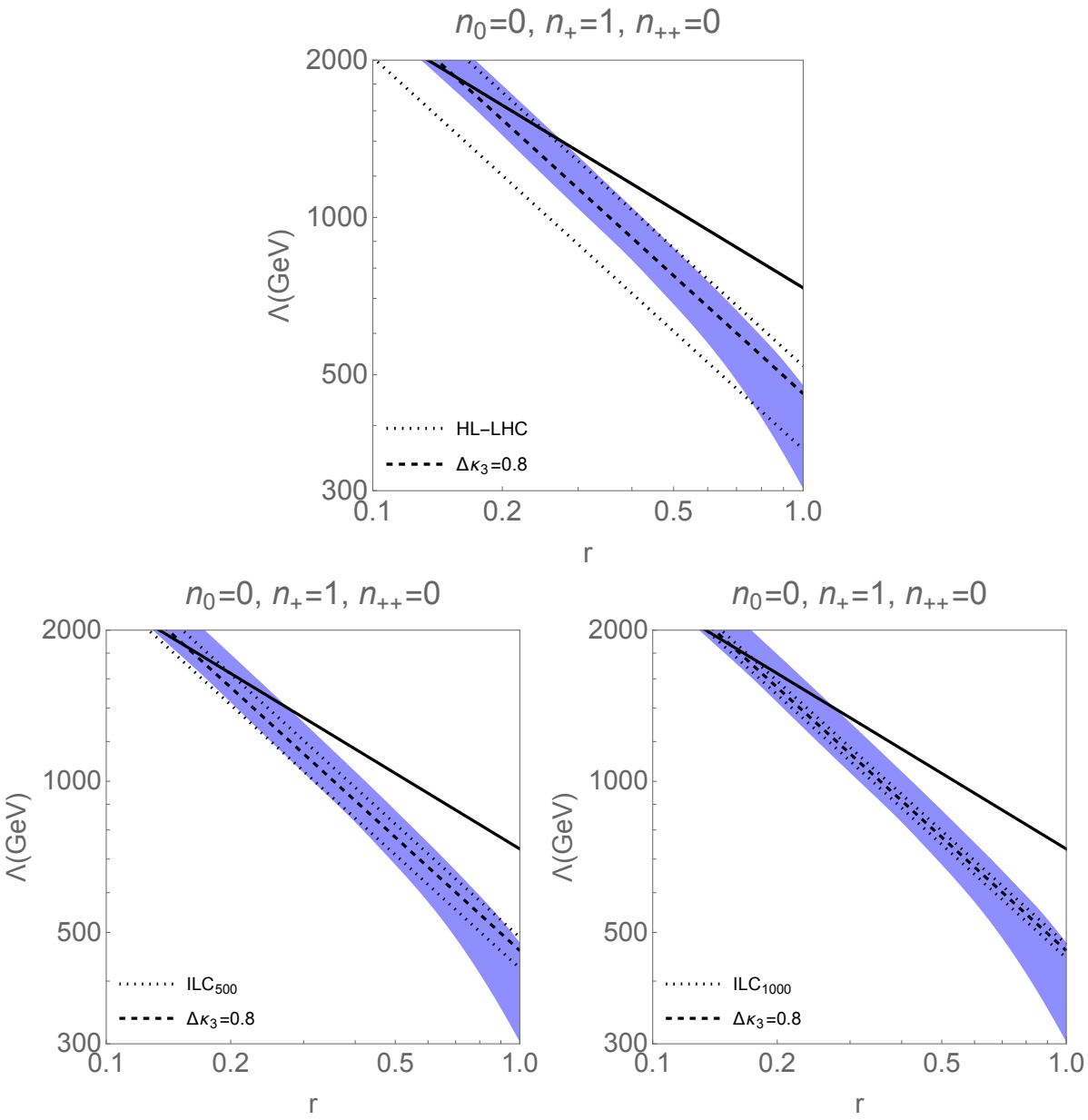



Figure 9.2: Scenario where $\kappa_3$ is measured at the ideal value for a SFOPT, $\kappa_3 = 1.8$, by each collider, with the precisions shown in table 9.3. The large dashed line represents this central value, while the smaller dashed lines represent the respective bounds by the respective collider measurements.

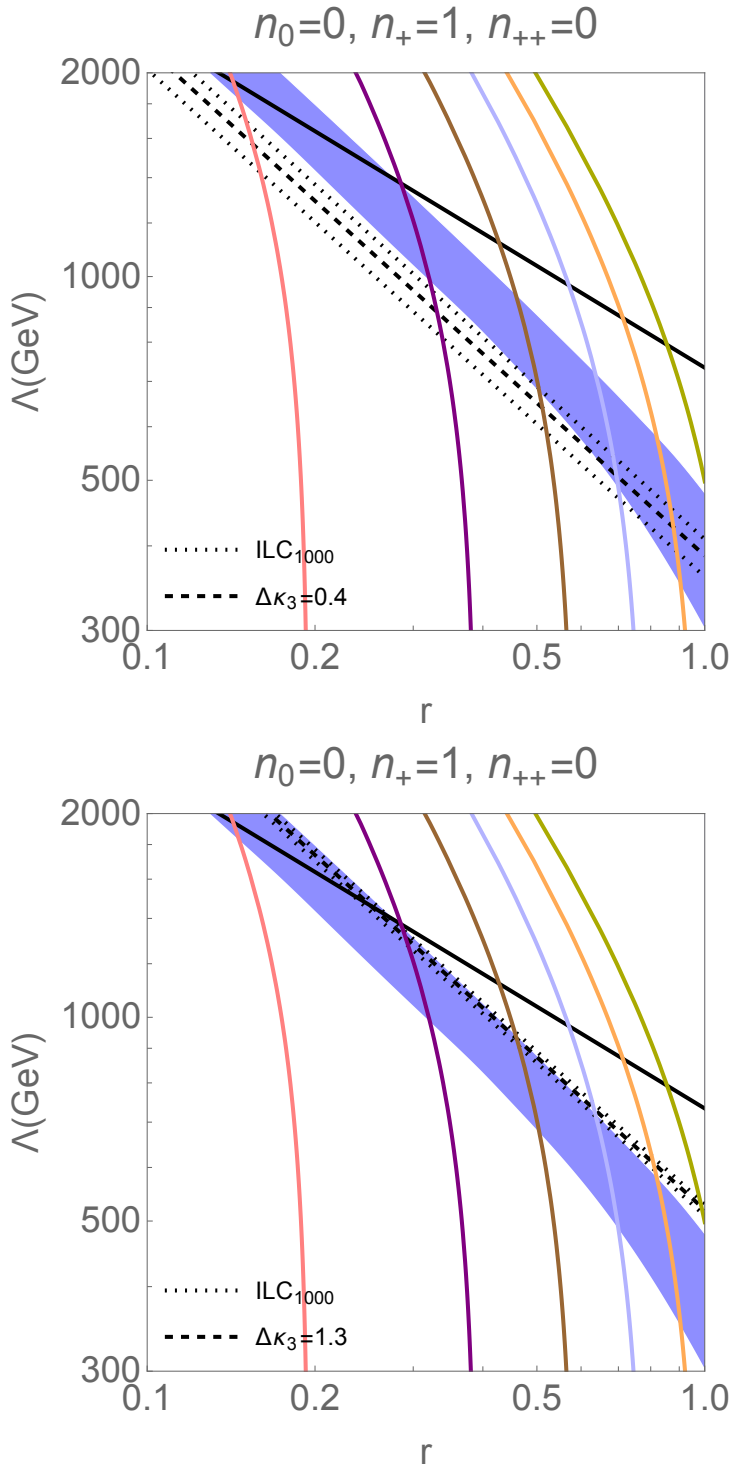



Figure 9.3: Two example scenarios, $\kappa_3 = 1.4$(left), $\kappa_3 = 2.3$(right), where determination of the nature of the SFOPT is impossible by the triple Higgs coupling alone. The $\kappa_{\gamma\gamma}$ contours show how the $h \to \gamma\gamma$ measurements can remedy this problem.

surements of $h \to \gamma\gamma$ can restrict the parameter space to a smaller section, such that, in conjunction with the $\kappa_3$ measurements, it can confirm or deny the SFOPT. This exemplifies once again the importance of the $h \to \gamma\gamma$ measurements in helping to probe the nature of the EWPT, in conjunction with the triple Higgs coupling measurements.

# Chapter 10

# Summary and Conclusions

This thesis started in Chapter 1 by providing an introduction to the topics covered and providing motivation for the research conducted in the context of this work. It was then organized into two different parts. Part I covered the background review of topics related to this research. Part II covered mainly the original research conducted. In this final chapter we summarize the contents of this thesis, and the main conclusions to be taken from it.

In Chapter 2 a review on the Standard Model of Particle Physics was presented. The theoretical framework of this model was laid out. The particle content was listed. An explanation of the Higgs mechanism was presented. Gauge invariance was used to construct the Lagrangian. The flavour structure of the model was explained. The concept of custodial symmetry was introduced. Finally, the full Standard Model Lagrangian was given.

In Chapter 3 a review of the experimental status of Standard Model phenomenology was given. A strong focus was given to Higgs sector phenomenology. Up to date results on the Higgs mass and various Higgs couplings were provided. This includes the Higgs triple self-couplings and the Higgs di-photon effective interaction, both of which are of special interest in this work. A section was dedicated to the status of electroweak precision experiments.

In Chapter 4 reviews on some important new physics models were given. These include the Two Higgs Doublet Model, the Higgs Triplet Model, and the Georgi-Machacek Model. These models are later used as benchmark model for our analysis using an effective field theory approach.

In Chapter 5 various topics on the Cosmology of the Electroweak Phase Transition were discussed. This began with a description of the problem of the observed Baryon Asymmetry of the Universe. It then discussed one of the most promising solutions to this problem, Electroweak Baryogenesis. It proceeded by giving an explanation of the sphaleron process, and how it can be used to produce baryon asymmetry. Then, the advent of bubble nucleation in first order phase transitions was explained, and the completion condition was presented. The sphaleron decoupling condition was then introduced, which is a necessary condition for the advent of a strongly first order phase transition. The generation of detectable gravitational waves and primordial black holes from fist order phase transitions was discussed.

In Chapter 6 the nearly-aligned Higgs Effective Field Theory was introduced. It's roots from chiral theory were explained. From it, the leading order Lagrangian, at chiral dimension 2, was derived. Corrections from finite temperature quantum field theory were calculated. It's validity and efficacy in describing non-decoupling effects were discussed with comparisons to the approach of effective cut-off by canonical dimension counting.

In Chapter 7 the non-decoupling effects in the Higgs di-photon effective interaction were studied. To this purpose, the naHEFT formalism was extended to include sub-leading order effects of chiral dimension four necessary to describe this interaction. Then, the parameters used for analysis were laid out, together with the list of used benchmark models. Finally, the behaviour of this effective interaction was studied by analysing the various figures produced.

Various conclusions were taken from the analysis in Section 7.3. For starters, it was shown the importance of the non-decoupling effects on this interaction, since the deviations grow with the mass scale of new physics. This includes effects from neutral particles, which indirectly affect the $\kappa_{\gamma\gamma}$ through the $\kappa_V$. The doubly charged scalars, on the other hand, lead to large deviations, and become strongly constrained by measurements. Finally, it was shown that large deviations in the Higgs triple self-coupling lead to large deviations in the Higgs di-photon coupling. It was concluded that models with charged scalars and a large triple Higgs coupling become constrained from Higgs di-photon experiments, unless the new physics scale is Higgs enough.

In Chapter 8 the main analysis of Electroweak Phase Transition signatures was

performed. After discussing the criteria used for the detectability of gravitational waves at interferometers, the parameter scan is performed. This scan took into account the sphaleron decoupling condition, which ensures the phase transition is strongly first order, necessary for successful electroweak baryogenesis. It also took into account the completion condition, making sure the transition is completed by the present day. To account for realistic unitarity bounds, a UV model was used. Detectability of gravitational waves and primordial black holes was also calculated, together with collider observables. Various benchmark models were considered with differently charged new scalar degrees of freedom.

Various conclusions were taken from the figures in Section 8.2, which both include contours of the deviations in $\kappa_{\gamma\gamma}$. Figure 8.2 includes contours of the Higgs triple self coupling, while Figure 8.3 focuses on $\kappa_V$ contours. From these, we corroborated that a first order phase transition requires large deviations in the triple Higgs coupling. It was also shown how models with charged particles predict a large Higgs di-photon coupling for a first order phase transition to be possible. The $\kappa_V$ interaction is also shown to be useful in constraining the parameter space since it will be measured with high precision in future experiments.

In Chapter 9 further topics were discussed building on the analysis performed in the previous chapters. Section 9.1 discussed how Higgs di-photon coupling measurements can be used to predict the triple Higgs coupling necessary for a first order phase transition in each model. It also put lower bounds on the Higgs di-photon absolute deviation for having a first order phase transition. Section 9.2, on the other hand, discussed how the triple Higgs coupling measurements will evolve at future colliders, and what kind of information we will be able to retrieve from those.

Various conclusions were taken from the discussions Section 9.1. In this discussion, the hypothetical future measurement of $\Delta\kappa_{\gamma\gamma} = -4\% \pm 1\%$ was considered. Then, in Table 9.1, specific predictions on the triple Higgs coupling were made. For example, in the simple charged singlet extension of the SM with $(n_0, n_+, n_{++}) = (0, 1, 0)$, it was concluded that a strongly first order electroweak phase transition requires the triple Higgs coupling deviation to be in the range $21\% - 137\%$. On the other hand, if such deviation is in the range $50\% - 114\%$, the phase transition is guaranteed to be first order. Moreover, in Figure 9.2, it was given an upper bound on the deviation in the Higgs

di-photon interaction of $-0.88\%$ in this same model, for the advent of a first order phase transition. These same bounds are made for each benchmark model.

Furthermore, various conclusions were taken from the discussions in Section 9.2. In this discussion, the expected precision of the triple Higgs coupling at future colliders shown in Table 9.3 were considered. Then, in Figure 9.1, by assuming a central value of $\kappa_3 = 1$, the expected bounds were plotted. It was concluded that only the final stage of the ILC will be able to completely exclude the strongly first order electroweak phase transition, in that scenario. Subsequently, in Figure 9.2, an ideal central value of $\kappa_3 = 1.8$ was considered. It was concluded that, once again, only the last stage of the ILC will be able to confirm the strongly first order phase transition. Finally, in Figure 9.3, it is exemplified that for other central values, for example $\kappa_3 = 1.4; 2.3$, no precise measurement of the triple Higgs coupling would ever be able to confirm or deny the strongly first order phase transition. Furthermore, the Higgs di-photon coupling contours are also shown in this figure. It was concluded that measurements of the Higgs di-photon coupling are ideal to solve this problem, by constraining the parameter space in a perpendicular way to the triple Higgs coupling and the other observables discussed before. This serves as further motivation of the usage of Higgs di-photon effective coupling measurements as a key component in determining the nature of the electroweak phase transition.

# Appendix A

# Theoretical Constraints on the naHEFT

Here we discuss the theoretical constraints on the naHEFT. We consider the case in which the scalar potential is given by

$$V = V_{SM} + \xi V_{CW}, \tag{A.1}$$

where $\xi = 1/(4\pi)^2$ is the loop factor, and $V_{CW}$ is a Coleman-Weingberg-like potential given by

$$V_{CW} = \frac{\kappa_0}{4}\left[\mathcal{M}^2(h)\right]^2 \ln\frac{\mathcal{M}^2(h)}{\mu^2}, \tag{A.2}$$

where $\kappa_0$ is the number of BSM degrees of freedom contributing to the loop corrections, $\mu^2$ is a renormalization scale, and the field depended mass is taken to be in the form

$$\mathcal{M}^2(h) = \Lambda^2 + \kappa_p\left(|\Phi|^2 - \frac{v^2}{2}\right), \tag{A.3}$$

where $\Lambda^2$ is the cut-off scale of the EFT, and $\kappa_p$ is the portal coupling between the Higgs field and the BSM fields, which can be related to the non-decouplingness by

$$r = \frac{\frac{\kappa_p}{2}v^2}{\Lambda^2}. \tag{A.4}$$

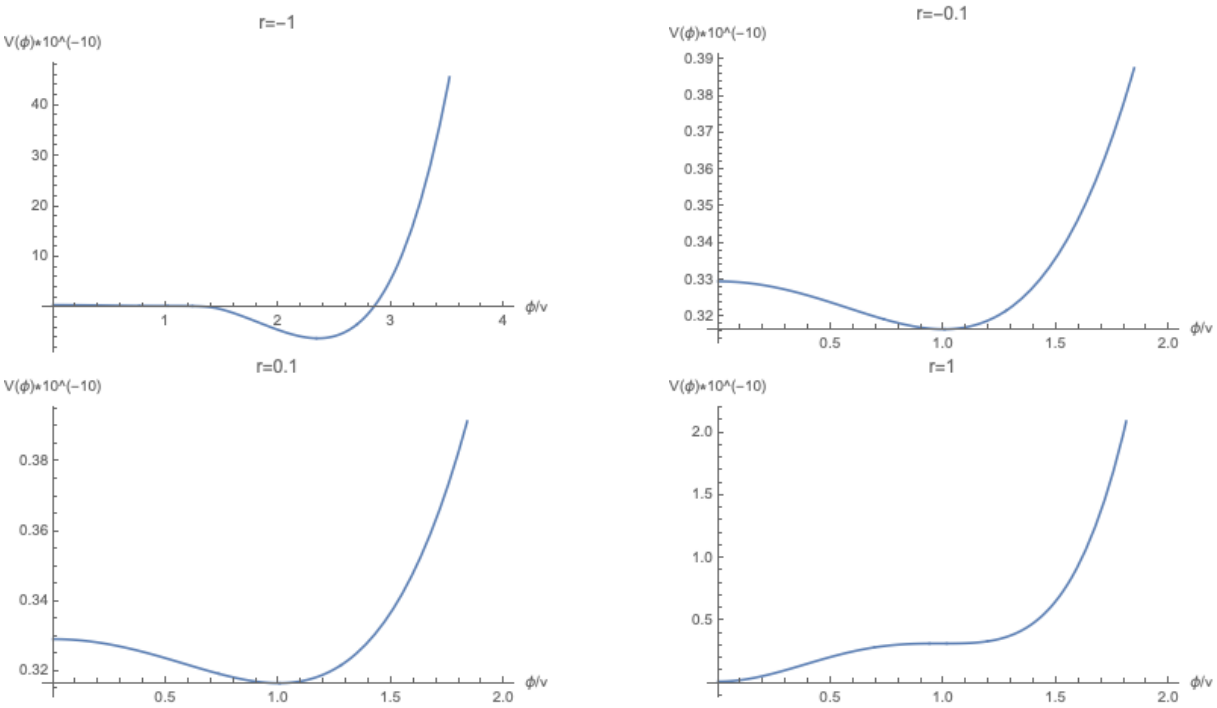



Figure A.1: Plots of the Higgs potential in the naHEFT for $\Lambda = 1TeV$, $\kappa_0 = 1$, and various values of $r$.

## A.1 Vacuum Stability

It is necessary to verify if the electroweak vacuum is the global minimum of the potential. After using the stationary and positivity of the minimum to replace $m$ and $\lambda$, the potential to study becomes

$$V(\phi) = \frac{M_h^2}{8v^2}(\phi^2 - v^2)^2 + \frac{\xi}{4}\kappa_0 \left[ [\mathcal{M}^2(\phi)]^2 \ln \frac{\mathcal{M}^2(\phi)}{\Lambda^2} - \frac{3}{2}[\mathcal{M}^2(\phi)]^2 + 2\Lambda^2\mathcal{M}^2(\phi) \right], \quad \text{(A.5)}$$

where

$$\mathcal{M}^2(\phi) = \Lambda^2 + \frac{\kappa_p}{2}(\phi^2 - v^2), \quad \text{(A.6)}$$

and the EW minimum is at $\phi = v$. Fixing $\Lambda = 1TeV$ and $\kappa_0 = 1$, and for various values of $r$, we obtaining the graphs in Figure A.1.

From the figures we conclude that for theories with non-decoupling effects, where $r \sim \mathcal{O}(1)$, the EW minimum is not ensured to be the global minimum. Vacuum stability must

be verified numerically.

## A.2 Perturbative Unitarity

We impose to the theory restriction from perturbative unitarity. The relevant part of the lagrangian is

$$\mathcal{L} = \frac{1}{2}\partial_\mu h \partial^\mu h + \frac{v^2}{4}\left(1 + 2\kappa_V \frac{h}{v} + \kappa_{VV}\frac{h^2}{v^2}\right) \mathrm{Tr}\left[\partial_\mu U^\dagger \partial^\mu U\right] - V(h), \tag{A.7}$$

where

$$V(h) = \frac{1}{2}M_h^2 h^2 + \frac{\kappa_3}{3!}\frac{3M_h^2}{v}h^3 + \frac{\kappa_4}{4!}\frac{3M_h^2}{v^2}h^4, \tag{A.8}$$

and the trace can be expanded as

$$\frac{v^2}{4}\mathrm{Tr}\left[\partial_\mu U^\dagger \partial^\mu U\right] = \frac{1}{2}\partial_\mu \boldsymbol{\pi}\cdot\partial^\mu\boldsymbol{\pi} + \frac{1}{6v^2}\left[(\boldsymbol{\pi}\cdot\partial_\mu\boldsymbol{\pi})^2 - \boldsymbol{\pi}^2(\partial_\mu\boldsymbol{\pi}\cdot\partial^\mu\boldsymbol{\pi})\right] + \mathcal{O}(\boldsymbol{\pi}^6). \tag{A.9}$$

From this expression, the following vertices can be obtained

$$V_{hhh} = -i\kappa_3 \frac{3M_h^2}{v}, \tag{A.10}$$

$$V_{hhhh} = -i\kappa_4 \frac{3M_h^2}{v^2}, \tag{A.11}$$

$$V_{h\pi^3\pi^3} = -i\kappa_V \frac{2p_{\pi_1^3} \cdot p_{\pi_2^3}}{v}, \tag{A.12}$$

$$V_{h\pi^+\pi^-} = -i\kappa_V \frac{2p_{\pi^+} \cdot p_{\pi^-}}{v}, \tag{A.13}$$

$$V_{hh\pi^+\pi^-} = -i\kappa_{VV} \frac{2p_{\pi^+} \cdot p_{\pi^-}}{v^2}, \tag{A.14}$$

$$V_{hh\pi^3\pi^3} = -i\kappa_{VV} \frac{2p_{\pi_1^3} \cdot p_{\pi_2^3}}{v^2}, \tag{A.15}$$

$$3iv^2 V_{\pi^+\pi^-\pi^+\pi^-} = p_{\pi_1^+} \cdot p_{\pi_2^+} + p_{\pi_1^-} \cdot p_{\pi_2^-} \tag{A.16}$$

$$- 2(p_{\pi_1^+} \cdot p_{\pi_1^-} + p_{\pi_1^+} \cdot p_{\pi_2^-} + p_{\pi_2^+} \cdot p_{\pi_1^-} + p_{\pi_2^+} \cdot p_{\pi_2^-}), \tag{A.17}$$

$$3iv^2 V_{\pi^+\pi^-\pi^3\pi^3} = p_{\pi^+} \cdot p_{\pi_1^3} + p_{\pi^-} \cdot p_{\pi_1^3} + p_{\pi^+} \cdot p_{\pi_2^3} + p_{\pi^-} \cdot p_{\pi_2^3} \tag{A.18}$$

$$- 2(p_{\pi^+} \cdot p_{\pi^-} + p_{\pi_1^3} \cdot p_{\pi_2^3}). \tag{A.19}$$

In order to calculate the amplitudes, we must set on-shell conditions. Here we neglect the on-shell masses setting them to zero. The amplitudes obtained are:

$$\mathcal{A}(\pi^+\pi^- \to \pi^+\pi^-) = -\frac{u}{v^2} - \frac{\kappa_V^2}{v^2}\left(\frac{s^2}{s-M_h^2} + \frac{t^2}{t-M_h^2}\right), \tag{A.20}$$

$$\mathcal{A}(\pi^3\pi^3 \to \pi^3\pi^3) = -\frac{\kappa_V^2}{v^2}\left(\frac{s^2}{s-M_h^2} + \frac{t^2}{t-M_h^2} + \frac{u^2}{u-M_h^2}\right), \tag{A.21}$$

$$\mathcal{A}(hh \to hh) = -\frac{3M_h^2}{v^2}\left[\kappa_4 + 3\kappa_3\left(\frac{M_h^2}{s-M_h^2} + \frac{M_h^2}{t-M_h^2} + \frac{M_h^2}{u-M_h^2}\right)\right], \tag{A.22}$$

$$\mathcal{A}(\pi^+\pi^- \to \pi^3\pi^3) = \frac{s}{v^2} - \frac{\kappa_V^2}{v^2}\frac{s^2}{s-M_h^2}, \tag{A.23}$$

$$\begin{aligned}\mathcal{A}(\pi^+\pi^- \to hh) = &-\frac{s}{v^2}(\kappa_{VV} - \kappa_V^2) - 3\kappa_3\frac{\kappa_V M_h^2}{v^2}\left(1 + \frac{M_h^2}{s-M_h^2}\right)\\ &- \frac{\kappa_V M_W^2}{v^2}\left(2\kappa_V + \kappa_V\frac{M_W^2}{t-M_W^2} + \kappa_V\frac{M_W^2}{u-M_W^2}\right),\end{aligned} \tag{A.24}$$

$$\begin{aligned}\mathcal{A}(\pi^+\pi^- \to hh) = &-\frac{s}{v^2}(\kappa_{VV} - \kappa_V^2) - 3\kappa_3\frac{\kappa_V M_h^2}{v^2}\left(1 + \frac{M_h^2}{s-M_h^2}\right)\\ &- \frac{\kappa_V M_h^2}{v^2}\left(-2\kappa_V + \kappa_V\frac{M_h^2}{t-M_W^2} + \kappa_V\frac{M_h^2}{u-M_W^2}\right),\end{aligned} \tag{A.25}$$

$$\begin{aligned}\mathcal{A}(\pi^3\pi^3 \to hh) = &-\frac{s}{v^2}(\kappa_{VV} - \kappa_V^2) - 3\kappa_3\frac{\kappa_V M_h^2}{v^2}\left(1 + \frac{M_h^2}{s-M_h^2}\right)\\ &- \frac{\kappa_V M_h^2}{v^2}\left(-2\kappa_V + \kappa_V\frac{M_h^2}{t-M_Z^2} + \kappa_V\frac{M_h^2}{u-M_Z^2}\right),\end{aligned} \tag{A.26}$$

$$\begin{aligned}\mathcal{A}(\pi^3 H \to \pi^3 h) = &-\frac{t}{v^2}(\kappa_{VV} - \kappa_V^2) - 3\kappa_3\frac{\kappa_V M_h^2}{v^2}\left(1 + \frac{M_h^2}{t-M_h^2}\right)\\ &- \frac{\kappa_V M_h^2}{v^2}\left(-2\kappa_V + \kappa_V\frac{M_h^2}{s-M_Z^2} + \kappa_V\frac{M_h^2}{u-M_Z^2}\right).\end{aligned} \tag{A.27}$$

The S wave amplitudes are now obtained from the formula

$$a_0(i) = \frac{1}{32\pi}\int_{-1}^{1}\mathcal{A}(i)d\cos\theta, \tag{A.28}$$

where once again we will have to consider some on-shell conditions for the replacement of $t$ and $u$ to $\cos\theta$. In order to obtain consistent results with [103], we must now consider all masses to be non-zero on shell. The results are as follows

$$a_0(\pi^+\pi^- \to \pi^+\pi^-) = \frac{s}{32\pi v^2}(1-\kappa_V^2) - \frac{M_h^2}{16\pi v^2}\kappa_V^2\left[2 + \frac{2M_W^2}{M_h^2}\frac{1+\kappa_V^2}{\kappa_V^2} + \frac{M_h^2}{s-M_h^2} - \frac{M_h^2}{s-4M_W^2}\log\left(1+\frac{s-4M_W^2}{M_h^2}\right)\right], \tag{A.29}$$

$$a_0(\pi^3\pi^3 \to \pi^3\pi^3) = -\frac{M_h^2}{16\pi v^2}\kappa_V^2\left[3 + \frac{4M_Z^2}{M_h^2} + \frac{M_h^2}{s-M_h^2} - \frac{2M_h^2}{s-4M_Z^2}\log\left(1+\frac{s-4M_Z^2}{M_h^2}\right)\right], \tag{A.30}$$

$$a_0(hh \to hh) = -\frac{M_h^2}{16\pi v^2}\left[3\kappa_4 + 9\kappa_3^2\frac{M_h^2}{s-M_h^2} - 18\kappa_3^2\frac{M_h^2}{s-4M_h^2}\log\left(\frac{s}{M_h^2}-3\right)\right], \tag{A.31}$$

$$a_0(\pi^+\pi^- \to \pi^3\pi^3) = \frac{s}{16\pi v^2}(1-\kappa_V^2) - \frac{M_h^2}{16\pi v^2}\kappa_V^2\left(1+\frac{M_h^2}{s-M_h^2}\right), \tag{A.32}$$

$$a_0(\pi^+\pi^- \to hh) = \frac{s}{16\pi v^2}(k_V^2-\kappa_{VV}) - \frac{M_h^2}{16\pi v^2}\kappa_V^2\left[3\kappa_3 - 2\kappa_V + 3\kappa_3\frac{M_h^2}{s-M_h^2} + \kappa_V\frac{2M_h^2}{\sqrt{(s-4M_W^2)(s-4M_h^2)}}\log\left(\frac{s-2M_h^2-\sqrt{(s-4M_W^2)(s-4M_h^2)}}{s-2M_h^2+\sqrt{(s-4M_W^2)(s-4M_h^2)}}\right)\right], \tag{A.33}$$

$$a_0(\pi^3\pi^3 \to hh) = \frac{s}{16\pi v^2}(k_V^2-\kappa_{VV}) - \frac{M_h^2}{16\pi v^2}\kappa_V^2\left[3\kappa_3 - 2\kappa_V + 3\kappa_3\frac{M_h^2}{s-M_h^2} + \kappa_V\frac{2M_h^2}{\sqrt{(s-4M_Z^2)(s-4M_h^2)}}\log\left(\frac{s-2M_h^2-\sqrt{(s-4M_Z^2)(s-4M_h^2)}}{s-2M_h^2+\sqrt{(s-4M_Z^2)(s-4M_h^2)}}\right)\right], \tag{A.34}$$

which mostly match [103] apart from some details in the term that goes as $1/s$ and are thus irrelevant for unitarity constraints.

The S wave scattering matrix can be obtained by

$$\mathcal{T}_0 = \begin{pmatrix} a_0(\pi^+\pi^- \to \pi^+\pi^-) & \frac{1}{\sqrt{2}}a_0(\pi^+\pi^- \to \pi^3\pi^3) & \frac{1}{\sqrt{2}}a_0(\pi^+\pi^- \to hh) & 0 \\ \frac{1}{\sqrt{2}}a_0(\pi^+\pi^- \to \pi^3\pi^3) & \frac{1}{2}a_0(\pi^3\pi^3 \to \pi^3\pi^3) & \frac{1}{2}a_0(\pi^3\pi^3 \to hh) & 0 \\ \frac{1}{\sqrt{2}}a_0(\pi^+\pi^- \to hh) & \frac{1}{2}a_0(\pi^3\pi^3 \to hh) & \frac{1}{2}a_0(hh \to hh) & 0 \\ 0 & 0 & 0 & a_0(\pi^3 h \to \pi^3 h) \end{pmatrix}. \tag{A.35}$$

When expanded in powers of $s$, this matrix will have two relevant components

$$\mathcal{T}_0 = \frac{s}{32\pi v^2}\mathcal{M}_1 - \frac{1}{8\pi v^2}\mathcal{M}_0 + \mathcal{O}\left(\frac{1}{s}\right), \tag{A.36}$$

where the second matrix shown can be further divided into the following contributions

$$\mathcal{M}_0 = M_h^2\mathcal{M}_h + M_W^2\mathcal{M}_W + M_Z^2\mathcal{M}_Z. \tag{A.37}$$

Two of the matrices can be readily obtained

$$\mathcal{M}_1 = \begin{pmatrix} \tilde{A} & \sqrt{2}\tilde{A} & \sqrt{2}\tilde{B} & 0 \\ \sqrt{2}\tilde{A} & 0 & \tilde{B} & 0 \\ \sqrt{2}\tilde{B} & \tilde{B} & 0 & 0 \\ 0 & 0 & 0 & -\tilde{B} \end{pmatrix}, \tag{A.38}$$

$$\mathcal{M}_h = \begin{pmatrix} A & \frac{1}{\sqrt{8}}B & \frac{1}{\sqrt{8}}C & 0 \\ \frac{1}{\sqrt{8}}B & \frac{3}{4}D & \frac{1}{4}C & 0 \\ \frac{1}{\sqrt{8}}C & \frac{1}{4}C & \frac{3}{4}E & 0 \\ 0 & 0 & 0 & \frac{1}{2}F \end{pmatrix}, \tag{A.39}$$

where

$$\tilde{A} = 1 - \kappa_V^2, \tag{A.40}$$

$$\tilde{B} = \kappa_V^2 - \kappa_{VV}, \tag{A.41}$$

$$A = B = D = \kappa_V^2, \tag{A.42}$$

$$C = \kappa_V(3\kappa_3 - 2\kappa_V), \tag{A.43}$$

$$E = \kappa_4, \tag{A.44}$$

$$F = 3\kappa_V(\kappa_3 - \kappa_V) + \kappa_{VV}. \tag{A.45}$$

By neglecting the gauge boson masses, we obtain the following eigenvalues

$$t_1 = \frac{s}{32\pi v^2}(\kappa_V^2 - 1) - \frac{M_h^2}{16\pi v^2}\kappa_V^2, \tag{A.46}$$

$$t_2 = \frac{s}{32\pi v^2}(1 - \kappa_V^2) - \frac{M_h^2}{16\pi v^2}\frac{3\kappa_4 + 5\kappa_V^2 + 4\sqrt{K(s)}}{4}, \tag{A.47}$$

$$t_2 = \frac{s}{32\pi v^2}(1 - \kappa_V^2) - \frac{M_h^2}{16\pi v^2}\frac{3\kappa_4 + 5\kappa_V^2 - 4\sqrt{K(s)}}{4}, \tag{A.48}$$

$$t_4 = \frac{s}{32\pi v^2}(\kappa_{VV} - \kappa_V^2) - \frac{M_h^2}{16\pi v^2}(3\kappa_V(\kappa_3 - \kappa_V) + \kappa_{VV}), \tag{A.49}$$

where

$$K(s) = \Delta_1\frac{s^2}{M_h^4} - \Delta_2\frac{s}{M_h^2} + \frac{1}{16}\left[9\kappa_4^2 + \kappa_V^2(73\kappa_V^2 - 144\kappa_3\kappa_V + 108\kappa_3^2 - 30\kappa_4)\right], \tag{A.50}$$

$$\Delta_1 = (\kappa_V^2 - 1)^2 - \frac{3}{2}(\kappa_V^2 - 1)(\kappa_{VV} - 1) + \frac{3}{4}(\kappa_{VV} - 1)^2, \tag{A.51}$$

$$\Delta_2 = \frac{9}{2}\kappa_3\kappa_V(\kappa_V^2 - \kappa_{VV}) + \frac{3}{4}\kappa_4(\kappa_V^2 - 1) - \frac{1}{4}\kappa_V^2(17\kappa_V^2 - 12\kappa_{VV} - 5). \tag{A.52}$$

Finally, by replacing $\Delta\kappa_{3,4}$ over $r, \Lambda$, and neglecting order $\Delta\kappa^2_{V,VV}$, the eigenvalues can be written as

$$t_1 = \frac{\Lambda^2}{16\pi v^2}\Delta\kappa_V, \tag{A.53}$$

$$t_2 = -\frac{3\Lambda^2}{64\pi v^2}\left[\Delta\kappa_{VV} + \frac{4}{3}\xi\kappa_0 r^3(6-r)\frac{\Lambda^2}{v^2}\right], \tag{A.54}$$

$$t_3 = -\frac{\Lambda^2}{8\pi v^2}\left[\Delta\kappa_V - \frac{3}{8}\Delta\kappa_{VV} + \frac{3}{2}\xi\kappa_0 r^3(2-r)\frac{\Lambda^2}{v^2}\right], \tag{A.55}$$

$$t_4 = -\frac{\Lambda^2}{32\pi v^2}\left[2\Delta\kappa_V - \Delta\kappa_{VV} + 8\xi\kappa_0 r^3\frac{\Lambda^2}{v^2}\right]. \tag{A.56}$$

# Bibliography


[1] H. Fritzsch and M. Gell-Mann, eConf **C720906V2** (1972), 135-165 [arXiv:hep-ph/0208010 [hep-ph]].

[2] H. Fritzsch, M. Gell-Mann and H. Leutwyler, Phys. Lett. B **47** (1973), 365-368 doi:10.1016/0370-2693(73)90625-4

[3] S. Weinberg, Phys. Rev. Lett. **31** (1973), 494-497 doi:10.1103/PhysRevLett.31.494

[4] S. Weinberg, Phys. Rev. D **8** (1973), 4482-4498 doi:10.1103/PhysRevD.8.4482

[5] D. J. Gross and F. Wilczek, Phys. Rev. D **8** (1973), 3633-3652 doi:10.1103/PhysRevD.8.3633

[6] S. L. Glashow, Nucl. Phys. **22** (1961), 579-588 doi:10.1016/0029-5582(61)90469-2

[7] S. Weinberg, Phys. Rev. Lett. **19** (1967), 1264-1266 doi:10.1103/PhysRevLett.19.1264

[8] A. Salam, Conf. Proc. C **680519** (1968), 367-377 doi:10.1142/9789812795915_0034

[9] P. W. Higgs, Phys. Rev. **145** (1966), 1156-1163 doi:10.1103/PhysRev.145.1156

[10] P. W. Higgs, Phys. Rev. Lett. **13** (1964), 508-509 doi:10.1103/PhysRevLett.13.508

[11] P. W. Higgs, Phys. Lett. **12** (1964), 132-133 doi:10.1016/0031-9163(64)91136-9

[12] F. Englert and R. Brout, Phys. Rev. Lett. **13** (1964), 321-323 doi:10.1103/PhysRevLett.13.321

[13] G. S. Guralnik, C. R. Hagen and T. W. B. Kibble, Phys. Rev. Lett. **13** (1964), 585-587 doi:10.1103/PhysRevLett.13.585

[14] S. Navas *et al.* [Particle Data Group], Phys. Rev. D **110** (2024) no.3, 030001 doi:10.1103/PhysRevD.110.030001

[15] G. Aad *et al.* [ATLAS], Phys. Lett. B **716** (2012), 1-29 doi:10.1016/j.physletb.2012.08.020 [arXiv:1207.7214 [hep-ex]].

[16] S. Chatrchyan *et al.* [CMS], Phys. Lett. B **716** (2012), 30-61 doi:10.1016/j.physletb.2012.08.021 [arXiv:1207.7235 [hep-ex]].

[17] N. Aghanim *et al.* [Planck], Astron. Astrophys. **641** (2020), A6 [erratum: Astron. Astrophys. **652** (2021), C4] doi:10.1051/0004-6361/201833910 [arXiv:1807.06209 [astro-ph.CO]].

[18] Y. Fukuda *et al.* [Super-Kamiokande], Phys. Rev. Lett. **81** (1998), 1562-1567 doi:10.1103/PhysRevLett.81.1562 [arXiv:hep-ex/9807003 [hep-ex]].

[19] M. A. Shifman, A. I. Vainshtein, M. B. Voloshin and V. I. Zakharov, Sov. J. Nucl. Phys. **30** (1979), 711-716 ITEP-42-1979.

[20] C. W. Chiang and K. Yagyu, Phys. Rev. D **87** (2013) no.3, 033003 doi:10.1103/PhysRevD.87.033003 [arXiv:1207.1065 [hep-ph]].

[21] A. Katz and M. Perelstein, JHEP **07** (2014), 108 doi:10.1007/JHEP07(2014)108 [arXiv:1401.1827 [hep-ph]].

[22] M. Kakizaki, S. Kanemura and T. Matsui, Phys. Rev. D **92** (2015) no.11, 115007 doi:10.1103/PhysRevD.92.115007 [arXiv:1509.08394 [hep-ph]].

[23] S. Kanemura, M. Kikuchi and K. Yagyu, Nucl. Phys. B **907** (2016), 286-322 doi:10.1016/j.nuclphysb.2016.04.005 [arXiv:1511.06211 [hep-ph]].

[24] S. Kanemura, M. Kikuchi and K. Yagyu, Nucl. Phys. B **917** (2017), 154-177 doi:10.1016/j.nuclphysb.2017.02.004 [arXiv:1608.01582 [hep-ph]].

[25] J. Braathen and S. Kanemura, Phys. Lett. B **796** (2019), 38-46 doi:10.1016/j.physletb.2019.07.021 [arXiv:1903.05417 [hep-ph]].

[26] J. Braathen and S. Kanemura, Eur. Phys. J. C **80** (2020) no.3, 227 doi:10.1140/epjc/s10052-020-7723-2 [arXiv:1911.11507 [hep-ph]].

[27] M. Aiko, S. Kanemura, M. Kikuchi, K. Sakurai and K. Yagyu, Comput. Phys. Commun. **301** (2024), 109231 doi:10.1016/j.cpc.2024.109231 [arXiv:2311.15892 [hep-ph]].

[28] A. Arhrib, M. Capdequi Peyranere, W. Hollik and S. Penaranda, Phys. Lett. B **579** (2004), 361-370 doi:10.1016/j.physletb.2003.10.006 [arXiv:hep-ph/0307391 [hep-ph]].

[29] M. Aoki, S. Kanemura, K. Tsumura and K. Yagyu, Phys. Rev. D **80** (2009), 015017 doi:10.1103/PhysRevD.80.015017 [arXiv:0902.4665 [hep-ph]].

[30] P. Posch, Phys. Lett. B **696** (2011), 447-453 doi:10.1016/j.physletb.2011.01.003 [arXiv:1001.1759 [hep-ph]].

[31] A. Arhrib, R. Benbrik and N. Gaur, Phys. Rev. D **85** (2012), 095021 doi:10.1103/PhysRevD.85.095021 [arXiv:1201.2644 [hep-ph]].

[32] D. Fontes, J. C. Romão and J. P. Silva, JHEP **12** (2014), 043 doi:10.1007/JHEP12(2014)043 [arXiv:1408.2534 [hep-ph]].

[33] S. Kanemura, M. Kikuchi and K. Yagyu, Phys. Lett. B **731** (2014), 27-35 doi:10.1016/j.physletb.2014.02.022 [arXiv:1401.0515 [hep-ph]].

[34] S. Kanemura, K. Tsumura, K. Yagyu and H. Yokoya, Phys. Rev. D **90** (2014), 075001 doi:10.1103/PhysRevD.90.075001 [arXiv:1406.3294 [hep-ph]].

[35] A. Arhrib, R. Benbrik, J. El Falaki and A. Jueid, JHEP **12** (2015), 007 doi:10.1007/JHEP12(2015)007 [arXiv:1507.03630 [hep-ph]].

[36] S. Kanemura, M. Kikuchi and K. Yagyu, Nucl. Phys. B **896** (2015), 80-137 doi:10.1016/j.nuclphysb.2015.04.015 [arXiv:1502.07716 [hep-ph]].

[37] K. Hashino, S. Kanemura and Y. Orikasa, Phys. Lett. B **752** (2016), 217-220 doi:10.1016/j.physletb.2015.11.044 [arXiv:1508.03245 [hep-ph]].

[38] S. Kanemura, M. Kikuchi and K. Sakurai, Phys. Rev. D **94** (2016) no.11, 115011 doi:10.1103/PhysRevD.94.115011 [arXiv:1605.08520 [hep-ph]].

[39] E. Senaha, Phys. Rev. D **100** (2019) no.5, 055034 doi:10.1103/PhysRevD.100.055034 [arXiv:1811.00336 [hep-ph]].

[40] J. Braathen, S. Kanemura and M. Shimoda, JHEP **03** (2021), 297 doi:10.1007/JHEP03(2021)297 [arXiv:2011.07580 [hep-ph]].

[41] R. R. Florentino, J. C. Romão and J. P. Silva, Eur. Phys. J. C **81** (2021) no.12, 1148 doi:10.1140/epjc/s10052-021-09956-2 [arXiv:2106.08332 [hep-ph]].

[42] G. Degrassi and P. Slavich, Eur. Phys. J. C **83** (2023) no.10, 941 doi:10.1140/epjc/s10052-023-12097-3 [arXiv:2307.02476 [hep-ph]].

[43] M. Aiko, J. Braathen and S. Kanemura, Eur. Phys. J. C **85** (2025) no.5, 489 doi:10.1140/epjc/s10052-025-14184-z [arXiv:2307.14976 [hep-ph]].

[44] A. G. Akeroyd and C. W. Chiang, Phys. Rev. D **81** (2010), 115007 doi:10.1103/PhysRevD.81.115007 [arXiv:1003.3724 [hep-ph]].

[45] A. Arhrib, R. Benbrik, M. Chabab, G. Moultaka and L. Rahili, JHEP **04** (2012), 136 doi:10.1007/JHEP04(2012)136 [arXiv:1112.5453 [hep-ph]].

[46] M. Aoki, S. Kanemura, M. Kikuchi and K. Yagyu, Phys. Lett. B **714** (2012), 279-285 doi:10.1016/j.physletb.2012.07.016 [arXiv:1204.1951 [hep-ph]].

[47] S. Kanemura and K. Yagyu, Phys. Rev. D **85** (2012), 115009 doi:10.1103/PhysRevD.85.115009 [arXiv:1201.6287 [hep-ph]].

[48] M. Aoki, S. Kanemura, M. Kikuchi and K. Yagyu, Phys. Rev. D **87** (2013) no.1, 015012 doi:10.1103/PhysRevD.87.015012 [arXiv:1211.6029 [hep-ph]].

[49] F. Arbabifar, S. Bahrami and M. Frank, Phys. Rev. D **87** (2013) no.1, 015020 doi:10.1103/PhysRevD.87.015020 [arXiv:1211.6797 [hep-ph]].

[50] A. D. Sakharov, Pisma Zh. Eksp. Teor. Fiz. **5** (1967), 32-35 doi:10.1070/PU1991v034n05ABEH002497

[51] V. A. Kuzmin, V. A. Rubakov and M. E. Shaposhnikov, Phys. Lett. B **155** (1985), 36 doi:10.1016/0370-2693(85)91028-7

[52] N. S. Manton, Phys. Rev. D **28** (1983), 2019 doi:10.1103/PhysRevD.28.2019

[53] F. R. Klinkhamer and N. S. Manton, Phys. Rev. D **30** (1984), 2212 doi:10.1103/PhysRevD.30.2212

[54] M. D'Onofrio and K. Rummukainen, Phys. Rev. D **93** (2016) no.2, 025003 doi:10.1103/PhysRevD.93.025003 [arXiv:1508.07161 [hep-ph]].

[55] M. B. Gavela, P. Hernandez, J. Orloff, O. Pene and C. Quimbay, Nucl. Phys. B **430** (1994), 382-426 doi:10.1016/0550-3213(94)00410-2 [arXiv:hep-ph/9406289 [hep-ph]].

[56] P. Huet and E. Sather, Phys. Rev. D **51** (1995), 379-394 doi:10.1103/PhysRevD.51.379 [arXiv:hep-ph/9404302 [hep-ph]].

[57] C. Grojean, G. Servant and J. D. Wells, Phys. Rev. D **71** (2005), 036001 doi:10.1103/PhysRevD.71.036001 [arXiv:hep-ph/0407019 [hep-ph]].

[58] S. Kanemura, Y. Okada and E. Senaha, Phys. Lett. B **606** (2005), 361-366 doi:10.1016/j.physletb.2004.12.004 [arXiv:hep-ph/0411354 [hep-ph]].

[59] K. Hashino, M. Kakizaki, S. Kanemura and T. Matsui, Phys. Rev. D **94** (2016) no.1, 015005 doi:10.1103/PhysRevD.94.015005 [arXiv:1604.02069 [hep-ph]].

[60] G. Aad *et al.* [ATLAS], Nature **607** (2022) no.7917, 52-59 [erratum: Nature **612** (2022) no.7941, E24] doi:10.1038/s41586-022-04893-w [arXiv:2207.00092 [hep-ex]].

[61] A. Tumasyan *et al.* [CMS], Nature **607** (2022) no.7917, 60-68 [erratum: Nature **623** (2023) no.7985, E4] doi:10.1038/s41586-022-04892-x [arXiv:2207.00043 [hep-ex]].

[62] G. Aad *et al.* [ATLAS], Phys. Lett. B **843** (2023), 137745 doi:10.1016/j.physletb.2023.137745 [arXiv:2211.01216 [hep-ex]].

[63] M. Cepeda, S. Gori, P. Ilten, M. Kado, F. Riva, R. Abdul Khalek, A. Aboubrahim, J. Alimena, S. Alioli and A. Alves, *et al.* CERN Yellow Rep. Monogr. **7** (2019), 221-584 doi:10.23731/CYRM-2019-007.221 [arXiv:1902.00134 [hep-ph]].

[64] P. Bambade, T. Barklow, T. Behnke, M. Berggren, J. Brau, P. Burrows, D. Denisov, A. Faus-Golfe, B. Foster and K. Fujii, *et al.* [arXiv:1903.01629 [hep-ex]].

[65] C. Grojean and G. Servant, Phys. Rev. D **75** (2007), 043507 doi:10.1103/PhysRevD.75.043507 [arXiv:hep-ph/0607107 [hep-ph]].

[66] P. Amaro-Seoane *et al.* [LISA], [arXiv:1702.00786 [astro-ph.IM]].

[67] S. Kawamura, M. Ando, N. Seto, S. Sato, T. Nakamura, K. Tsubono, N. Kanda, T. Tanaka, J. Yokoyama and I. Funaki, *et al.* Class. Quant. Grav. **28** (2011), 094011 doi:10.1088/0264-9381/28/9/094011

[68] J. Luo *et al.* [TianQin], Class. Quant. Grav. **33** (2016) no.3, 035010 doi:10.1088/0264-9381/33/3/035010 [arXiv:1512.02076 [astro-ph.IM]].

[69] W. H. Ruan, Z. K. Guo, R. G. Cai and Y. Z. Zhang, Int. J. Mod. Phys. A **35** (2020) no.17, 2050075 doi:10.1142/S0217751X2050075X [arXiv:1807.09495 [gr-qc]].

[70] V. Corbin and N. J. Cornish, Class. Quant. Grav. **23** (2006), 2435-2446 doi:10.1088/0264-9381/23/7/014 [arXiv:gr-qc/0512039 [gr-qc]].

[71] T. H. Jung and T. Okui, Phys. Rev. D **110** (2024) no.11, 115014 doi:10.1103/PhysRevD.110.115014 [arXiv:2110.04271 [hep-ph]].

[72] K. Kawana and K. P. Xie, Phys. Lett. B **824** (2022), 136791 doi:10.1016/j.physletb.2021.136791 [arXiv:2106.00111 [astro-ph.CO]].

[73] K. Hashino, S. Kanemura and T. Takahashi, Phys. Lett. B **833** (2022), 137261 doi:10.1016/j.physletb.2022.137261 [arXiv:2111.13099 [hep-ph]].

[74] J. Liu, L. Bian, R. G. Cai, Z. K. Guo and S. J. Wang, Phys. Rev. D **105** (2022) no.2, L021303 doi:10.1103/PhysRevD.105.L021303 [arXiv:2106.05637 [astro-ph.CO]].

[75] P. Lu, K. Kawana and K. P. Xie, Phys. Rev. D **105** (2022) no.12, 123503 doi:10.1103/PhysRevD.105.123503 [arXiv:2202.03439 [astro-ph.CO]].

[76] K. Hashino, S. Kanemura, T. Takahashi and M. Tanaka, Phys. Lett. B **838** (2023), 137688 doi:10.1016/j.physletb.2023.137688 [arXiv:2211.16225 [hep-ph]].

[77] M. Lewicki, P. Toczek and V. Vaskonen, JHEP **09** (2023), 092 doi:10.1007/JHEP09(2023)092 [arXiv:2305.04924 [astro-ph.CO]].

[78] K. Kawana, T. Kim and P. Lu, Phys. Rev. D **108** (2023) no.10, 103531 doi:10.1103/PhysRevD.108.103531 [arXiv:2212.14037 [astro-ph.CO]].

[79] Y. Gouttenoire and T. Volansky, Phys. Rev. D **110** (2024) no.4, 4 doi:10.1103/PhysRevD.110.043514 [arXiv:2305.04942 [hep-ph]].

[80] R. Jinno, J. Kume and M. Yamada, Phys. Lett. B **849** (2024), 138465 doi:10.1016/j.physletb.2024.138465 [arXiv:2310.06901 [hep-ph]].

[81] M. M. Flores, A. Kusenko and M. Sasaki, Phys. Rev. D **110** (2024) no.1, 015005 doi:10.1103/PhysRevD.110.015005 [arXiv:2402.13341 [hep-ph]].

[82] S. Kanemura, M. Tanaka and K. P. Xie, JHEP **06** (2024), 036 doi:10.1007/JHEP06(2024)036 [arXiv:2404.00646 [hep-ph]].

[83] Y. Gouttenoire, Phys. Lett. B **855** (2024), 138800 doi:10.1016/j.physletb.2024.138800 [arXiv:2311.13640 [hep-ph]].

[84] H. Niikura, M. Takada, N. Yasuda, R. H. Lupton, T. Sumi, S. More, T. Kurita, S. Sugiyama, A. More and M. Oguri, *et al.* Nature Astron. **3** (2019) no.6, 524-534 doi:10.1038/s41550-019-0723-1 [arXiv:1701.02151 [astro-ph.CO]].

[85] H. Niikura, M. Takada, S. Yokoyama, T. Sumi and S. Masaki, Phys. Rev. D **99** (2019) no.8, 083503 doi:10.1103/PhysRevD.99.083503 [arXiv:1901.07120 [astro-ph.CO]].

[86] Kondo, Iona and Sumi, Takahiro and Koshimoto, Naoki and Rattenbury, Nicholas J. and Suzuki, Daisuke and Bennett, David P., The Astronomical Journal **165** (2023) no.6, 254 doi:10.3847/1538-3881/acccf9

[87] J. Fardeen, P. McGill, S. E. Perkins, W. A. Dawson, N. S. Abrams, J. R. Lu, M. F. Ho and S. Bird, Astrophys. J. **965** (2024) no.2, 138 doi:10.3847/1538-4357/ad3243 [arXiv:2312.13249 [astro-ph.GA]].

[88] W. Buchmuller and D. Wyler, Nucl. Phys. B **268** (1986), 621-653 doi:10.1016/0550-3213(86)90262-2

[89] K. Hagiwara, S. Ishihara, R. Szalapski and D. Zeppenfeld, Phys. Rev. D **48** (1993), 2182-2203 doi:10.1103/PhysRevD.48.2182

[90] B. Grzadkowski, M. Iskrzynski, M. Misiak and J. Rosiek, JHEP **10** (2010), 085 doi:10.1007/JHEP10(2010)085 [arXiv:1008.4884 [hep-ph]].

[91] F. Feruglio, Int. J. Mod. Phys. A **8** (1993), 4937-4972 doi:10.1142/S0217751X93001946 [arXiv:hep-ph/9301281 [hep-ph]].

[92] R. Alonso, M. B. Gavela, L. Merlo, S. Rigolin and J. Yepes, Phys. Lett. B **722** (2013), 330-335 [erratum: Phys. Lett. B **726** (2013), 926] doi:10.1016/j.physletb.2013.04.037 [arXiv:1212.3305 [hep-ph]].

[93] I. Brivio, T. Corbett, O. J. P. Éboli, M. B. Gavela, J. Gonzalez-Fraile, M. C. Gonzalez-Garcia, L. Merlo and S. Rigolin, JHEP **03** (2014), 024 doi:10.1007/JHEP03(2014)024 [arXiv:1311.1823 [hep-ph]].

[94] G. Buchalla, O. Catà and C. Krause, Nucl. Phys. B **880** (2014), 552-573 [erratum: Nucl. Phys. B **913** (2016), 475-478] doi:10.1016/j.nuclphysb.2014.01.018 [arXiv:1307.5017 [hep-ph]].

[95] G. Buchalla, O. Cata, A. Celis, M. Knecht and C. Krause, Nucl. Phys. B **928** (2018), 93-106 doi:10.1016/j.nuclphysb.2018.01.009 [arXiv:1710.06412 [hep-ph]].

[96] A. Falkowski and R. Rattazzi, JHEP **10** (2019), 255 doi:10.1007/JHEP10(2019)255 [arXiv:1902.05936 [hep-ph]].

[97] T. Cohen, N. Craig, X. Lu and D. Sutherland, JHEP **03** (2021), 237 doi:10.1007/JHEP03(2021)237 [arXiv:2008.08597 [hep-ph]].

[98] H. Sun, M. L. Xiao and J. H. Yu, JHEP **05** (2023), 043 doi:10.1007/JHEP05(2023)043 [arXiv:2206.07722 [hep-ph]].

[99] H. Sun, M. L. Xiao and J. H. Yu, JHEP **04** (2023), 086 doi:10.1007/JHEP04(2023)086 [arXiv:2210.14939 [hep-ph]].

[100] I. Banta, T. Cohen, N. Craig, X. Lu and D. Sutherland, JHEP **02** (2022), 029 doi:10.1007/JHEP02(2022)029 [arXiv:2110.02967 [hep-ph]].

[101] I. Banta, JHEP **06** (2022), 099 doi:10.1007/JHEP06(2022)099 [arXiv:2202.04608 [hep-ph]].

[102] G. Buchalla, F. König, C. Müller-Salditt and F. Pandler, Phys. Rev. D **110** (2024) no.1, 016015 doi:10.1103/PhysRevD.110.016015 [arXiv:2312.13885 [hep-ph]].

[103] S. Kanemura and R. Nagai, JHEP **03** (2022), 194 doi:10.1007/JHEP03(2022)194 [arXiv:2111.12585 [hep-ph]].

[104] S. Kanemura, R. Nagai and M. Tanaka, JHEP **06** (2022), 027 doi:10.1007/JHEP06(2022)027 [arXiv:2202.12774 [hep-ph]].

[105] R. R. Florentino, S. Kanemura and M. Tanaka, Phys. Lett. B **856** (2024), 138940 doi:10.1016/j.physletb.2024.138940 [arXiv:2406.03957 [hep-ph]].

[106] R. R. Florentino, S. Kanemura and M. Tanaka, EPJ Web Conf. **315** (2024), 01012 doi:10.1051/epjconf/202431501012 [arXiv:2410.04773 [hep-ph]].

[107] [ATLAS], ATLAS-CONF-2025-006.

[108] [CMS], CMS-PAS-HIG-21-018.

[109] G. Aad *et al.* [ATLAS and CMS], [arXiv:2504.00672 [hep-ex]].

[110] G. Aad *et al.* [ATLAS and CMS], Phys. Rev. Lett. **114** (2015), 191803 doi:10.1103/PhysRevLett.114.191803 [arXiv:1503.07589 [hep-ex]].

[111] M. Aaboud *et al.* [ATLAS], Phys. Lett. B **784** (2018), 345-366 doi:10.1016/j.physletb.2018.07.050 [arXiv:1806.00242 [hep-ex]].

[112] [ATLAS], ATLAS-CONF-2020-005.

[113] A. M. Sirunyan *et al.* [CMS], JHEP **11** (2017), 047 doi:10.1007/JHEP11(2017)047 [arXiv:1706.09936 [hep-ex]].

[114] A. M. Sirunyan *et al.* [CMS], Phys. Lett. B **805** (2020), 135425 doi:10.1016/j.physletb.2020.135425 [arXiv:2002.06398 [hep-ex]].

[115] G. Aad *et al.* [ATLAS], Phys. Rev. Lett. **131** (2023) no.25, 251802 doi:10.1103/PhysRevLett.131.251802 [arXiv:2308.04775 [hep-ex]].

[116] A. Hayrapetyan *et al.* [CMS], Phys. Rev. D **111** (2025) no.9, 092014 doi:10.1103/PhysRevD.111.092014 [arXiv:2409.13663 [hep-ex]].

[117] S. Heinemeyer *et al.* [LHC Higgs Cross Section Working Group], doi:10.5170/CERN-2013-004 [arXiv:1307.1347 [hep-ph]].

[118] A. David *et al.* [LHC Higgs Cross Section Working Group], [arXiv:1209.0040 [hep-ph]].

[119] G. Aad *et al.* [ATLAS], Phys. Rev. Lett. **133** (2024) no.10, 101801 doi:10.1103/PhysRevLett.133.101801 [arXiv:2406.09971 [hep-ex]].

[120] [CMS], [arXiv:2510.07527 [hep-ex]].

[121] M. E. Peskin and T. Takeuchi, Phys. Rev. D **46** (1992), 381-409 doi:10.1103/PhysRevD.46.381

[122] I. Maksymyk, C. P. Burgess and D. London, Phys. Rev. D **50** (1994), 529-535 doi:10.1103/PhysRevD.50.529 [arXiv:hep-ph/9306267 [hep-ph]].

[123] A. Crivellin, A. Kokulu and C. Greub, Phys. Rev. D **87** (2013) no.9, 094031 doi:10.1103/PhysRevD.87.094031 [arXiv:1303.5877 [hep-ph]].

[124] T. D. Lee, Phys. Rev. D **8** (1973), 1226-1239 doi:10.1103/PhysRevD.8.1226

[125] S. L. Glashow and S. Weinberg, Phys. Rev. D **15** (1977), 1958 doi:10.1103/PhysRevD.15.1958

[126] E. A. Paschos, Phys. Rev. D **15** (1977), 1966 doi:10.1103/PhysRevD.15.1966

[127] H. E. Haber, G. L. Kane and T. Sterling, Nucl. Phys. B **161** (1979), 493-532 doi:10.1016/0550-3213(79)90225-6

[128] J. F. Donoghue and L. F. Li, Phys. Rev. D **19** (1979), 945 doi:10.1103/PhysRevD.19.945

[129] L. J. Hall and M. B. Wise, Nucl. Phys. B **187** (1981), 397-408 doi:10.1016/0550-3213(81)90469-7

[130] J. F. Gunion, H. E. Haber, G. L. Kane and S. Dawson, Front. Phys. **80** (2000), 1-404 doi:10.1201/9780429496448

[131] V. D. Barger, J. L. Hewett and R. J. N. Phillips, Phys. Rev. D **41** (1990), 3421-3441 doi:10.1103/PhysRevD.41.3421

[132] G. C. Branco, P. M. Ferreira, L. Lavoura, M. N. Rebelo, M. Sher and J. P. Silva, Phys. Rept. **516** (2012), 1-102 doi:10.1016/j.physrep.2012.02.002 [arXiv:1106.0034 [hep-ph]].

[133] A. Pomarol and R. Vega, Nucl. Phys. B **413** (1994), 3-15 doi:10.1016/0550-3213(94)90611-4 [arXiv:hep-ph/9305272 [hep-ph]].

[134] H. E. Haber and D. O'Neil, Phys. Rev. D **83** (2011), 055017 doi:10.1103/PhysRevD.83.055017 [arXiv:1011.6188 [hep-ph]].

[135] D. Das and A. Santamaria, Phys. Rev. D **94** (2016) no.1, 015015 doi:10.1103/PhysRevD.94.015015 [arXiv:1604.08099 [hep-ph]].

[136] P. Nath, B. D. Nelson, H. Davoudiasl, B. Dutta, D. Feldman, Z. Liu, T. Han, P. Langacker, R. Mohapatra and J. Valle, *et al.* Nucl. Phys. B Proc. Suppl. **200-202** (2010), 185-417 doi:10.1016/j.nuclphysbps.2010.03.001 [arXiv:1001.2693 [hep-ph]].

[137] J. Garayoa and T. Schwetz, JHEP **03** (2008), 009 doi:10.1088/1126-6708/2008/03/009 [arXiv:0712.1453 [hep-ph]].

[138] H. E. Haber and H. E. Logan, Phys. Rev. D **62** (2000), 015011 doi:10.1103/PhysRevD.62.015011 [arXiv:hep-ph/9909335 [hep-ph]].

[139] I. Low and J. Lykken, JHEP **10** (2010), 053 doi:10.1007/JHEP10(2010)053 [arXiv:1005.0872 [hep-ph]].

[140] I. Low, J. Lykken and G. Shaughnessy, Phys. Rev. D **86** (2012), 093012 doi:10.1103/PhysRevD.86.093012 [arXiv:1207.1093 [hep-ph]].

[141] J. F. Gunion, R. Vega and J. Wudka, Phys. Rev. D **43** (1991), 2322-2336 doi:10.1103/PhysRevD.43.2322

[142] H. E. Logan and M. A. Roy, Phys. Rev. D **82** (2010), 115011 doi:10.1103/PhysRevD.82.115011 [arXiv:1008.4869 [hep-ph]].

[143] A. Falkowski, S. Rychkov and A. Urbano, JHEP **04** (2012), 073 doi:10.1007/JHEP04(2012)073 [arXiv:1202.1532 [hep-ph]].

[144] D. de Florian *et al.* [LHC Higgs Cross Section Working Group], CERN Yellow Rep. Monogr. **2** (2017), 1-869 doi:10.23731/CYRM-2017-002 [arXiv:1610.07922 [hep-ph]].

[145] E. W. Kolb and M. S. Turner, Front. Phys. **69** (1990), 1-547 Taylor and Francis, 2019, ISBN 978-0-429-49286-0, 978-0-201-62674-2 doi:10.1201/9780429492860

[146] G. Steigman, Ann. Rev. Astron. Astrophys. **14** (1976), 339-372 doi:10.1146/annurev.aa.14.090176.002011

[147] M. Fukugita and T. Yanagida, Phys. Lett. B **174** (1986), 45-47 doi:10.1016/0370-2693(86)91126-3

[148] I. Affleck and M. Dine, Nucl. Phys. B **249** (1985), 361-380 doi:10.1016/0550-3213(85)90021-5

[149] A. G. Cohen and D. B. Kaplan, Phys. Lett. B **199** (1987), 251-258 doi:10.1016/0370-2693(87)91369-4

[150] M. M. Anber and E. Sabancilar, Phys. Rev. D **92** (2015) no.10, 101501 doi:10.1103/PhysRevD.92.101501 [arXiv:1507.00744 [hep-th]].

[151] G. Elor, M. Escudero and A. Nelson, Phys. Rev. D **99** (2019) no.3, 035031 doi:10.1103/PhysRevD.99.035031 [arXiv:1810.00880 [hep-ph]].

[152] E. W. Kolb, A. Riotto and I. I. Tkachev, Phys. Lett. B **423** (1998), 348-354 doi:10.1016/S0370-2693(98)00134-8 [arXiv:hep-ph/9801306 [hep-ph]].

[153] H. Davoudiasl, R. Kitano, G. D. Kribs, H. Murayama and P. J. Steinhardt, Phys. Rev. Lett. **93** (2004), 201301 doi:10.1103/PhysRevLett.93.201301 [arXiv:hep-ph/0403019 [hep-ph]].

[154] H. Aoki and H. Kawai, Prog. Theor. Phys. **98** (1997), 449-456 doi:10.1143/PTP.98.449 [arXiv:hep-ph/9703421 [hep-ph]].

[155] M. Trodden, Rev. Mod. Phys. **71** (1999), 1463-1500 doi:10.1103/RevModPhys.71.1463 [arXiv:hep-ph/9803479 [hep-ph]].

[156] J. M. Cline, M. Joyce and K. Kainulainen, JHEP **07** (2000), 018 doi:10.1088/1126-6708/2000/07/018 [arXiv:hep-ph/0006119 [hep-ph]].

[157] M. Losada, Nucl. Phys. B **537** (1999), 3-31 doi:10.1016/S0550-3213(98)00563-X [arXiv:hep-ph/9806519 [hep-ph]].

[158] M. Quiros, [arXiv:hep-ph/9901312 [hep-ph]].

[159] M. Carena, G. Nardini, M. Quiros and C. E. M. Wagner, Nucl. Phys. B **812** (2009), 243-263 doi:10.1016/j.nuclphysb.2008.12.014 [arXiv:0809.3760 [hep-ph]].

[160] K. Funakubo and E. Senaha, Phys. Rev. D **79** (2009), 115024 doi:10.1103/PhysRevD.79.115024 [arXiv:0905.2022 [hep-ph]].

[161] V. Cirigliano, Y. Li, S. Profumo and M. J. Ramsey-Musolf, JHEP **01** (2010), 002 doi:10.1007/JHEP01(2010)002 [arXiv:0910.4589 [hep-ph]].

[162] J. Kang, P. Langacker, T. Li and T. Liu, JHEP **04** (2011), 097 doi:10.1007/JHEP04(2011)097 [arXiv:0911.2939 [hep-ph]].

[163] S. W. Ham, S. a. Shim and S. K. Oh, [arXiv:1001.1129 [hep-ph]].

[164] K. Blum, C. Delaunay, M. Losada, Y. Nir and S. Tulin, JHEP **05** (2010), 101 doi:10.1007/JHEP05(2010)101 [arXiv:1003.2447 [hep-ph]].

[165] J. Grant and M. Hindmarsh, Phys. Rev. D **64** (2001), 016002 doi:10.1103/PhysRevD.64.016002 [arXiv:hep-ph/0101120 [hep-ph]].

[166] A. Tranberg and B. Wu, JHEP **07** (2012), 087 doi:10.1007/JHEP07(2012)087 [arXiv:1203.5012 [hep-ph]].

[167] K. Enqvist, P. Stephens, O. Taanila and A. Tranberg, JCAP **09** (2010), 019 doi:10.1088/1475-7516/2010/09/019 [arXiv:1005.0752 [astro-ph.CO]].

[168] J. M. No, [arXiv:1504.07840 [hep-ph]].

[169] G. 't Hooft, Phys. Rev. D **14** (1976), 3432-3450 [erratum: Phys. Rev. D **18** (1978), 2199] doi:10.1103/PhysRevD.14.3432

[170] G. 't Hooft, Phys. Rev. Lett. **37** (1976), 8-11 doi:10.1103/PhysRevLett.37.8

[171] K. Kajantie, M. Laine, K. Rummukainen and M. E. Shaposhnikov, Phys. Rev. Lett. **77** (1996), 2887-2890 doi:10.1103/PhysRevLett.77.2887 [arXiv:hep-ph/9605288 [hep-ph]].

[172] F. Karsch, T. Neuhaus, A. Patkos and J. Rank, Nucl. Phys. B Proc. Suppl. **53** (1997), 623-625 doi:10.1016/S0920-5632(96)00736-0 [arXiv:hep-lat/9608087 [hep-lat]].

[173] M. Gurtler, E. M. Ilgenfritz and A. Schiller, Phys. Rev. D **56** (1997), 3888-3895 doi:10.1103/PhysRevD.56.3888 [arXiv:hep-lat/9704013 [hep-lat]].

[174] K. Rummukainen, M. Tsypin, K. Kajantie, M. Laine and M. E. Shaposhnikov, Nucl. Phys. B **532** (1998), 283-314 doi:10.1016/S0550-3213(98)00494-5 [arXiv:hep-lat/9805013 [hep-lat]].

[175] F. Csikor, Z. Fodor and J. Heitger, Phys. Rev. Lett. **82** (1999), 21-24 doi:10.1103/PhysRevLett.82.21 [arXiv:hep-ph/9809291 [hep-ph]].

[176] Y. Aoki, F. Csikor, Z. Fodor and A. Ukawa, Phys. Rev. D **60** (1999), 013001 doi:10.1103/PhysRevD.60.013001 [arXiv:hep-lat/9901021 [hep-lat]].

[177] P. B. Arnold and L. D. McLerran, Phys. Rev. D **36** (1987), 581 doi:10.1103/PhysRevD.36.581

[178] J. M. Moreno, D. H. Oaknin and M. Quiros, Nucl. Phys. B **483** (1997), 267-290 doi:10.1016/S0550-3213(96)00562-7 [arXiv:hep-ph/9605387 [hep-ph]].

[179] A. Ahriche, Phys. Rev. D **75** (2007), 083522 doi:10.1103/PhysRevD.75.083522 [arXiv:hep-ph/0701192 [hep-ph]].

[180] C. W. Chiang, M. J. Ramsey-Musolf and E. Senaha, Phys. Rev. D **97** (2018) no.1, 015005 doi:10.1103/PhysRevD.97.015005 [arXiv:1707.09960 [hep-ph]].

[181] R. Zhou, L. Bian and H. K. Guo, Phys. Rev. D **101** (2020) no.9, 091903 doi:10.1103/PhysRevD.101.091903 [arXiv:1910.00234 [hep-ph]].

[182] R. Zhou and L. Bian, Phys. Lett. B **829** (2022), 137105 doi:10.1016/j.physletb.2022.137105 [arXiv:2001.01237 [hep-ph]].

[183] K. Funakubo, A. Kakuto, S. Tao and F. Toyoda, Prog. Theor. Phys. **114** (2006), 1069-1082 doi:10.1143/PTP.114.1069 [arXiv:hep-ph/0506156 [hep-ph]].

[184] A. Ahriche, Eur. Phys. J. C **66** (2010), 333-340 doi:10.1140/epjc/s10052-010-1234-5 [arXiv:0904.0700 [hep-ph]].

[185] A. Ahriche, T. A. Chowdhury and S. Nasri, JHEP **11** (2014), 096 doi:10.1007/JHEP11(2014)096 [arXiv:1409.4086 [hep-ph]].

[186] K. Fuyuto and E. Senaha, Phys. Lett. B **747** (2015), 152-157 doi:10.1016/j.physletb.2015.05.061 [arXiv:1504.04291 [hep-ph]].

[187] X. Gan, A. J. Long and L. T. Wang, Phys. Rev. D **96** (2017) no.11, 115018 doi:10.1103/PhysRevD.96.115018 [arXiv:1708.03061 [hep-ph]].

[188] M. Spannowsky and C. Tamarit, Phys. Rev. D **95** (2017) no.1, 015006 doi:10.1103/PhysRevD.95.015006 [arXiv:1611.05466 [hep-ph]].

[189] S. Kanemura and M. Tanaka, Phys. Lett. B **809** (2020), 135711 doi:10.1016/j.physletb.2020.135711 [arXiv:2005.05250 [hep-ph]].

[190] V. Q. Phong, P. H. Khiem, N. P. D. Loc and H. N. Long, Phys. Rev. D **101** (2020) no.11, 116010 doi:10.1103/PhysRevD.101.116010 [arXiv:2003.09625 [hep-ph]].

[191] A. D. Linde, Nucl. Phys. B **216** (1983), 421 [erratum: Nucl. Phys. B **223** (1983), 544] doi:10.1016/0550-3213(83)90072-X

[192] L. Carson, X. Li, L. D. McLerran and R. T. Wang, Phys. Rev. D **42** (1990), 2127-2143 doi:10.1103/PhysRevD.42.2127

[193] L. Carson and L. D. McLerran, Phys. Rev. D **41** (1990), 647 doi:10.1103/PhysRevD.41.647

[194] K. Fuyuto and E. Senaha, Phys. Rev. D **90** (2014) no.1, 015015 doi:10.1103/PhysRevD.90.015015 [arXiv:1406.0433 [hep-ph]].

[195] X. Gan, A. J. Long and L. T. Wang, Phys. Rev. D **96** (2017) no.11, 115018 doi:10.1103/PhysRevD.96.115018 [arXiv:1708.03061 [hep-ph]].

[196] M. Lewicki, M. Merchand and M. Zych, JHEP **02** (2022), 017 doi:10.1007/JHEP02(2022)017 [arXiv:2111.02393 [astro-ph.CO]].

[197] M. Hindmarsh, S. J. Huber, K. Rummukainen and D. J. Weir, Phys. Rev. D **92** (2015) no.12, 123009 doi:10.1103/PhysRevD.92.123009 [arXiv:1504.03291 [astro-ph.CO]].

[198] C. Caprini, M. Hindmarsh, S. Huber, T. Konstandin, J. Kozaczuk, G. Nardini, J. M. No, A. Petiteau, P. Schwaller and G. Servant, *et al.* JCAP **04** (2016), 001 doi:10.1088/1475-7516/2016/04/001 [arXiv:1512.06239 [astro-ph.CO]].

[199] J. R. Espinosa, T. Konstandin, J. M. No and G. Servant, JCAP **06** (2010), 028 doi:10.1088/1475-7516/2010/06/028 [arXiv:1004.4187 [hep-ph]].

[200] I. Musco, J. C. Miller and L. Rezzolla, Class. Quant. Grav. **22** (2005), 1405-1424 doi:10.1088/0264-9381/22/7/013 [arXiv:gr-qc/0412063 [gr-qc]].

[201] T. Harada, C. M. Yoo and K. Kohri, Phys. Rev. D **88** (2013) no.8, 084051 [erratum: Phys. Rev. D **89** (2014) no.2, 029903] doi:10.1103/PhysRevD.88.084051 [arXiv:1309.4201 [astro-ph.CO]].

[202] C. W. Bernard, Phys. Rev. D **9** (1974), 3312 doi:10.1103/PhysRevD.9.3312

[203] L. Dolan and R. Jackiw, Phys. Rev. D **9** (1974), 3320-3341 doi:10.1103/PhysRevD.9.3320

[204] S. Weinberg, Phys. Rev. D **9** (1974), 3357-3378 doi:10.1103/PhysRevD.9.3357

[205] G. Aad *et al.* [ATLAS], JHEP **07** (2023), 088 doi:10.1007/JHEP07(2023)088 [arXiv:2207.00348 [hep-ex]].

[206] C. W. Chiang, A. L. Kuo and K. Yagyu, Phys. Lett. B **774** (2017), 119-122 doi:10.1016/j.physletb.2017.09.061 [arXiv:1707.04176 [hep-ph]].

[207] C. W. Chiang, A. L. Kuo and K. Yagyu, Phys. Rev. D **98** (2018) no.1, 013008 doi:10.1103/PhysRevD.98.013008 [arXiv:1804.02633 [hep-ph]].

[208] T. Appelquist and J. Carazzone, Phys. Rev. D **11** (1975), 2856 doi:10.1103/PhysRevD.11.2856

[209] J. M. Cline, A. Friedlander, D. M. He, K. Kainulainen, B. Laurent and D. Tucker-Smith, Phys. Rev. D **103** (2021) no.12, 123529 doi:10.1103/PhysRevD.103.123529 [arXiv:2102.12490 [hep-ph]].

[210] M. S. Turner, E. J. Weinberg and L. M. Widrow, Phys. Rev. D **46** (1992), 2384-2403 doi:10.1103/PhysRevD.46.2384

[211] S. Kanemura and M. Tanaka, Phys. Rev. D **106** (2022) no.3, 035012 doi:10.1103/PhysRevD.106.035012 [arXiv:2201.04791 [hep-ph]].

[212] B. Di Micco, M. Gouzevitch, J. Mazzitelli, C. Vernieri, J. Alison, K. Androsov, J. Baglio, E. Bagnaschi, S. Banerjee and P. Basler, *et al.* Rev. Phys. **5** (2020), 100045 doi:10.1016/j.revip.2020.100045 [arXiv:1910.00012 [hep-ph]].

[213] Y. Wu, L. Xiao and Y. Zhang, [arXiv:2505.04496 [hep-ph]].